Characterization of a Cell Death Mechanism in a Mouse Model of Multiple Sulfatase Deficiency: Role of Mitochondrial Autophagy

Thesis

UNRESTRICTED

The Open University

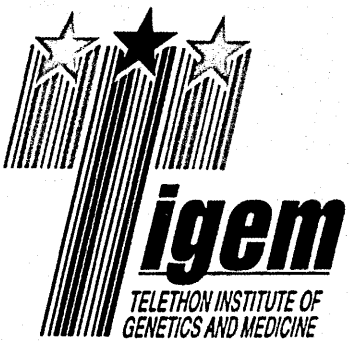

Characterization of a cell death mechanism in a mouse model of Multiple Sulfatase Deficiency: role of mitochondrial autophagy

Thesis submitted for the degree of

DOCTOR OF PHILOSOPHY

The OPEN UNIVERSITY, January 2011

by

RAQUEL DE PABLO LATORRE, B.Sc. M.Sc.

DATE of SUBMISSION: 28 JAN 2011

DATE of AWARD: 8 JUNE 2011

ProQuest LLC.
789 East Eisenhower Parkway
P.O. Box 1346
Ann Arbor, MI 48106 – 1346

"If we knew what it was we were doing, it would not be called research, would it?"

Albert Einstein

ABSTRACT

Mitochondria are organelles recognized as central players in cell death. Dysfunctional mitochondria are a well-known hallmark of disease since the accumulation of aberrant mitochondria can alter cell homeostasis thus resulting in tissue degeneration. Lysosomal storage disorders (LSDs) are a group of genetic diseases characterized by the accumulation of un-degraded material inside lysosomes that leads to autophagic-lysosomal function failure. In LSDs, mitochondrial aberrations have been associated to autophagic stress. However, the mechanisms by which autophagic deregulation determines mitochondrial dysfunction and how such alterations are involved in tissue pathogenesis remain largely unexplored. Normally, mitochondrial clearance occurs by a selective form of autophagy, known as mitophagy, which relies on a parkin- mediated mitochondrial priming and subsequent engulfment by autophagosomes. Here, we have performed a comprehensive analysis of mitophagy in a mouse model of Multiple sulfatase deficiency (MSD), an LSD characterized by both severe neurological and systemic involvement. We demonstrated that, in MSD liver, reduced parkin results in an inefficient mitochondrial turnover thus determining the accumulation of effete organelles outside autophagic vesicles. As consequence, dysfunctional mitochondria release cytochrome *c* into the cytosol ultimately leading to apoptotic cell death. Otherwise, in MSD brain, we observed minor morphological and functional changes that could not be directly associated to specific defects in mitochondrial priming machinery. Together these data provide new evidences on the mechanisms underlying mitochondrial dysfunction in LSDs and indicate that mitochondrial alterations differently contribute to tissue pathogenesis in a mouse model of LSD.

ACKNOWLEDGEMENTS

First of all, I would really like to thank both my supervisors, Prof. Andrea Ballabio and Prof. David C. Rubinsztein, whose advice and personal guidance have been essential for the completion of my thesis project.

Thanks to Dr. Elena and Roman Polishuck, who actively contributed to this work.

Thanks to all my colleagues, especially to Alberto, Cristina, Carmine, Diego, Edo, Fabio, Mina and Valentina, for their unselfish and unfailing technical and moral support. A special mention is to my dear Susy, whose helpfulness and friendship have been of great worth.

I am deeply grateful to Alessandro Fraldi, to whom I will always be indebted for all his support.

I warmly thank all people at TIGEM, for every single moment passed together. You have made me feel like home.

I owe my loving thanks to all my family, my parents Mercè and Lluís, my brother Albert and my grandparents Titi, Pepita and Luis. They have lost a lot due to my research abroad but I know that they are so proud of me. This is the best reward I could have ever got.

Finally, a special thank to my boyfriend, Andrea, who wiped away my tears in the hardest moments and shared the joyful for each little success. I could have never done it without you.

TABLE OF CONTENTS

LIST OF TABLES

TABLE **PAGE**

LIST OF FIGURES

ABREVIATIONS

α-GalA	Alpha-galactosidase A
AAV	Adeno-associated vector
AD	Alzheimer's disease
ALS	Autophagy-lysosome system
ARS	Arylsulfatase
ATG	Autophagy genes
AV	Autophagosome vesicle
BECN-1	Beclin-1
Bp	Base pair
CCCP	Carbonyl cyanide m-chlorophenyl hydrazone
CD-MPR	Cation-dependent mannose phosphate receptor
CI-MPR	Cation-independent mannose phosphate receptor
CDPX1	Chondrodisplasia punctata 1
CLEAR	Coordinated Lysosomal Expression and Regulation
COX IV	Cytochrome oxidase IV
DAPI	4',6-diamidino-2-phenylindole
DIOC6	3,3′-dihexyloxacarbocyanine iodide
DLP-1	Dynamin-like protein 1
DMEM	Dulbecco's modified eagle medium
DTT	Dithiothreitol
EE	Early endosome
EM	Electron Microscopy
ELM	Embryonic liver macrophages
ER	Endoplasmic reticulum
ERT	Enzyme replacement therapy
FBS	Fetal bovine serum
FGE	Formylglycine- generating enzyme
FGly	Formilglycine

FIS1	Fission protein 1
FLU	Fluorescence units
GAG	Glycosaminoglycans
GM1	Monosialotetrahexosylganglioside
HAT	Hypoxanthine-aminopterin-thymidine
HD	Huntington's disease
HSCT	Hematopoietic stem cell transplantation
Htt	Huntingtin
IMM	Inner mitochondrial membrane
IMS	Intermembrane space
JC-1	5,5',6,6'-tetrachloro-1,1',3,3'-tetraethylbenzimi- dazolylcarbocyanine iodide
LAMP-1/2	Lysosomal associated membrane protein 1/2
LC3	Light chain 3
LE	Late endosome
LSD	Lysosomal storage disorders
LYS	Lysosome
M6-P	Mannose 6-phosphate
MEF	Mouse embryonic fibroblasts
MFN1/2	Mitofusins 1/2
MHC II	Major histocompatibility complex II
ML	Mucolipidoses
MLD	Metachromatic Leukodystrophy
MPS	Mucopolysaccharidoses
MPT	Mitochondrial permeability transition
MRI	Magnetic resonance imaging
MSD	Multiple Sulfatase Deficiency
mTOR	Mammalian target of rapamycin
NPC	Niemann-Pick C disease
OMM	Outer mitochondrial membrane
OPA-1	Optic atrophy 1
PBS	Phosphate buffer solution

PCR	Polymerase chain reaction
PD	Parkinson's disease
PFA	Paraformaldehyde
PINK1	PTEN induced putative kinase 1
PVDF	Poly(vinylidene fluoride)
ROS	Reactive oxygen species
SDS-PAGE	Sodium Dodecyl Sulphate - PolyAcrylamide Gel Electrophoresis
SNARE	Soluble NSF Attachment Protein REceptors
SQSTM1	Sequestosome 1
SRT	Substrate reduction therapy
STS	Steroid sulfatase
SUMF1	Sulfatase modifying factor 1
SV40	Simian vacuolating virus 40
TFEB	Transcription factor elongation B
TGN	Trans Golgi network
TUNEL	Terminal deoxynucleotidyl transferase dUTP nick end labeling
VDAC1	Voltage-dependent anion channel 1
VPS	Vacuolar protein sorting
XLI	X-linked icthyiosis

Chapter 1. Lysosomes

Lysosomes are single-membrane-delimited organelles engaged in the degradation of several types of macromolecules. They were first described by de Duve as "a special type of cytoplasmic granules with sedimentation properties between those of mitochondria and microsomes" (1). Lysosomes contain in their lumen more than 40 hydrolases including proteases, glycosidases, sulfatases, phosphatases and lipases. These enzymes have an optimum pH below 6 and this acidic microenvironment, essential for several lysosomal functions, is maintained by a vacuolar-type H^+- ATPase enclosed in the limiting membrane. The membrane is formed by a single phospholipid bilayer that retains many integral proteins (i.e. LAMP-1 and -2) that control the passage of material into and out of lysosomes by both permeability and its ability to fuse with other vacuoles. This material is delivered from the cells own cytoplasm (i.e. autophagy) as well as macromolecules taken up from the extracellular space (endocytosis) by an interconnected network of membranes known as the endo-lysosomal system (2, 3).

1.1. Synthesis and sorting of lysosomal enzymes

Lysosomal hydrolases are glycoproteins originally synthesized with an N-terminal sequence of 20-25 aminoacids recognized by the signal recognition particle, which enables the nascent polypeptides to be translocated across the

membrane of the rough endoplasmic reticulum (ER) (figure 1). Subsequent to the removal of the signal peptide and N-glycosylation, they move to the Golgi compartment where they acquire a mannose 6-phosphate (M6-P) ligand. The acquisition of the M6-P marker is required to guarantee the targeting of proteins to lysosomes although M6-P-independent trafficking to lysosomes has also been described. However, In most cases, the failure of acquisition of the M6-P ligand results in either mistargeting of lysosomal enzymes or their secretion.

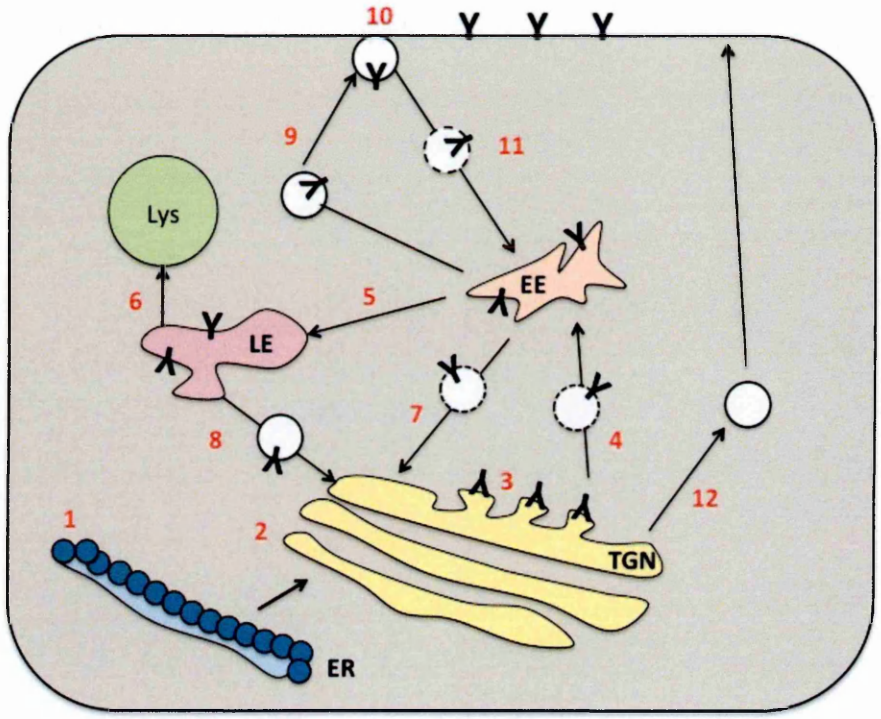

Figure 1.Model for the intracellular transport of MPR and proteins to lysosomes. Soluble lysosomal enzymes are synthesized and translocated into the ER lumen (1). Once in the Golgi (2), the MP6 tag is added (3) and recognized by MPRs. Receptor-ligand complexes are transported to the early endosomal compartment (EE, 4). A lower pH produces complex dissociation and the lysosomal enzymes are delivered to the lysosome (Lys; 5 and 6). MPRs return back to the TGN (7 and 8) or to the plasma membrane (9). Exogenous M6P-containing proteins can be internalized by CI-MPR (10) and directed to lysosomes along the endocytic pathway (11). Enzymes that do not bind to MPR are secreted (12).

In mammalian cells two MPR exist: the 46 KDa cation-dependent MPR (CD-MPR, MPR46) and the 300 KDa cation-independent MPR (CI-MPR, MPR300). Subsequently, receptor-ligand complexes exit from the TGN in clathrin-coated vesicles and fuse with membranes of the endosomal compartment. Once in the acidic environment of lysosomes, hydrolases undergo additional post-translational modifications including proteolysis, folding and aggregation (2, 4, 5).

1.2. Lysosome biogenesis

Acidic hydrolases can be found in each type of cell except for erythrocytes. It is therefore not surprising that genes encoding some lysosomal enzymes have regions upstream of the coding sequence that are common to promoters of housekeeping genes.

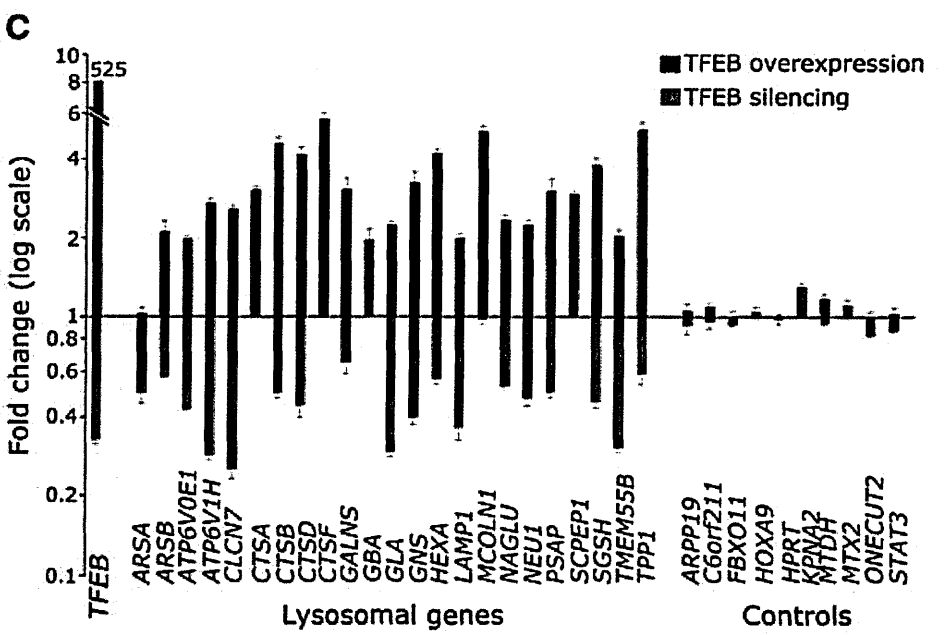

Figure 2.Expression analysis of lysosomal genes after TFEB over- expression and silencing. Blue bars show the fold change of the mRNA levels of lysosomal genes in TFEB- versus pcDNA3- transfected cells. Red bars show the fold change of mRNA levels in mimic-miR-128–transfected cells versus cells transfected with a standard control miRNA (mimic-miR-cel-67). Randomly chosen nonlysosomal genes were used as controls. Gene expression was normalized relative to glyceraldehyde-3-phosphate dehydrogenase (GAPDH).

Recently, a comprehensive analysis of promoter regions of 96 lysosomal genes resulted in the identification of a palindromic sequence, called CLEAR, highly enriched in this promoter set. Among the transcription factors that bind sequences similar to the CLEAR consensus, only TFEB resulted in the upregulation of lysosomal genes (figure 2). The increase in the number of lysosomes and the upregulation of some non-lysosomal enzymes tightly related to lysosomal function (i.e. *M6PR*) make TFEB a master regulator of lysosomal biogenesis (6).

Chapter 2. Lysosomal storage disorders (LSDs)

Lysosomal storage disorders are a group of inherited metabolic disorders that result from defective lysosomal acid hydrolysis of endogenous macromolecules. Although the first description of a lysosomal storage disorder was that of Tay-Sachs disease in 1881, the link between an enzyme deficiency and a storage disorder was only demonstrated by Hers in 1963 (4, 5). Currently, over 40 LSDs involving soluble hydrolases and integral membrane proteins have been described (Table I from ref.7).

LSDs can be classified according to the defective enzyme or protein but perhaps, the most useful classification is made on the basis of the kind of substrate that accumulates. For example, in Mucopolysaccharidoses (MPS), glycosaminoglycans (mucopolysaccharides) accumulate due to the impaired function of any 1 of 11 lysosomal enzymes that include exoglycosidases, sulphatases and one transferase. In some cases, a defect in a single enzyme can lead to the accumulation of different substrates (7).

However, it is important to highlight that these disorders are not simply a consequence of pure storage but result from perturbation of complex cell signaling mechanisms that give rise to secondary structural and biochemical changes.

Table I. **Lysosomal storage disorders**

Disease	Defective protein	Main storage materials
Sphingolipidoses		
Fabry	α- Galactosidase A	Globotriasylceramide and blood-group-B substances
Faber lipogranulomatosis	Ceramide	Ceramide
Gaucher	β- Glucosidase Saposin-C activator	Glucosylceramide Glucosylceramide
Niemann-Pick A and B	Sphingomyelinase	Sphingomyelin
Sphingolipid-activator deficiency	Sphingolipid activator	Glycolipids
GM1 gangliosidosis	β- Galactosidase	GM1 ganglioside
GM2 gangliosidosis (Tay-Sachs)	β- Hexosaminidase A	GM2 ganglioside and related glycolipids
GM2 gangliosidosis (Sandhoff)	β- Hexosaminidase A and B	GM2 ganglioside and related glycolipids
GM2 gangliosidosis (GM2-activator deficiency)	GM2-activator protein	GM2 ganglioside and related glycolipids
Mucopolysaccharidoses (MPS)		
MPS I (Hurler, Scheie, Hurler/Scheie)	α-iduronidase	Dermatan sulphate and heparan sulphate
MPS II (Hunter)	Iduronate-2-sulphatase	Dermatan sulphate and heparan sulphate
MPSIIIA (Sanfilippo)	Heparan *N*-sulphatase (sulphamidase)	Heparan sulphate
MPSIIIB (Sanfilippo)	*N*-Acetyl-α-glucosaminidase	Heparan sulphate
MPSIIIC (Sanfilippo)	Acetyl-CoA:α-glucosamide *N*-acetyltransferase	Heparan sulphate
MPSIIID (Sanfilippo)	*N*-Acetylglucosamine-6-sulphatase	Heparan sulphate
Morquio-A disease	*N*-Acetylgalactosamine-6-sulphate-sulphatase	Keratan sulphate, chondroitin 6-sulphate
Morquio-B disease	β-Galactosidase	Keratan sulphate
MPS VI (Maroteaux-Lamy)	*N*-Acetylgalactosamine-4-sulphatase (arylsulphatase B)	Dermatan sulphate
MPS VII (Sly)	β- Glucuronidase	Heparan sulphate, dermatan sulphate, chondroitin-4- and -6-sulphates

Table 1. **Lysosomal storage disorders (continue)**

Disease	Defective protein	Main storage materials
Oligosaccharidoses and glycoproteinosis		
Pompe (glycogen-storage-disease type II)	α- Glucosidase	Glycogen
Diseases caused by defects in integral membrane proteins		
Cystinosis	Cystinosin	Cystine
Danon disease	LAMP2	Cytoplasmic debris and glycogen
Infantile sialic-acid-storgae disease and Salla disease	Sialin	Sialic acid
Mucolipidosis (ML) IV	Mucolipin-1	Lipids and acid mucopolysaccharides
Niemann-Pick C (NPC)	NPC1 and 2	Cholesterol and sphingolipids
Others		
Galactosialidosis	Cathepsin A	Sialyloligosaccharides
I Cell and pseudo-Hurler polydystrophy (ML II and ML III, respectively)	UDP-*N*-acetylglucosamine:lysosomal enzyme *N*-acetylglucosaminyl-1-phosphotransferase	Oligosaccharides, mucopolysaccharides and lipids
Multiple sulfatase deficiency	Cα-formylglicine-generating enzyme	Sulphatides
Neuronal ceroid lipofuscinosis (NCL) 1 (Batten disease)	CLN1 (protein palmitoylthioesterase-1)	Lipidated thioesters
NCL2 (Batten disease)	CLN2 (tripeptidyl amino peptidase-1)	Subunit c of the mitochondrial ATP synthase
NCL3 (Batten disease)	Arginine transporter	Subunit c of the mitochondrial ATP synthase

2.1. Genetics

LSDs are monogenetic disorders usually inherited in an autosomal-recessive fashion except for Fabry disease, MPS II and Danon disease that are X-linked. The prevalence is 1 in 5000 to 8000 births in USA, Europe and Australia. Different

mutations have been described in the same gene and these include missense, nonsense and splice-site mutations, and partial deletions and insertions. Depending on the type of mutation, complete or partial loss of enzyme activity can be found. The levels of enzyme activity account for the severity of the phenotype: the lower the residual activity, the earlier the age of onset and the more severe the disease (5, 7).

2.2. Clinical features and diagnosis

In LSDs, the severity of the disease is related to the type and amount of substrate that accumulates and the tissues or cells in which it accumulates. The most severe, the infantile forms, present acute brain involvement and patients usually die within the first years of life. In adult forms, symptoms develop more slowly and disability often arises mainly from peripheral symptoms. Juvenile forms are intermediate between infantile and adult forms. Neurological symptoms can include seizures, dementia and brainstem dysfunction. Among the peripheral symptoms we find enlargement of the spleen and liver (hepatosplenomegaly), heart and kidney injury, abnormal bone formation, muscle atrophy and ocular disease. Several LSDs are characterized by prominent neurological involvement and minimal peripheral impairment (for example, Sanfilippo disease), whereas others have peripheral dysfunction with rare brain involvement (for example, Fabry disease) (7).

The identification of a LSD can be complex and lengthy. Certain symptoms, especially when appearing in clusters, should alert physicians to the possibility of a

LSD as the underlying cause. However, many of these appear with other more common diseases leading to delays caused by misdiagnosis.

Table II. Presenting features in some Lysosomal storage disorders

Disease	Signs and symptoms	Samples for diagnosis
GM1 gangliosidosis	IO: hypotonia, DD, coarse facial features, HM, CRS (±) LO: DD, ataxia, dysarthria, PR, dystonia	L, P, F
Metachromatic Leukodystrophy	Late IO: weakness, hypotonia, DD, genu recurvatum JO: weakness, PR, ataxia, behavior changes AO: pyramidal or cerebellar signs, behavior changes, psychoses, dementia	L, F, U
MPS IIIA (Sanfilippo)	Aggressive behavior, DD, mildly coarse facial features, hirsute, coarse hair, mild DM	F
Multiple sulfatase deficiency	DD, ichthyosis, coarse facial features, deafness, mild DM, PR	L, F
Mucolipidosis IV	DD, corneal opacities, retinal degeneration, strabismus	F
Pompe disease	Hypotonia, DD, cardiac enlargement	F

Abbreviations: AO, adult onset; DD, developmental delay; DM, dysostosis multiplex; F, fibroblasts; HM, hepatomegaly; HSM, hepatosplenomegaly; IO, infantile onset; JO, juvenile onset; LO, late onset; L, leukocytes; MR, mental retardation; P, plasma; PR, psychomotor regression; U, urine.

The main method of validating a clinical suspicion is enzyme assay, available for most LSDs. These tests compare enzyme levels in a patient sample (generally blood, urine, or skin fibroblasts) against normal benchmarks (Table II). Low levels of a particular enzyme confirm the LSD associated with that enzyme defect. In some cases, other methods may be used, such as brain MRIs, electroretinogram, or biopsy of enlarged tissue. Mutation analysis can check for a gene mutation known to cause a particular disorder but it is not always conclusive as several mutations may cause a certain LSD (8).

2.3. Treatment

The phenotypic heterogeneity has resulted in considerable difficulty especially when considering treatment. Specific therapy can be broadly divided into those that address the symptoms and those that address the cause.

Metabolic cross-correction

- Stem cell transplantation (HSCT)

  Hematopoietic cells from donors are able to build up sufficient amounts of enzyme to correct the deficient activity. Engraftment after transplantation results in a rapid decline in GAG excretion, reduction of liver and spleen volume, and improvement of obstructive airway symptoms. However, the skeleton does not respond as well and patients often need surgical intervention (9).

- Enzyme replacement therapy (ERT)

  Exogenously enzymes are taken up by cells. The results of ERT vary considerably from disease to disease and depend on the age of onset, rapidity of progression and the presence or absence of neurological involvement. Recombinant enzymes are already available for some LSDs (Pompe, Fabry, MPSI, II and VI and Gaucher) (5, 9) (Table III).

Table III. Metabolic cross-correction of some types of LSDs

Category	Diagnosis	BMT	ERT
Mucopolysaccharidosis	MPS I	Yes	Yes
	MPS II	Yes	Yes
	MPS III A-D	Yes	-
	MPS IV A-B	Yes	-
	MPS VI	Yes	Yes
Glycoproteinosis	Aspartylglucosaminuria	Yes	-
	Fucosidosis	Yes	
	Mannosidosis α and β	Yes	
Sphingolipidosis	Fabry's	-	Yes
	Farber's	Yes	-
	Gaucher's I-III	Yes	Yes
	GM_1 gangliosidosis	Yes	-
	Niemann-Pick A and B	Yes	-
	Tay-Sachs disease	Yes	-
	Krabbe disease	Yes	-
	MLD	Yes	-
Other lipidosis	Ceroid lipofuscinosis	Yes	-

BMT, bone marrow transplantation; ERT, enzyme replacement therapy

Substrate reduction therapy (SRT)

The concept of this therapeutic principle is to reduce the amount of storage material instead of enhancing the activity of the degrading enzymes. For example, N- butyldeoxynojirimycin (Miglustat, Zavesca1, Actelion Pharmaceuticals, Allschwil/Basel, Switzerland) has the ability to inhibit ceramide glucosyltransferase, the enzyme that synthesizes glucosylceramide, the storage compound in Gaucher disease (10). This compound has also successfully been used in other LSDs such as NPC as glycosphingolipids directly derivate from glucosylceramide (11).

Chaperone-mediated therapy

Mutations that affect accurate folding prevent the lysosomal enzymes from reaching their final destination so that they cannot fulfill their function. Chaperones are small molecular weight ligands that stabilize misfolded proteins and ensure their correct targeting to the lysososome. One of the advantages of pharmacological chaperones is their better biodistribution profile in comparison with recombinant enzymes. Unfortunately, this therapy is likely to be effective only in patients with mutations outside the catalytic site (5, 9).

For example, in Fabry disease, it has been demonstrated that subinhibitory doses of the competitive inhibitor of α-GalA, 1-deoxygalactonojirimycin (DGJ), stabilize mutant α-GalA *in vitro* and correct the trafficking defect (12).

Gene therapy

- *In vivo* Gene therapy

  Vector delivery systems (i.e. retroviruses, AAVs) containing the correct copy of a gene are administrated to effectively transduce organs, which become a source of enzyme for metabolic correction. Intravenous delivery of AAV2 vectors has resulted in biochemical, histological, and clinical improvements in several murine models of LSD. Moreover, numerous studies have been done to test the hypothesis that directed brain gene transfer can be therapeutic in animal models of LSD with neurologic involvement. Unfortunately, in some cases, the expression of

the delivered gene can be transient due to the severe immune reactions directed against the vector (13).

- *Ex vivo* Gene therapy

  The goal of this strategy is to transplant autologous genetically modified hematopoietic stem cells that express the defective protein thus creating a reservoir of enzyme that can be secreted into the circulation and correct the disease at distant sites. Although the preclinical hematopoietic-directed gene therapy experiments are promising, the success has not translated into the clinic as pre-clinical experiments in small animals suggest that there is no selective advantage for enzyme-positive cells in LSDs (13).

However, in the last years, research in LSDs has been largely addressed to understand the relationship between storage and cellular dysfunction. Understanding what is occurring in each cell at a molecular level would allow us to find common features/pathways with other type of storage disorders (i.e. Alzheimer's, Parkinson's) and design new therapeutic strategies.

Chapter 3. Sulfatase Deficiencies

3.1. Sulfatases family

Sulfatases are a family of enzymes that carry out the hydrolysis of sulfate ester bounds from a wide variety of substrates such as glycosaminoglycans, sulfolipids and steroid sulfates (14).

$$R\text{-}OSO_3^- + H_2O \rightarrow R\text{-}OH + H^+ + SO_4^{2-}$$

$$R\text{-}NHSO_3^- + H_2O \rightarrow R\text{-}NH_3^+ + SO_4^{2-}$$

The similarities shared by sulfatases include: 1) 20–60% sequence homology over the entire protein length, 2) a highly conserved N- terminal region containing the consensus sulfatase motifs, and 3) a unique active-site aldehyde residue, α-formylglycine (FGly), which is installed post-translationally (15). The significant sequence conservation strongly suggests that sulfatases are members of an evolutionary conserved gene family sharing a common ancestor (16).

The first sulfatases described were identified through the study of a disease (i.e. STS, steroid sulfatase). Years after, positional cloning strategies first and analysis of the human genome sequence allowed the identification of many new sulfatases (17). To date, 17 different sulfatases have been described in humans (Table IV from ref.17)

Table IV. **Human Sulfatases**

Gene	Chromosomal localization	Enzyme	Subcellular localization	Human disorder
ARSA	22q13	Arylsulfatase A	Lysosomal	Metachromatic leukodystrophy
ARSB	5q13	Arylsulfatase B	Lysosomal	Maroteaux-Lamy syndrome
IDS	Xq27-28	Iduronate sulfatase	Lysosomal	Hunter syndrome
SGSH	17q25.3	Sulfamidase	Lysosomal	Sanfilippo A syndrome
G6S	12q14	Glucosamine-6-sulfatase	Lysosomal	Sanfilippo D syndrome
GAL6S	16q24	Galactose-6-sulfatase	Lysosomal	Morquio A syndrome
ARSC/STS	Xp22.3	Arylsulfatase C / Steroid sulfatase	Microsomal	X-linked Ichthyosis
ARSD	Xp22.3	Arylsulfatase D	ER	N.I.
ARSE	Xp22.3	Arylsulfatase E	Golgi	Chondrodysplasia Punctata I
ARSF	Xp22.3	Arylsulfatase F	ER	N.I.
ARSH	Xp22.3	Arylsulfatase H	N.D.	N.I.
HSULF1	8q13.2-13.3	Hsulf1	Cell surface	N.I.
HSULF2	20q13.12	Hsulf2	Cell surface	N.I.
ARSG	17q23-24	Arylsulfatase G	Lysosomal (?)	N.I.
ARSJ	4q26	Arylsulfatase J	ER	N.I.
ARSI	5q32	Arylsulfatase I	ER	N.I.
TSULF	5q15	T.Sulfatase	N.D.	N.I.

ER, endoplasmic reticulum; ND, not determined; NI, not identified

Classification

- Lysosomal sulfatases

  Sulfatases localized into the lysosomes are soluble enzymes that exert their activity (mostly catabolic) at an acidic pH. They demonstrate substrate

specificity and little functional redundancy. Six diseases are due to deficiencies of lysosomal sulfatases. They include (17):

a) MLD (Metachromatic Leukodystrophy), in which sulfatide accumulation destroys myelin sheaths of the nervous system;

b) and five different types of Mucopolysaccharidoses,

   i. MPS II (Hunter), heparan and dermatan sulfate storage.

   ii. MPS IIIA and D (Sanfilippo), heparan sulfate accumulation.

   iii. MPS IVA (Morquio), keratan sulfate storage.

   iv. MPS VI (Maroteaux-Lamy), dermatan and chondroitin sulfate accumulation.

- Non-lysosomal sulfatases

Sulfatases localized in non-acidic subcellular compartments such as the ER, the Golgi and the cell surface; are membrane-bound enzymes involved in biosynthetic pathways (15). Extracellular matrix sulfatases (Sulf1/2) have a pivotal role in signaling and embryonic development based on the modulation of interactions between GAGs and signaling molecules. Mutations in the ER/Golgi sulfatases (STS/ARSC and ARSE) are, respectively, responsible for:

a) X-linked ichthyosis (XLI),

b) and X-linked recessive chondrodysplasia punctata 1 (CDPX1), characterized by abnormalities in cartilage and bone development (17).

Animal models

Currently, animal models for sulfatases deficiencies are available except for the two non-lysosomal sulfatases deficiencies. Although rare genetic disorders are as infrequent in animals as they are in humans, most of these animal models are spontaneous models (table V from ref.17). Fortunately, these animal models resemble the human phenotype thus becoming of great importance for the study of new therapeutic approaches for these types of disorders.

Table V. **Animal models of sulfatases deficiencies**

Sulfatase disorder	Animal model
MLD	Mouse
MPSVI	Cat*, rat*, dog*, mouse
MPS II	Dog*, mouse
MPS III A	Dog*, mouse*
MPS III D	Goat*
MPS IV A	Mouse
XLI	Not available
CDPX	Not available

* spontaneous models

3.2. Sulfatase Modifying Factors (SUMFs)

Two highly homologous amino acid motifs, recognized as the sulfatase signature sequences I and II, are found within the first third of the N-terminal sequence of all known hydrolytic sulfatases (18). The signature sequence I (C/S-X-P-S/X-R-X-X-X-L/X-T/X-G/X-R/X) is critical for directing the post-translational

modification of the initial cysteine or serine residue into the catalytically active residue formylglycine (FGly) (19, 20). This step occurs within the ER before the sorting to different cellular compartments and is directed by the product of the *SUMF1* gene.

The identification of the *SUMF1* gene was carried out by two different approaches, one biochemical (21) and the other genetic (22). In this case, Cosma and collaborators used a panel of human/mouse hybrid cell lines containing individual normal human chromosomes tagged with the dominant selectable marker HyTK and fused to an immortalized cell line from a patient with Multiple Sulfatase Deficiency (MSD) (see chapter section 3.3).

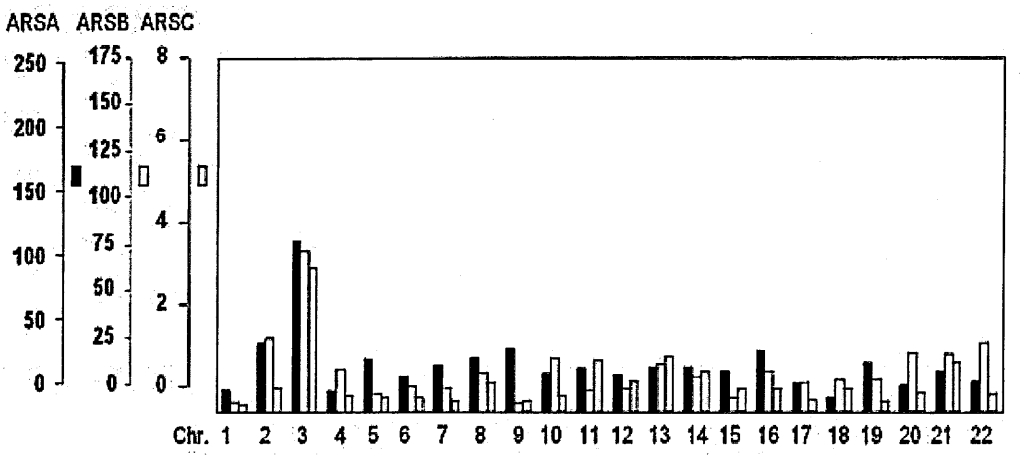

Figure 3. Mapping of the MSD gene by microcell-mediated chromosome transfer. ARSA, ARSB and ARSC activities are expressed in enzymatic units x mg total protein^{-1} x 3 hr^{-1}. Chromosome 3 clones complement the MSD defect (from ref. 22).

All 22 human autosomes were transferred one by one to the patient cell line and hybrids were selected in hygromcyin and HAT-containing medium. Subsequently, cells were harvested for ARSA, ARSB and ARSC enzymatic assay.

Several clones deriving from the chromosome 3 transfer were significantly higher compared to clones from all other chromosomes (figure 3).

Further analysis determined 3p26 as the specific chromosomal region containing the *SUMF1* gene. This gene is composed of 9 exons, spans approximately 106 kb and encodes a glycoprotein of 374 aminoacids, the formylglycine-generating enzyme (FGE). Northern blot analysis revealed an ubiquitous expression pattern of *SUMF1* with a higher abundance in kidney and liver (22).

Highly conserved *SUMF1* homologues were found in many eukaryotic and prokaryotic species, which is not surprising given the importance of the FGly modification. Catalytic and functional conservation among FGE homologues was demonstrated by the production of active human sulfatases co-expressed with *SUMF1* cDNAs from mice and *Drosophila* (figure 4) (22).

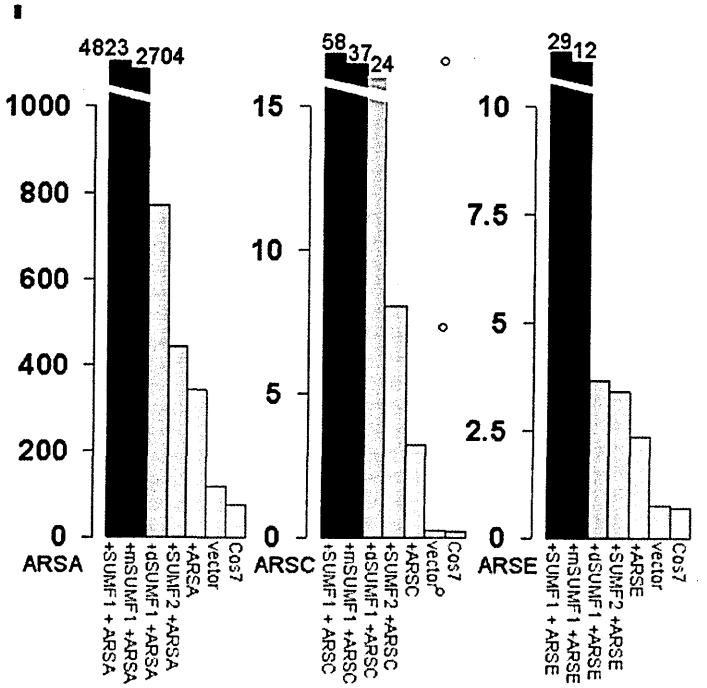

Figure 4. Murine *SUMF1*, Drosophila *SUMF1* and human *SUMF2* enhance human sulfatase activities in Cos-7 cells (from ref.22).

Sequence comparison identified the presence of a *SUMF1* gene paralogue located on human chromosome 7q11 that was designated *SUMF2*. The product of this gene also showed FGE activity, albeit much less efficient than that of *SUMF1* (22).

3.3. The Multiple Sulfatase Deficiency (MSD)

Genetics

The Multiple Sulfatase Deficiency (OMIM #272220) is an autosomal recessive disorder caused by mutations in the *SUMF1* gene (figure 5).

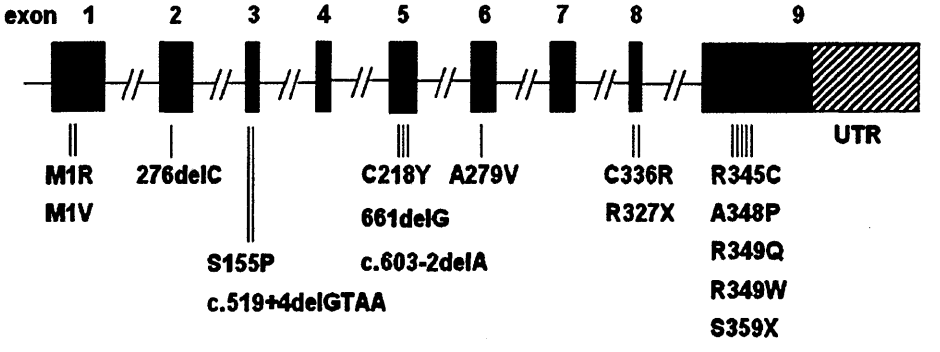

Figure 5. Localization of the mutations associated with MSD.

Most MSD patients have residual sulfatases activity due to hypomorphic mutations in the *SUMF1* gene thus suggesting that complete loss of *SUMF1* function is likely to be lethal in humans (23). Nevertheless, this residual activity is not sufficient for the proper modification of sulfatases.

Clinical features

Patients suffering from MSD combine clinical symptoms of the different single sulfatase defects and can be classified into four clinical forms (table VI from ref.24): very severe neonatal MSD, whose diagnosis is established in the first months of life and whose symptomatology is very similar to mucopolysaccharidosis (MPS) with death within the first 12 months of life; severe late-infantile MSD, whose onset is in the first year of life and neurological problems are similar to the late-infantile form of metachromatic leukodystrophy (MLD); mild late-infantile MSD, with symptoms occurring between the age of 2 and 4 years, absence of intrauterine manifestations, facial dysmorphism, visceromegaly, and cardiopathy, and presence of a milder/slower neurodegeneration; and juvenile MSD, which is a rare subtype associated with a few of the symptoms of MSD, such as ichthyosis and mental retardation (25).

Table VI. **Classification of MSD patients and associated clinical phenotype**

Symptoms	Neonatal (very severe)	Late Infantile (Severe)	Late Infantile (Mild)	Juvenile (Mild)
Retardation	+++	+++	+++	++
Neurodegeneration	+++	+++	+++	++
Ichthyosis	+++	+++	++	+
Dysmorphism	+++	+++	-	+
Organomegaly	+++	+++	-	-
Skeletal changes	+++	++	+	-
Intrauterine manifestation	+++	+++	-	-
Heart disease	+++	-	-	-
Corneal clouding	+++	-	-	-
Hydrocefalus	+++	-	-	-

Age at onset: +++ <2 years, ++ 2–4 years, + >4 years, - not observed).

No genotype-phenotype correlation has been established so far with any clinical form, but the severe neonatal subtype appears to be related to nonsense mutations and large deletions as well as to missense mutations that directly affect the active site of FGE (26).

Diagnosis

Biochemically, MSD is distinct and classifiable. Patients with MSD show a mixed excretion of glycosaminoglycans (GAGs) and storage of the different sulfatase substrates. The residual activities of different sulfatases measured in leukocytes and fibroblasts of patients can be sub-grouped into two classes with less than 15% compared to normal activities into group I (severe) and more than 15%, sometimes reaching normal values, into group II (mild) (reviewed in 24).

Treatment

Currently, there are no available therapies for the treatment of MSD. However, a patient treated with human recombinant arylsulfatase B (Galsufase) showed significant improvement (26). In that case, the main clinical manifestations were similar to those of MPS VI but, in general, the severity of the phenotype makes MSD unsuitable to be treated by enzyme replacement or bone marrow transplantation.

Recently, an *in vivo* gene-therapy approach has been tested on an MSD mouse model. Combined administration (intra-cerebral and systemic) of an AAV9

vector encoding *SUMF1* resulted in the global activation of sulfatases and the near-complete clearance of GAGs (27).

3.4. The *Sumf1-/-* mouse: an animal model for Multiple Sulfatase Deficiency (MSD)

In 2007, in our lab, a transgenic mouse (C57B6/S129j background) carrying a null mutation in the *SUMF1* gene was generated.

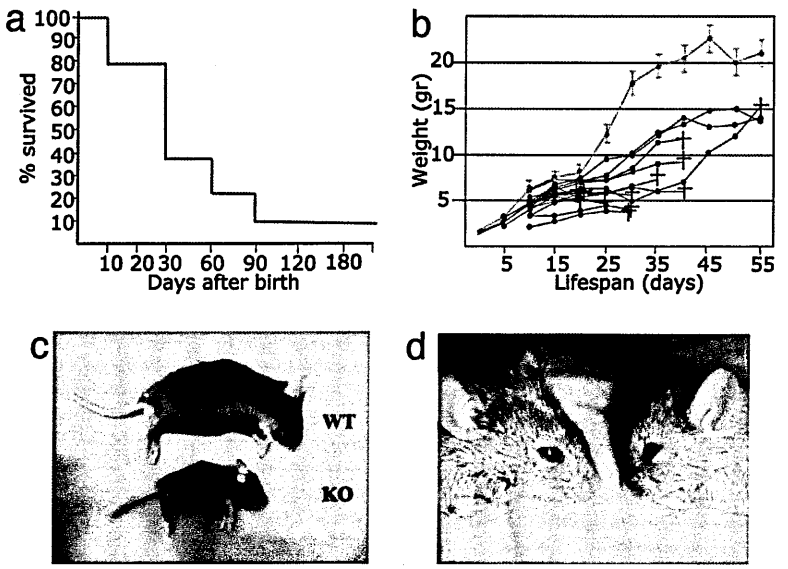

Figure 6. Growth and survival rates in *Sumf1-/-* mice. (a) Kaplan–Meyer survival curve of *Sumf1-/-*mice. (b) Mean weight values of WT (purple) and individual weight values of *Sumf1-/-* mice (blue). (c) *Sumf1-/-* mice (KO) are smaller than their WT littermates at P40. (d) *Sumf1-/-* mice (on the left) display the typical flat facial profile of patients affected by MPSs.

Although *Sumf1-/-* mice differ from patients for the total absence of SUMF1 protein (FGE), they share a common phenotype: *Sumf1-/-* mice display congenital

growth retardation and frequent mortality in the first weeks of life, with only 10% reaching 3 months of age (figure 6) (28). Hind limb clasping, head tremor and seizures were also detected, indicating neurological involvement. Hepatosplenomegaly and skeletal abnormalities are other typical features of this disorder due to the accumulation of storage material in peripheral organs. Strong signs of inflammation have been observed in all tissues of *Sumf1-/-* mice. Detailed analysis of the accumulated material pointed out macrophages as the primary site of GAG storage, thus indicating a link between storage and inflammation. Moreover, immunohistochemical analysis revealed a remarkably astroglyosis, progressive loss of Purkinje cells and massive apoptosis at a late stage of disease (28).

As SUMF1 regulates not only lysosomal sulfatases but also sulfatases localized in other cellular compartments (i.e. extracellular matrix, ER/Golgi), some of the clinical features observed in MSD may be due to alterations in signaling pathways since GAGs are involved in developmental processes.

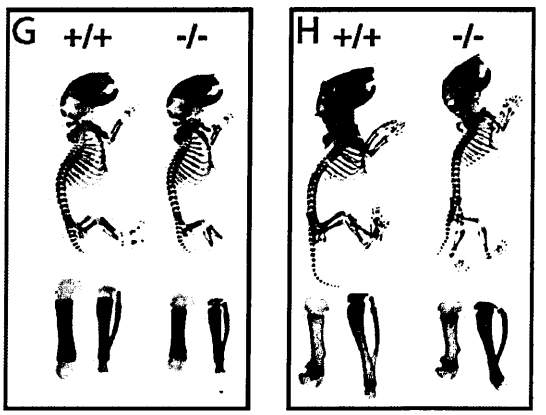

Figure 7. Skeletal development in *Sumf1-/-* mice. (G) Newborn, (H) and P4 with femur and tibia magnification.

A study of Settembre and collaborators in 2008 (29) have shown that some of the skeletal abnormalities observed in *Sumf1-/-* mice are due to altered proteoglycan desulfation, a critical step for chondrocyte differentiation and proliferation (figure 7).

Research on MSD has underlined the general importance of studying inherited diseases even if only very few patients are affected. However, many questions need to be answered to unravel the steps from the basic molecular defect to the manifestation of the disease in order to gain deeper insight into complex pathophysiological mechanisms. Hence, the MSD mouse (*Sumf1-/-*) represents a good animal model to study the pathogenic mechanisms of this rare genetic disorder as it recapitulates most of the clinical features described in MSD patients.

Chapter 4. Autophagy and Mitochondria in LSDs

In order to maintain cell homeostasis, a well-controlled balance between protein synthesis/degradation and organelle biogenesis/turnover is required. The cell's major pathways of degradation are autophagy-lysosome system (ALS) and the proteasome. Whereas proteasome degradation depends on specific tagging of target proteins by ubiquitin molecules, autophagy is a dynamic process by which parts of the cytoplasm and organelles are delivered to lysosomes for their degradation (30) (figure 8).

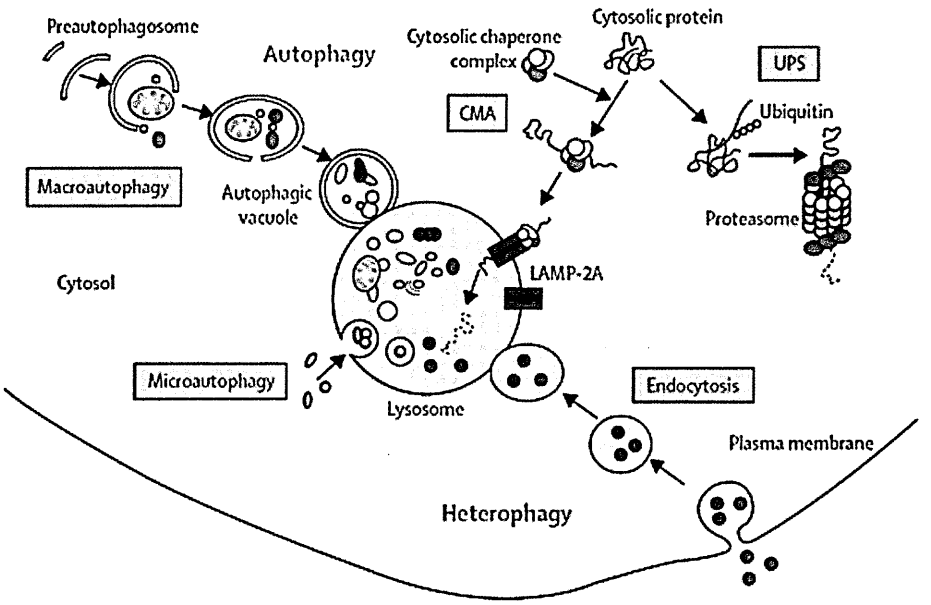

Figure 8. Proteolytic systems in mammalian cells (31)

Depending on the delivery route, three different autophagic routes are known (reviewed in 32):

1) *macroautophagy* (usually referred simply as autophagy), in which a double-membrane vesicle, called autophagosome, encircles part of the cytoplasm and fuses with lysosomes for the degradation of its content;

2) *microautophagy*, in which the lysosomal membrane itself sequesters a portion of the cytoplasm;

3) *chaperone-mediated autophagy*, by which only proteins with a specific sequence signal are recognized by cytosolic chaperones and transported from the cytosol to the lysosomal lumen.

The process of macroautophagy can be divided into at least 4 steps: induction, formation of the autophagosome, autophagosome docking and fusion and autophagic body breakdown (30) (figure 9).

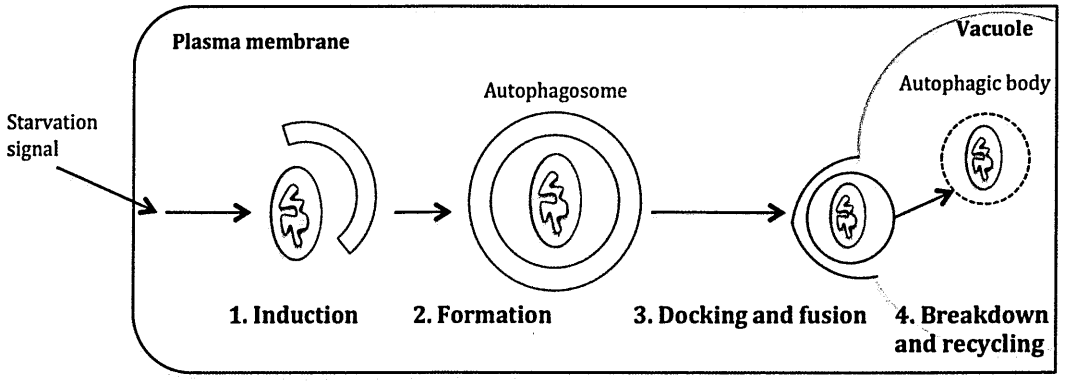

Figure 9. Schematic model of macroautophagy.

1) *Induction of macroautophagy*

This process is both developmentally and nutritionally regulated. Under nutrient-rich conditions, autophagy is inhibited by mTOR (mammalian target of Rapamycin), a member of the phosphatidylinositol 3-kinase-related kinase protein with a conserved role in sensing cellular nutrients, energy levels and redox status. During starvation instead, mTOR kinase is inactivated and autophagy is induced. Downstream of TOR kinase, more than 20 *ATG* genes (yeast) encode proteins essential for the execution of autophagy (figure 10).

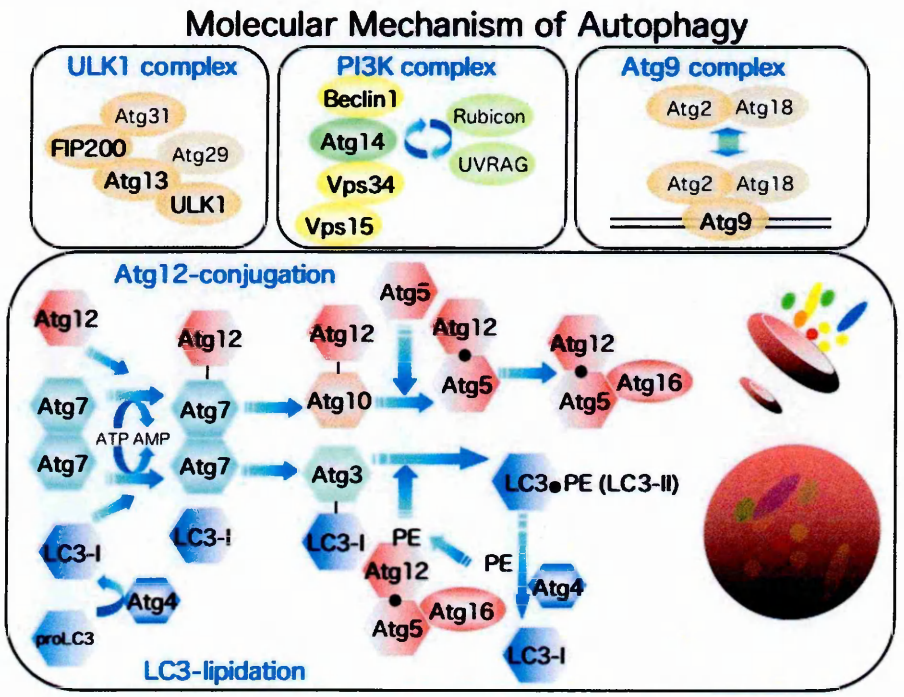

Figure 10. ATG proteins take part in the induction and formation of new autophagosome membranes.

In the initial steps of autophagy we find numerous proteins including:

- Atg1-Atg13-Atg17, a serine/threonine kinase complex (ULK1 complex) that responds to upstream signals (i.e. mTOR)

- Atg6-Atg14-Vps34-Vps15, a lipid kinase- signaling complex (PI3K complex) that mediates vesicle nucleation. Beclin-1 is the mammalian orthologue of the yeast *Atg6* gene and when over-expressed, it can induce autophagy. Moreover, Beclin-1 can bind to Bcl-2, an important regulator of apoptosis, leading to the inhibition of autophagosome formation (reviewed in 32).

2) *Formation of the autophagosome*

After induction, a double-membrane vesicle begins to form in the cytosol. The origins of this membrane is still unknown but for mammalian cells it is generally thought to be the ER (33) and/or mitochondria (34), despite a recent study has demonstrated the involvement of plasma membrane (35). LC3, a mammalian homologue of yeast Agp8p, is widely used as a marker for tracking autophagosomes (36). There are two forms of LC3: the cytosolic LC3-I and the membrane bound LC3-II. During autophagy, LC3-I gets lipidated and converted to

LC3-II, which is found specifically on autophagosomes. Therefore, the amount of LC3-II is correlated with the extent of autophagosome formation.

3) *Autophagosome docking and fusion*

Once autophagosomes have sequestered their cargo, this is delivered to lysosomes. Specific proteins on both autophagosome and lysosome membranes are required for the proper docking and/or fusion. These proteins are called SNARE (Soluble NSF Attachment Protein REceptors) and are a large superfamily of more than 60 members that mediate vesicle fusion. Besides SNARE proteins, fusion also depends on microtubule and maintenance of proper acidification of vesicles (reviewed in 30).

4) *Autophagic body breakdown*

Fusion with lysosomes causes the release of the single-membrane bound inner vesicle of the autophagosome (called autophagic body) into the vacuole lumen while the outer membrane is incorporated into the limiting membrane of the receptor vesicle. Once inside the lumen, cargo is broken down by the activity of acidic hydrolases.

Autophagy has many physiological functions in mammalian cells (resumed in figure 11 from 32). Among the main functions of this pathway we highlight its pivotal role in:

- *Stress response*. Production of energy and nutrients during stress conditions (i.e. starvation).
- *Quality control*. Turnover of organelles and aggregate-prone proteins.
- *Innate and adaptive immunity*. Delivery of cytosolic proteins for MHC class II presentation.
- *Cell death*. Clearance of apoptotic cells during embryonic development in mice and cross- talk between Atg proteins and apoptotic factors.
- *Aging and longevity*. Increased autophagic turnover of cytoplasmic constituents contributes to longer life.

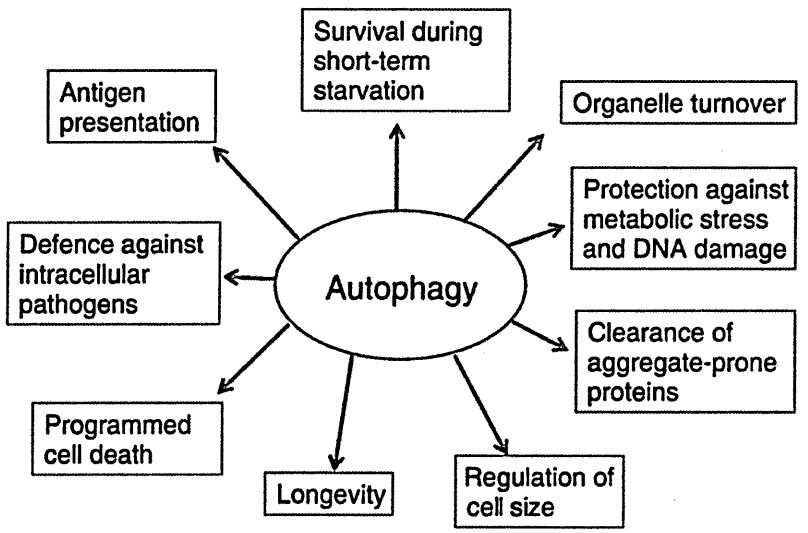

Figure 11. A summary of the functions of autophagy.

Maintenance of proper activity of this pathway is essential to guarantee cell survival. When autophagy is impaired (i.e. mutations in *ATG* genes or reduction/increasement of the autophagic flux), cell homeostasis is altered and this imbalance can lead to a pathogenic state and subsequently to cell death.

4.1. Mitophagy as a selective form of autophagy

Among the principal functions of mitochondria we find: 1) energy production by oxidative phosphorilation, 2) calcium signaling, 3) regulation of cellular metabolism and proliferation, and 4) apoptosis-programmed cell death. Mitochondrial life cycle consists of a series of fusion and fission events that allows the maintenance of a healthy population of mitochondria (figure 12). Mediators of fusion and fission were first described in *D. melanogaster* (37). In mammals, mitochondrial fusion involves multiple steps, including mitochondrial tethering and fusion of OMMs, docking and fusion of IMMs and mixing of intramitochondrial components. The fusion machinery is composed by mitofusins MFN1/2, located on the OMM (38), which form *trans* complexes on adjacent mitochondria during fusion processes; and OPA-1, which controls IMMs fusion (39). On the other side, fission processes are driven by the OMM protein Fis1 and the cytosolic protein DLP1, which is recruited to mitochondrial surfaces and associates with Fis 1 (40, 41).

Twig et al (42) have demonstrated that fusion triggers fission and that fission is essential for autophagy. Fission events can produce metabolically different daughter units; one with high membrane potential ($\Delta\psi m$) and the other with low $\Delta\psi m$. Whereas mitochondria with high $\Delta\psi m$ can re-enter the cycle by fusing with the mitochondrial network, the one with low $\Delta\psi m$ is less likely to re-fuse and is targeted by autophagy. This means that fusion is a selective process that depends on the metabolic state of the organelle and that fission targets depolarized mitochondria for digestion and elimination.

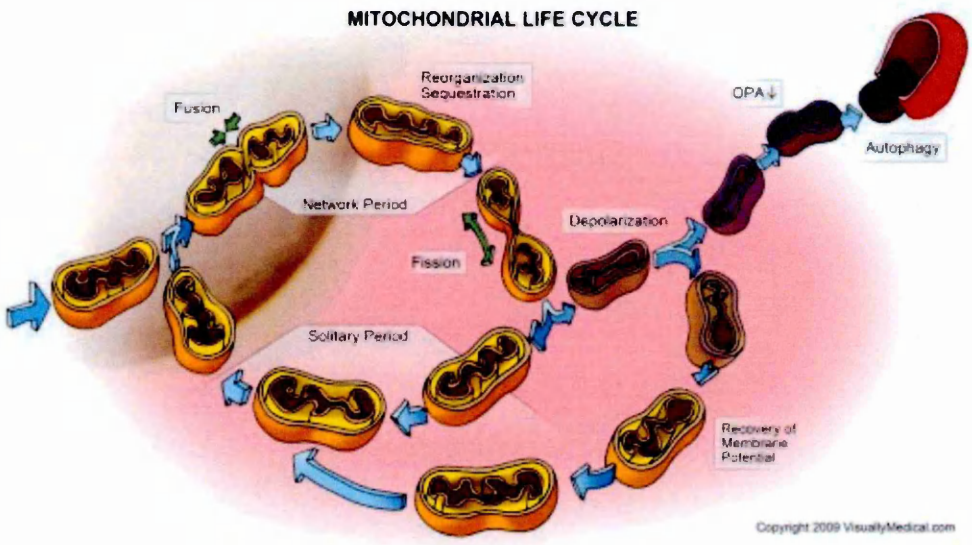

Figure 12. Scheme of the different steps of mitochondria life cycle.

How are depolarized mitochondria recognized by the autophagic machinery? Although long assumed to be a random process, increasing evidence indicates that mitochondrial autophagy (also called mitophagy) is a selective process. This idea gave raise as a result of a study carried out by Kissova et al (43), who identified an outer membrane protein, Uth1p, as an essential protein for efficient mitophagy in yeast. Recently, two independent studies have described the existence of a specific receptor for autophagy on the mitochondrial surface of yeast (44, 45). However, a mammalian homologue for this receptor, known as Atg32, has not been found yet. Interestingly, it seems that selective recognition of damaged mammalian mitochondria depends on the PINK1-dependent recruitment of Parkin. Many studies have addressed this issue in the last two years (46-49). PINK1 (PTEN-induced putative kinase 1) is a putative serine/threonine kinase with a

mitochondrial targeting sequence that recognizes depolarized mitochondria and promotes the translocation of cytosolic parkin onto the mitochondrial surface. The fact that PINK1 and parkin act in a common genetic pathway was demonstrated in *Drosophila PINK1* mutants, which shared marked similarities with parkin mutants. Moreover, parkin could compensate for the PINK1 loss-of-function phenotype but not viceversa (50).

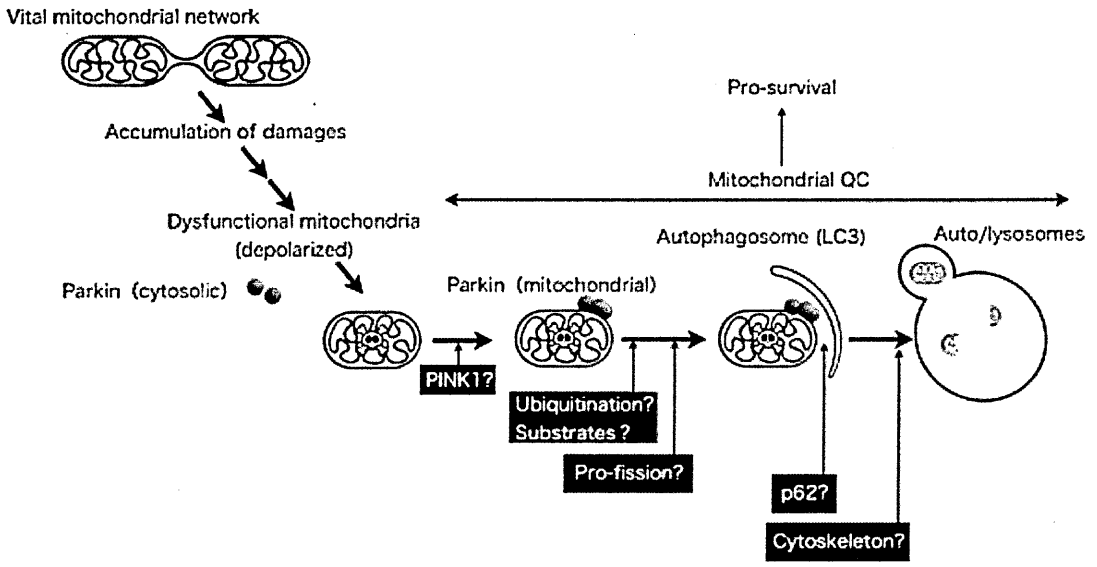

Figure 13. PINK1-dependent Parkin recruitment of mitochondria for autophagic degradation (from ref.51)

Among the principal substrates of parkin, an E3 ubiquitin ligase, VDAC1 and mitofusins have been pointed out as the main candidates. Poly-ubiquitin-positive clusters of mitochondria are then recognized by the autophagic adaptor p62/SQSTM1 and directly targeted to autophagosomes for degradation (figure 13).

Mutations in the parkin gene (*PARK2*) and PINK1 (*PARK6*) are associated with autosomal recessive inheritance of Parkinson's disease (PD). Parkin loss-of-function *Drosophila* exhibit increased sensitivity to ROS, dopaminergic cell loss and swollen mitochondria with fragmented cristae (52). Thus, dysfunctional parkin, or its non-recruitment, prevents proper targeting of irreparably damaged mitochondria for mitophagy, leading to a buildup of toxic, dysfunctional mitochondria, ultimately leading to death. Alterations in mitochondrial function have also been described in Alzheimer's disease and Huntington's disease (53) suggesting the involvement of mitochondria dynamics in the pathogenesis of these neurodegenerative disorders.

4.2. Autophagy impairment in Lysosomal Storage Disorders

Autophagy has become a growing research field in the past years. This process has been studied in many diseases such as neurodegenerative disorders, inflammatory diseases and cancer (reviewed in 54). However, the reason behind autophagic failure can be very diverse because of the different steps required for autophagy and the molecular players involved in each of them. Understanding the step(s) affected in each disorder could explain differences in the course of these pathologies and will be essential to develop targeted therapeutic approaches for each disease based on modulation of autophagy. Among the possible defects that could be behind macroautophagy we can find: 1) reduced autophagy induction; 2) enhanced autophagy repression; 3) altered cargo recognition; 4) inefficient autophagosome/lysosome fusion, and 5) inefficient degradation of the autophagic cargo (figure 14 from ref.55).

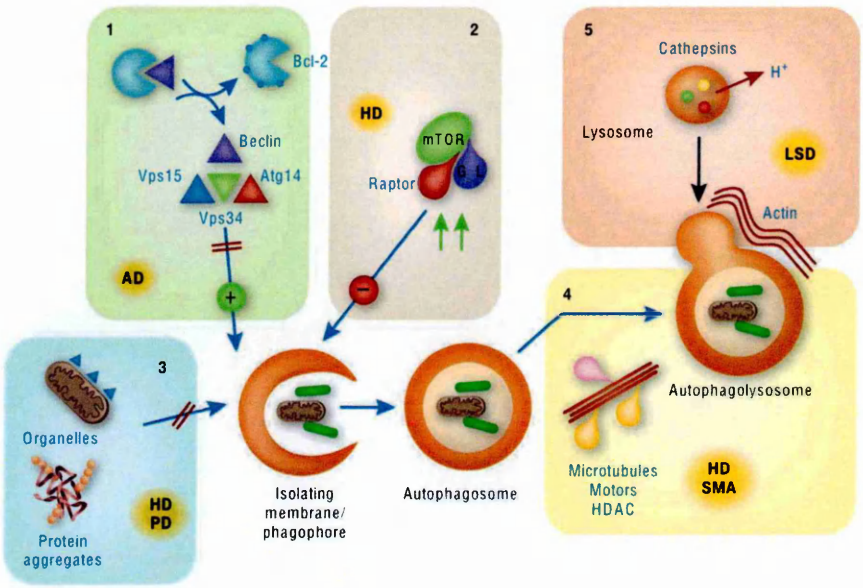

Figure 14. Possible alterations in macroautophagy under pathological conditions.

As lysosomes are the final destination for autophagic cargo, autophagy has become an attractive target for new studies in LSDs. This pathway had already been studied in some neurodegenerative disorders such as Alzheimer's, Parkinson's and Huntington's (55). Although the etiology of LSD is different, the similarities shared with these disorders have given rise to a new line of research. To date, autophagy has been studied in Mucopolysaccharidosis type IIIA (MPS IIIA) (56), GM_1-Gangliosidosis (57), Niemann-Pick Disease type C (NPC) (58), Neuronal Ceroid Lipofuscinosis (NCL) (59), Mucolipidosis type IV (60), Danon Disease (61) and Multiple Sulfatase Deficiency (56). In all disorders, an increase in the number of autophagosomes has been described (reviewed in 62). However, whereas in some cases the accumulation of autophagic vesicles was due to a block in autophagosome maturation (i.e. NCL), in other cases it was a consequence of autophagy induction

(i.e. NPC). Nevertheless, despite numerous studies in LSDs animal models, the precise mechanism leading to malfunction of the autophagic pathway remains still elusive.

Autophagy impairment in Multiple Sulfatase deficiency

In a study carried out in 2008 and published on *Human Molecular Genetics* we speculated an impairment of the autophagic pathway in two different mouse models of LSDs: Multiple Sulfatase Deficiency (MSD) and Mucopolysaccharidosis type IIIA (MPS IIIA) (56). Using different approaches we showed the accumulation of autophagosomes in MSD tissue (brain) and cells (embryonic fibroblast and liver macrophages). We postulated that this abnormal accumulation of vesicles was due to defective clearance caused by impaired autophagosome-lysosome fusion. The results obtained supported our hypothesis:

1) Reduced co-localization of LAMP1 (lysosomal marker) and LC3-II (autophagic marker) in MSD MEFs.

2) MSD MEFs had increased levels of autophagy substrates like mutant proteins (α- synuclein and huntingtin) overexpressed.

3) Chemical induction of autophagy by rapamycin increased LC3-II levels in both control and MSD MEFs.

4) Treatment of MSD MEFs with Bafilomycin A1 (an inhibitor of autophagosome-lysosome fusion), alone or in combination with rapamycin; equally increased the number of autophagosomes (63).

5) Accumulation of endogenous autophagic substrates (poly-ubiquitinated proteins, p62/SQSTM1 aggregates and mitochondria) in MSD brain (figure 15).

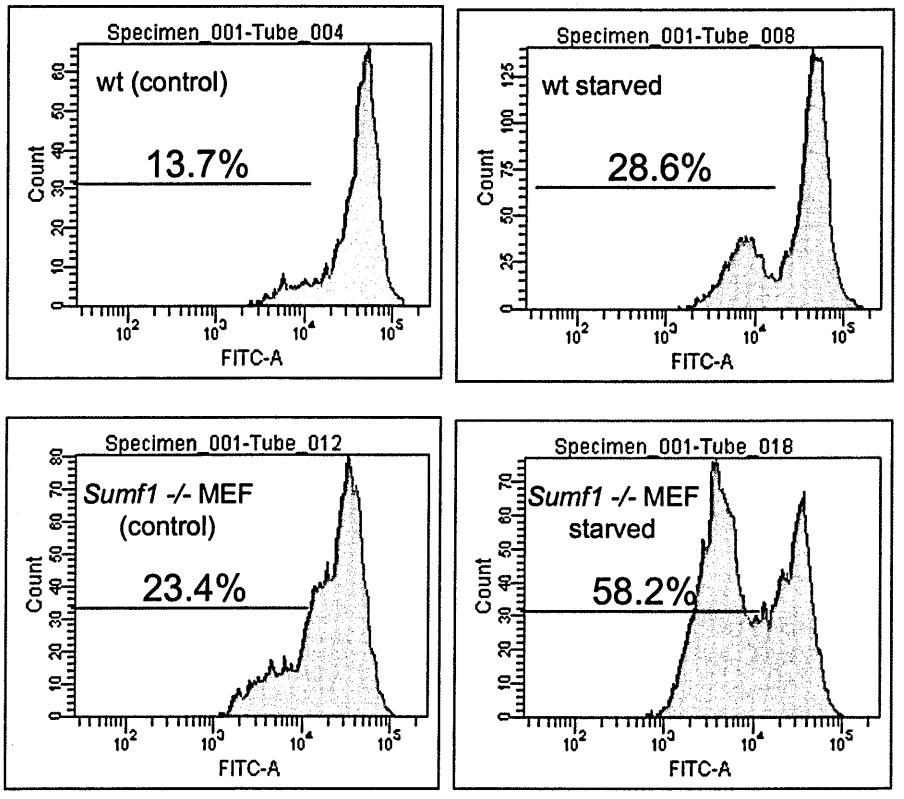

Figure 15. Mitochondrial membrane potential in MSD MEFs. Control and MSD MEFs were grown in either normal serum or starved conditions (4 h). Cells were then stained with 40 nM DiOC6 and 1 mg/ml propidium iodine. $\Delta\psi m$ was measured by flow cytometry. Propidium iodine was used as counterstain. All experiments were performed in triplicate and analyzed using Stat-View software and ANOVA test. Results were considered significant if $P < 0.05$.

According to these results, lysosomal accumulation of undegraded material results in defective fusion between autophagosomes and lysosomes and causes a block of the autophagic pathway. Our data suggest that LSDs may share common mechanisms with other neurodegenerative disorders (i.e. Alzheimer's, Parkinson's and Huntington's) raising the possibility of overlapping therapeutic strategies.

A study recently published by our group (64) further confirms the block of autophagy in LSDs and demonstrates that this impairment is caused by dysfunction of SNARE proteins involved in the autophagosome/lysosome fusion machinery.

4.3. Mitochondrial aberrations in LSDs

Mitochondrial aberrations have already been described in some LSDs. In GM1-gangliosidosis, measurement of cytochrome *c* oxidase activity in brains from *β*-gal-/- mice revealed decreasing mitochondria functionality, which was parallel to disease progression. Primary astrocytes obtained from these mice showed abnormally small fragmented mitochondria with reduced membrane potential (57). Cultured skin fibroblasts from MLIV patients have been used to investigate the mitochondrial-autophagosomal axis in mucolipidoses. In these cells, mitochondria appeared fragmented and had reduced buffering capacity (60). Similar results were obtained in MLII, MLIII and NCL2 fibroblasts (65).

All these studies suggest that the presence of dysfunctional mitochondria may be due to defects in the autophagic pathway as the modulation of this pathway can rescue the mitochondrial phenotype.

However, most of these data describe the accumulation of mitochondria as a merely consequence of autophagy impairment. A detailed study on mitochondrial autophagy in LSDs would allow us to see whether mitochondrial priming/engulfment is altered in these types of disorders. Currently, it is unclear whether mitochondria are eventually degraded or if mitophagy fails to efficiently eliminate mitochondria.

AIM OF THE THESIS

1) To elucidate whether the accumulation of dysfunctional mitochondria is a consequence of impaired mitochondrial targeting to autophagosomes and, in turn, whether this impairment is due to defects in the mitophagic machinery.

2) To establish the role of dysfunctional mitochondria in MSD pathology.

MATERIALS & METHODS

1. *Sumf1-/-* mice genotyping

1.1. Genomic DNA extraction

Tails were cut off from mice around P20 and lysed in 500µl lysis buffer (50mM TrisHCl pH 8, 100mM EDTA, 100mM NaCl, SDS 1%,) supplemented with 20 µl proteinase K (20mg/ml) at 55°C O/N. After removal of cellular debris (5 minutes centrifugation at maximum speed), DNA was precipitated by adding 1 ml of 100% ethanol (EtOH) to each tube and gently mixed by inverting the tubes. Subsequently, DNA was washed once with 70% EtOH, air-dried and resuspended in 500 µl H_2O.

1.2. PCR Amplification

We genotyped the mice by PCR on tail DNAs using β-gal-specific primers coupled with *Sumf1*- specific primers (figure 16):

Int3rev 5'- AGA AAC CAC CTC ACC AAA GCA GAG- 3'

Int3for 5'- TTT GTG CCT TTA CTG CCC TCT TGG-3',

βgeorev 5'-CAA AGT CAG GGT CAC AAG GTT CAT-3'.

PCR conditions using the Takara LA Taq mixture (Takara Bio Inc., Japan):

1) 95 °C 2 min;

2) 95 °C 30 sec/68 °C 30 sec/68 °C 1 min for 30 cycles;

3) 72 °C 10 min.

Resolution in a 1.5% agarose gel: 1153 bp band (*Sumf1+/+*), 800 bp band (*Sumf1-/-*) or both (*Sumf1+/-*).

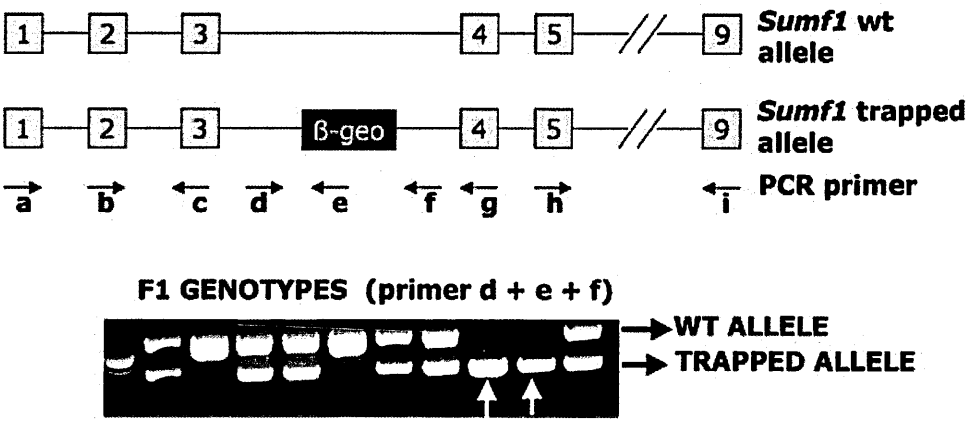

Figure 16. Gene trapping insertion site within the *SUMF1* gene. Genomic PCR analysis of DNAs from *Sumf1+/+, Sumf1+/-* and *Sumf1-/-* littermates demonstrates that the insertion site is in intron 3 of the Sumf1 gene

2. Generation of immortalized MEFs (Mouse Embryonic Fibroblasts)

MEFs were isolated by trypsinization of littermate embryos collected at E14.5 and grown in DMEM supplemented with 20% FBS and 1% penicillin/streptomycin. Immortalization was performed by transfection of the pMSSVLT plasmid containing

the *SV40* gene. Selection of immortalized clones by neomycin treatment was carried out for 3 weeks and the immortalized cells were maintained in DMEM supplemented with 10% FBS and antibiotics.

3. Immunoblotting of total lysates

3.1.Total protein extraction of tissue samples

Mice were anesthetized with avertin (20µl/g weight) and then perfused with PBS. Brain and liver samples were collected and homogenized in ice-cold lysis buffer (50mM TrisHCl pH 7.4, 150mM NaCl, 1mM EDTA, 1% Triton X-100, 0.1% SDS, 0.5% Na deoxycholate) in presence of protease inhibitors (Sigma-Aldrich, MO, USA). Mechanical disruption of samples was perfomed using the TissueLyser equipment (Qiagen, Netherlands). Homogenates were incubated on ice for 30 minutes and then centrifugated at maximum speed to eliminate cellular debris. Proteins were quantified by the Bradford method (Bio-Rad, CA, USA) and stored at -80°C.

3.2. SDS-PAGE electrophoresis

Mini-protean SDS-PAGE gels were prepared according to protocol. Proteins (10-50µg) were prepared in sample buffer 4x containing β-mercaptoethanol, boiled for 5 minutes and loaded. Pre-stained protein marker (175-7KDa) was from New England Biosciencies (MA, USA). Electrophoresis was run at 80V for almost 3 hours at RT. Proteins on SDS-PAGE gels were transferred to PVDF membranes (Millipore, MA, USA) at 30V O/N 4°C. The day after, membranes were blocked in TBS/Tween

5% milk for 1 hour at RT followed by incubation with primary antibody (1-2 hours). Filters were washed 3 times in TBS/Tween and incubated with secondary HRP-conjugated antibody (GE healthcare, WI, USA). Detection was performed using the enhanced chemioluminescence (ECL) from Pierce (Thermo Scientific, MA, USA).

Primary antibodies used on tissue total lysates were: rabbit anti-COXIV 1:1,000 (#4844 Cell Signaling Technology Inc., MA, USA), rabbit anti-LC3 1:1,000 (NB100-2331, Novus biologicals, CO, USA), mouse anti-Parkin 1:1,000 (#4211, Cell Signaling Technology, MA, USA), rabbit anti-BECN1 1:1,000 (sc-11427, Santa Cruz biotech., CA, USA), mouse anti-OPA-1 1:1,000 (612607, BD Biosciences, NJ, USA), mouse anti-DLP1 1:1,000 (611112, BD Biosciences, NJ, USA) and mouse anti-β-actin 1:10,000(A1978, Sigma-Aldrich, MO, USA).

4. Immunoblotting of subcellular fractions

4.1. Subcellular fractioning

Brain and liver samples were collected from PBS-perfused mice. Tissue was weighted and homogenized in 10 volumes of ice-cold hypotonic buffer (300mM sucrose, 10mM HEPES pH 7.4, 0.2mM EDTA) in presence of protease inhibitors (Sigma-Aldrich, MO, USA). Samples were mechanically disrupted with micropestles (Eppendorf, Germany) and then passed through a 20G- and a 26G-needle for several times. The same amount of protein (1 mg) was processed in an equal volume of buffer for all samples. The supernatant of the first centrifugation (5 minutes, 600 g) was further centrifugated at 16,000 g for 15 minutes. Supernatants

were conserved as the cytosolic fraction. Pellets were washed in buffer and re-centrifugated. The resultant pellets (mitochondria) were resuspended in the same volume of lysis buffer (50mM TrisHCl pH 7.4, 150mM NaCl, 1mM EDTA, 1% Triton X-100, 0.1% SDS, 0.5% Na deoxycholate). Samples were quantified by the Bradford method (BioRad, CA, USA) and stored at -80°C.

4.2. SDS-PAGE electrophoresis

Sample preparation and electrophoresis run were performed as described in 3.2. For parkin immunoblotting, same amounts of protein were loaded (10-20μg). For cytochrome *c* and ubiquitin immunoblotting, same volumes of each subcellular fraction were loaded (10-20μl).

The antibodies used were: mouse anti- Cytochrom *c* 1:1,000 (Cat.556433 BD Pharmingen, NJ, USA), mouse anti-Parkin 1:1,000 (#4211, Cell Signaling Technology, MA, USA) and rabbit anti-Ubiquitin 1:500 (Z0458, Dako cytomation, CO, USA). Rabbit anti- COX IV 1:1,000 (#4844 Cell Signaling Technology Inc., MA, USA) and mouse anti- ATPase β subunit 1:10,000 (ab14730, Abcam, UK) were used as mitochondrial markers.

5. Electron Microscopy

5.1. Tissue processing

Tissue was fixed in 1% gluteraldehyde solution (in 0.2 M HEPES) and postfixed in OsO_4 and uranyl acetate. After dehydration in graded series of ethanol, tissue

samples were cleared in propylene oxide, embedded in Epoxy resin (Epon 812) and polymerized at 60°C for 24 h. From each sample, ultrathin sections (70 nm- thick) were cut with a Leica EM UC6 ultramicrotome. EM images were acquired using a FEI Tecnai-12 electron microscope equipped with an ULTRA VIEW CCD digital camera (FEI, Einhoven, The Netherlands). All these steps were performed by both Dr. Elena Polishchuk and Dr. Roman Polishchuk.

5.2. Analysis of mitochondrial morphology

Quantification of the mitochondrial dimensions (diameter) was performed using the AnalySIS software (Soft Imaging Systems GmbH, Munster, Germany). The morphological analysis was performed by Dr. Elena Polishchuk.

5.3. Analysis of autophagosome content

EM images were qualitatively analyzed and autophagosomes were classified as "empty" (electron-clear vesicles) or "filled" (electron-dense vesicles).

6. Real-time PCR

6.1. RNA extraction and retrotranscription (RT-PCR)

Total RNA was extracted from tissue using the RNeasy® kit (QIAgen, Netherlands): homogenization of samples was performed mechanically using the TissueLyser equipment and processed according to manufacturer's manual. RNA

samples were quantified using a NanoDrop 8000 spectophotometer (Thermo Scientific, MA, USA) and 1 μg of each sample was retrotranscribed with the QuantiTect® Reverse Transcription kit (Qiagen, Netherlands).

6.2. cDNA amplification

Amplification of cDNA was performed using the SYBR Green I Master for LightCycler® 480 (Roche, Switzerland). Primer sequences were designed using the GenScript Primer Design tool (https://www.genscript.com/ssl-bin/app/primer):

- *PARK2*
  - forward 5'- GCA GCC ATA CCC TGC CGG TG-3'
  - reverse 5'- TGT GGC AGG GGC CTT TGC AG-3'
- *PGC1α*
  - forward 5'- CCC AGA GTC ACC AAA TGA CCC CA-3'
  - reverse 5'- TGA GGA GGA GTT GTG GGA GGA GT-3'

7. Analysis of mitochondrial functionality

7.1. Mitochondria isolation

Isolation of tissue mitochondria was performed using the Mitochondria Isolation kit protocol (MITOISO1, Sigma-Aldrich, MO, USA). Briefly, small amounts of tissue samples (75-150mg) were homogenized in Extraction Buffer A using

micropestles (Eppendorf, Germany) and 20G- and 26G- needles. After a series of centrifuges, the final pellet of mitochondria was resuspended in storage buffer (10mM HEPES pH 7.4, 250mM sucrose, 1mM ATP, 0.08 mM ADP, 5mM sodium succinate, 2mM K_2HPO_4, 1mM DTT) and proteins were quantified by the Bradford method (Bio-Rad, CA, USA). All functional assays were performed by 4 hours after mitochondria isolation.

7.2. Analysis of mitochondrial membrane integrity

Mitochondria (10μg) obtained from MSD and control mice (n=3) were incubated with the JC-1 working solution (Sigma-Aldrich, MO, USA) for 7 minutes. Subsequently, fluorescence (excitation: 485, emission: 590) was measured in a Fluoroskan Ascent FL fluorometer (Thermo Scientific, MA, USA).

7.3. Analysis of mitochondrial ATP content

Mitochondria obtained from MSD and control mice (n=3) were resuspended in an ATP-free storage buffer. ATP was measured using the ATP determination kit (Invitrogen, CA, USA). The assay is based on luciferase's requirement for ATP in producing light from the reaction:

$$\text{Luciferin} + \text{ATP} + O_2 \rightarrow \text{oxyluciferin} + \text{AMP} + \text{pyrophosphatase} + CO_2 + \text{light}$$

Luciferase was added to mitochondria samples (5-10μl) and luminescence was measured in a GloMax 96-well luminometer (Promega, WI, USA). Results were normalized by the amount of mitochondrial protein.

8. Detection of apoptotic cells

Paraffin-embedded tissues were sectioned (7 µM) in a Leica RM165 microtome (Germany) and fixed (PFA 4%). Apoptotic nuclei were detected using the *In Situ* cell death detection kit (Roche, Switzerland). Images were acquired in a Zeiss Axioimager A.1 fluorescence microscope (Carl Zeiss, Germany).

9. Analysis of mitochondrial morphology and dynamics in MEFs

9.1. Plasmids transfection

All plasmids transfections were performed using the Lipofectamine 2000 reagent (Invitrogen, CA, USA). Four hours after transfection, medium was replaced with a growth medium containing antibiotics.

The plasmids used in our experiments were: GFP-LC3 (52), GFP-myc-Parkin and DsREDmito, which are a kindly gift of Prof. Wolfdieter Springer (University of Tübingen) and Prof. Luca Scorrano (University of Geneva) respectively.

9.2. Analysis of mitochondrial morphology

In vitro morphological analysis of mitochondria was performed by transfection of the DsREDmito plasmid into MSD and control iMEFs. Cells from four independent experiments were analyzed (≈ 185 cells/experiment) and classified following a pre-established criteria of mitochondria size/shape.

9.3. Analysis of mitochondrial dynamics

Plasmids couples GFP-LC3/DsREDmito and GFP-Parkin/DsREDmito were co-expressed in MEFs. 24 hours after transfection, cells were treated with 20μM CCCP (Sigma-Aldrich, MO, USA) for 20 hours. Cells were fixed in PFA 4% and mounted in vectashield + DAPI (Vector laboratories, CA, USA).

Images were acquired in a Zeiss LM 710 confocal microscope (Germany) with a 63x/1.4 Oil DIC Plan Apo lens. Laser lines at 488 nm (GFP) and 561 nm (DsRED) were used.

10. Data Analysis

10.1. Immunoblotting quantification

Quantification of immunoblotting bands was performed using the Image J software. For all experiments, data from four control and four MSD mice were processed and the average was expressed as the fold-change respect to control.

10.2. Statistics

Data were analyzed by Student's *t* distribution. A p-value < 0.05 was considered statistically significant.

1. Morphologically- altered mitochondria accumulate in a tissue-specific and time-dependent manner in MSD

In order to evaluate the pattern of mitochondrial accumulation, we determined the content of mitochondria in two of the most affected tissues of MSD mice: brain and liver. For this purpose we used COX IV, a component of the mitochondrial electron transport chain, which has been widely used as a marker for quantifying the number of mitochondria (56). Levels of COX IV were determined by western blot analysis on brain and liver total homogenates obtained from MSD (n=4) and control mice (n=4) at four different ages (P15, 1-, 2- and 3 months) (figure 17). In MSD brain, levels of COX IV were comparable to control mice (P15, 0.85 ± 0.04; 1 month, 0.80 ± 0.07; 2 months, 1.02 ± 0.02; 3 months, 1.01 ± 0.023) thus indicating that mitochondrial content remained unaltered over time. The same amount of COX IV protein was observed in MSD liver at an early stage compared to control (P15, 0.87 ± 0.08; 1 month, 0.97 ± 0.01) whereas increased levels were detected at a late stage (2 months, 1.57 ± 0.04; 3 months, 1.32 ± 0.04; p-value< 0.01). Further analysis of *PGC1α* mRNA levels by qPCR, a master transcriptional co-activator that controls many genes involved in mitochondrial biogenesis, excluded the possibility that the accumulation observed in MSD was due to enhanced mitochondrial biogenesis (Brain 3 months, 0.7 ± 0.13; Liver 3 months, 0.91 ± 0.44), thus suggesting a defect in mitochondrial removal (figure 18).

Since abnormal accumulation of mitochondria can result in morphological changes, we then wondered whether mitochondria from MSD tissues were ultrastructurally altered. For this purpose, we measured the size (diameter) of

mitochondria in both cerebellum and liver ultra-thin sections of control (average number of mitochondria measured ≈ 53) and MSD mice (av. number of mitochondria measured ≈ 73) using the AnalySIS software (figure 19).

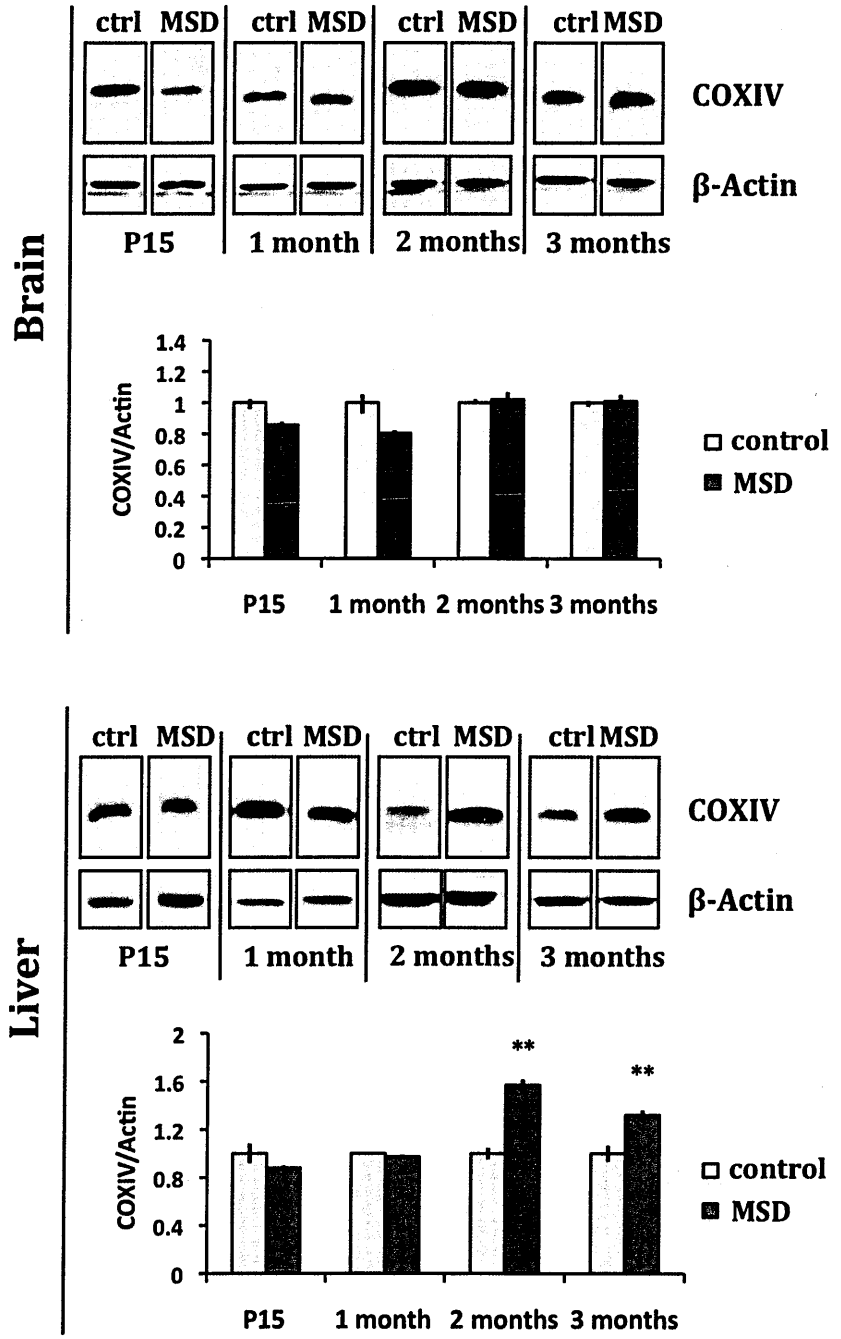

Figure 17. Accumulation of mitochondria in MSD tissues. . Levels of COX IV in brain and liver total lysates obtained from MSD (n=4) and control mice (n=4) at P15, 1-, 2- and 3 months. Here we show the most representative blot as obtained after quantification with Image J software. The COX IV/Actin ratio is expressed in terms of fold-change compared to control . ** p-value< 0.01

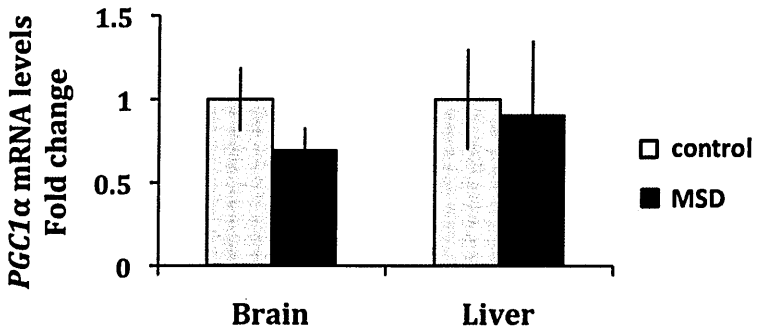

Figure 18. *PGC1α* mRNA levels in MSD tissues. Relative expression of *PGC1α* measured by quantitative PCR in both brain and liver extracts of MSD mice (n=3) at 3 months. . Results are represented in terms of fold-change compared to control.

Mitochondria of MSD cerebellum exhibited a similar morphology as their control littermates at an early stage (control, 498 ± 38; MSD, 503 ± 36) but significantly increased in size at 2 months (control, 625 ± 40; MSD, 929 ± 77). Surprinsingly, mitochondria appeared smaller (fragmented) at an advanced stage (control, 604 ± 43; MSD, 481 ± 18). Morphological analysis of liver samples showed that mitochondria of MSD mice (av. num. mitochondria measured ≅ 75) were larger (giant) compared to control mice (av. num. mitochondria measured ≅ 56) as soon as 15 days after birth (control, 994 ± 35; MSD, 1211 ± 30). Similar results were obtained at advanced ages (1 month; control, 840 ± 39; MSD, 1760 ± 131; 2 months; control, 712 ± 37; MSD, 1112 ± 84; 3 months; control 820 ± 34; MSD, 1277 ± 62).

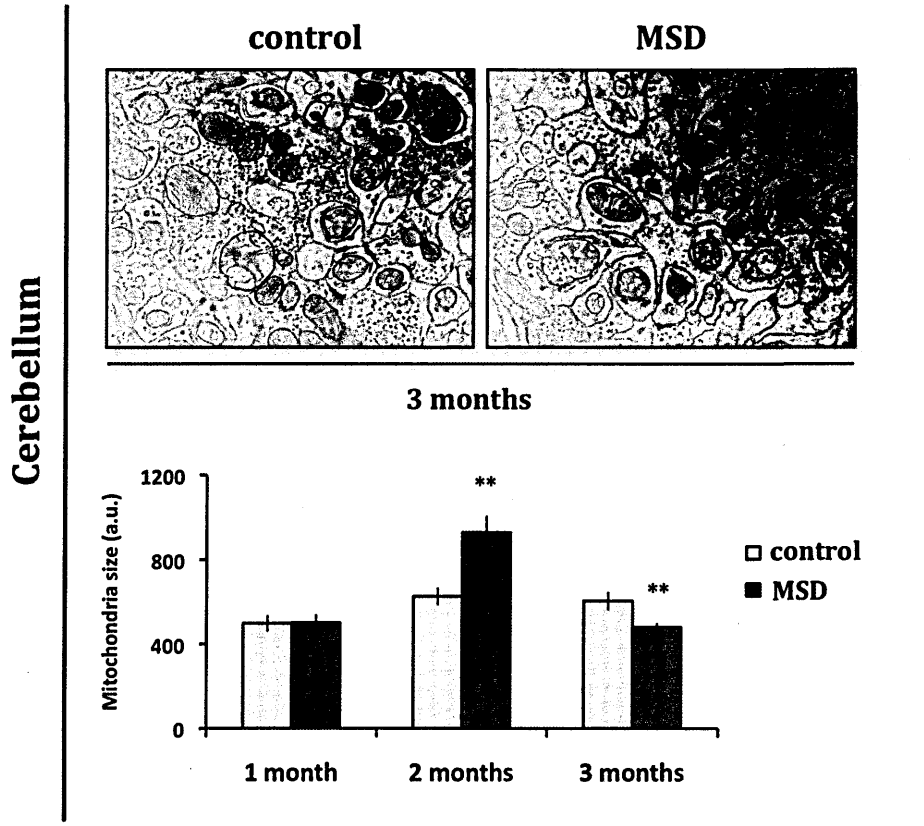
Cerebellum
control
MSD
3 months
Mitochondria size (a.u.)
1200
800
400
0
**
**
control
MSD
1 month
2 months
3 months

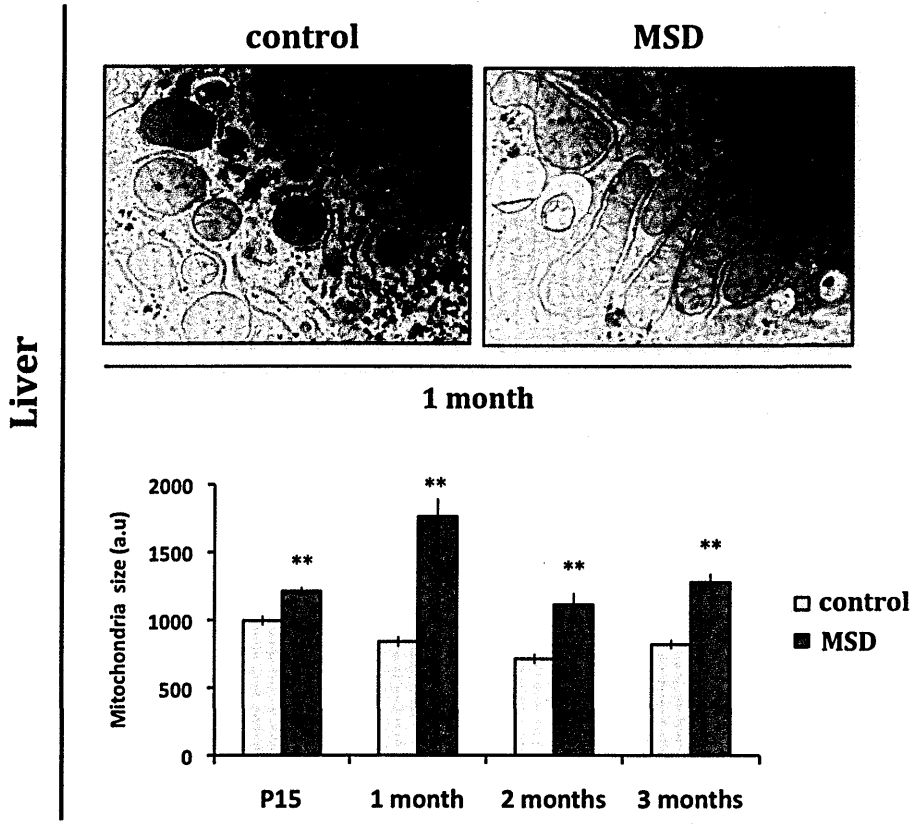
Liver
control
MSD
1 month
Mitochondria size (a.u)
2000
1500
1000
500
0
**
**
**
**
control
MSD
P15
1 month
2 months
3 months

Figure 19. Analysis of mitochondrial morphology in MSD tissues. Electron microscopy images from cerebellum and liver ultra-thin sections of MSD and control mice (*, mitochondria). Mitochondrial size (diameter) was measured using the AnalySIS software on EM images obtained from cerebellum and liver ultra-thin sections of MSD and control mice at different time points (P15, 1-, 2-, and 3 months). Measurements have been expressed in arbitrary units (a.u.). ** p-value< 0.01

The presence of giant mitochondria may be explained by: 1) Enhanced fusion, 2) defective fission and/or 3) impaired mitophagy. We therefore checked for the levels of both the fusion protein OPA-1 and the fission protein DLP1 in total brain and liver homogenates at 3 months.

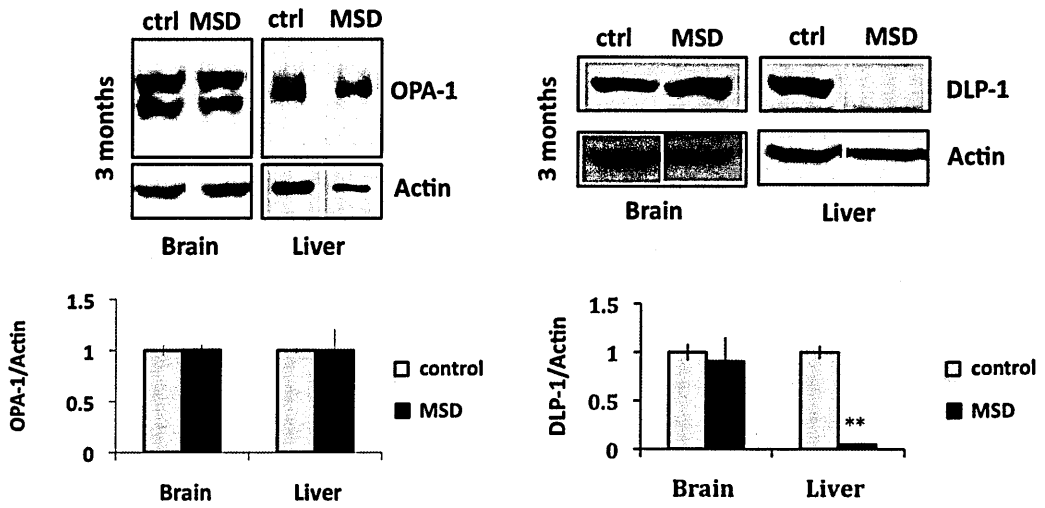

Figure 20. Fusion and fission protein levels in MSD tissues. OPA-1 (left) and DLP-1 (right) protein levels in total brain and liver homogenates obtained from MSD (n=3) and control mice (n=3) at 3 months. Here we show the most representative blot as obtained after quantification with Image J software. Both OPA-1/Actin and DLP-1/Actin ratio are expressed in terms of fold-change compared to control. ** p-value< 0.01

As shown in figure 20 (left), OPA-1 levels were similar to control in both brain (1 ± 0.05) and liver (0.99 ± 0.21) of MSD mice thus indicating no changes in

fusion rates. Similar results were obtained for the fission protein DLP-1 in MSD brain (right) (0.90 ± 0.24). On the contrary, DLP-1 levels were dramatically reduced in liver (0.05 ± 0.004, p-value< 0.01) when compared to control.

These data suggest that the morphology observed in liver mitochondria of MSD may be a consequence of impaired fission. Moreover, these mitochondrial alterations are tissue-specific and time-related features of MSD pathology since they are mostly observed in liver rather than brain.

2. Mitochondria accumulate outside autophagosome membranes

As previously described in *Chapter 4*, abnormal mitochondria are recycled by mitophagy through their targeting to autophagosomes. However, mitochondrial fission is an essential event for proper mitochondrial segregation (42). Defects in fission proteins, as observed in MSD liver, might result in impaired mitochondrial degradation. Therefore, we investigated whether mitochondria were properly sequestered inside autophagic vesicles. To this end, we analyzed the content of autophagosomes by electron microscopy (figure 21). Qualitative analysis of ultra-thin sections revealed the presence of autophagosomes with fuzzy content in both brain and liver of MSD mice. After a detailed analysis of AVs, the number of vesicles with no-recognizable structures, called "empty" autophagosomes (eAVs), represented out of 35% of the total number of vesicles screened in brain. Interestingly, this percentage remained constant over time: P15, 35.7%; 1 month, 34.9%; 2 months, 33.3%; 3 months, 35.3%. Otherwise, in MSD liver, the percentage

of eAVs increased over time (P 15, 17.7%; 1 month, 54.3%; 2 months, 47%; 3 months, 80%) thus suggesting a progressive impairment of autophagic cargo sequestration.

To confirm these observations, we transiently co-expressed GFP-LC3 and DsREDmito plasmids in MSD and control mouse embryonic fibroblasts (MEFs). As previously demonstrated by our group (56), MSD MEFs present a higher percentage of depolarized mitochondria in steady-state conditions. However, it is hardly difficult to detect a mitophagic event unless depolarization is not exacerbated by drug treatments. We then treated cells with CCCP (20μM, 20h), a mitochondrial-uncoupling agent that induces mitochondria depolarization and promotes their elimination by autophagy (figure 22). Upon CCCP treatment, mitochondria from both MSD and control cells appeared fragmented (round-shaped), indicating the loss of membrane potential. Under this condition, depolarized mitochondria were surrounded by autophagic membranes in control MEFs, as shown by co-localization of autophagy-mitochondria markers. On the contrary, only few mitochondria were engulfed by autophagosomes in MSD cells even if CCCP treatment was as efficient as in control cells. Moreover, as shown in figure 23, a detailed analysis of mitochondrial morphology indicated that MSD MEFs presented a higher population of intermediate-fragmented mitochondria in both untreated and CCCP- treated conditions compared to control.

Together these data indicate that mitochondria accumulate outside autophagosomes thus suggesting a defect in the mechanism responsible for mitochondrial targeting.

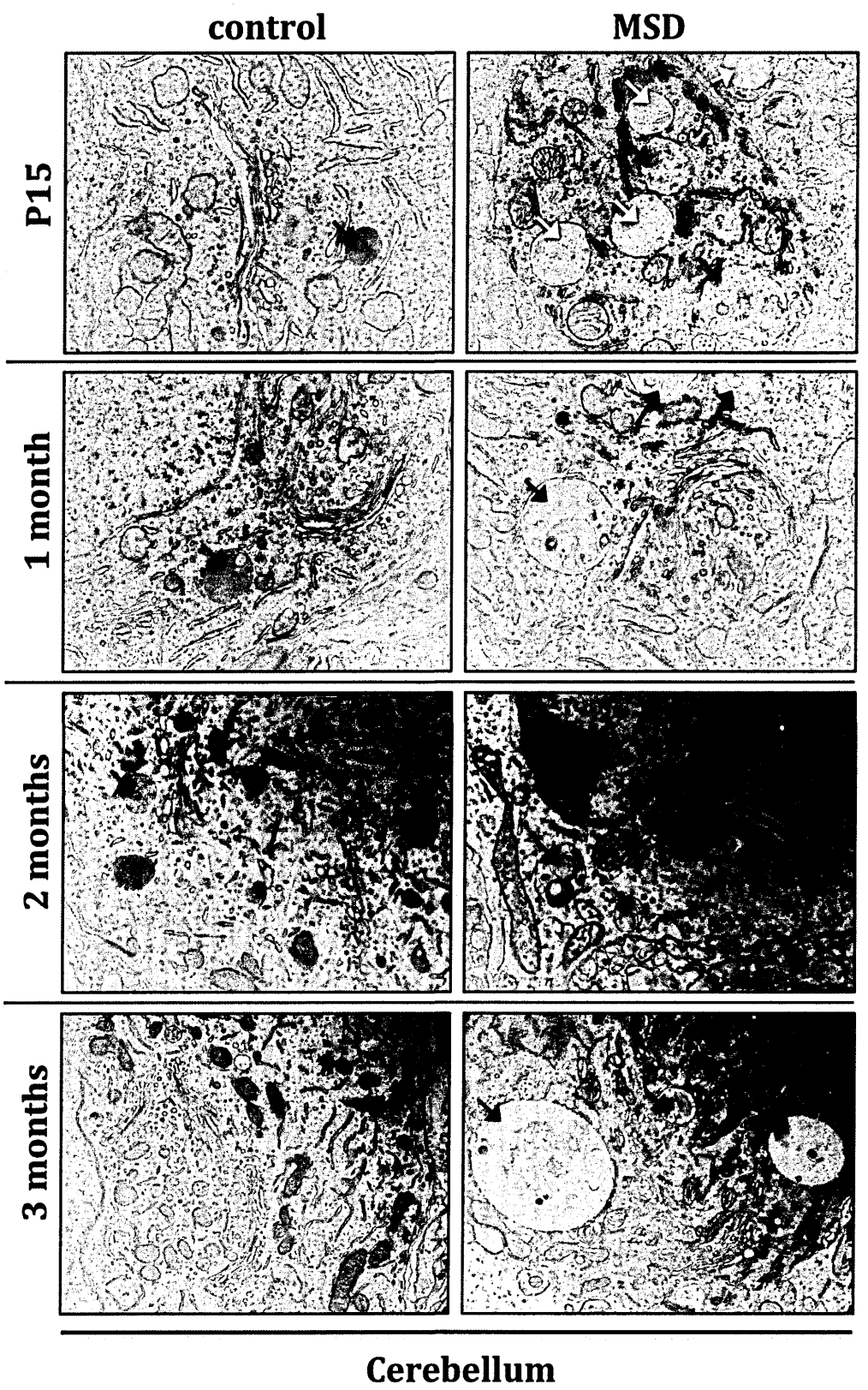

Figure 21.

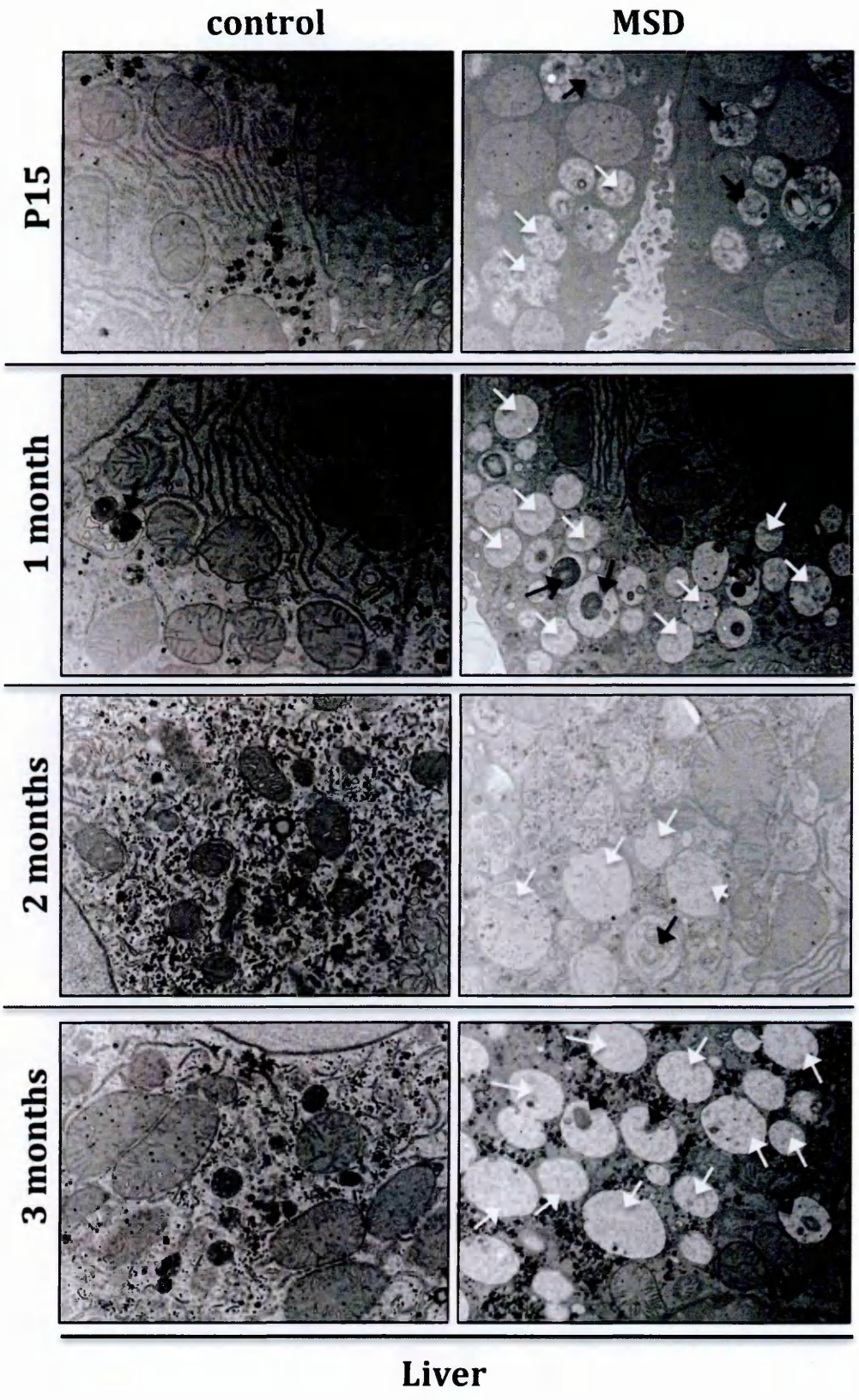

Figure 21 (cont.)

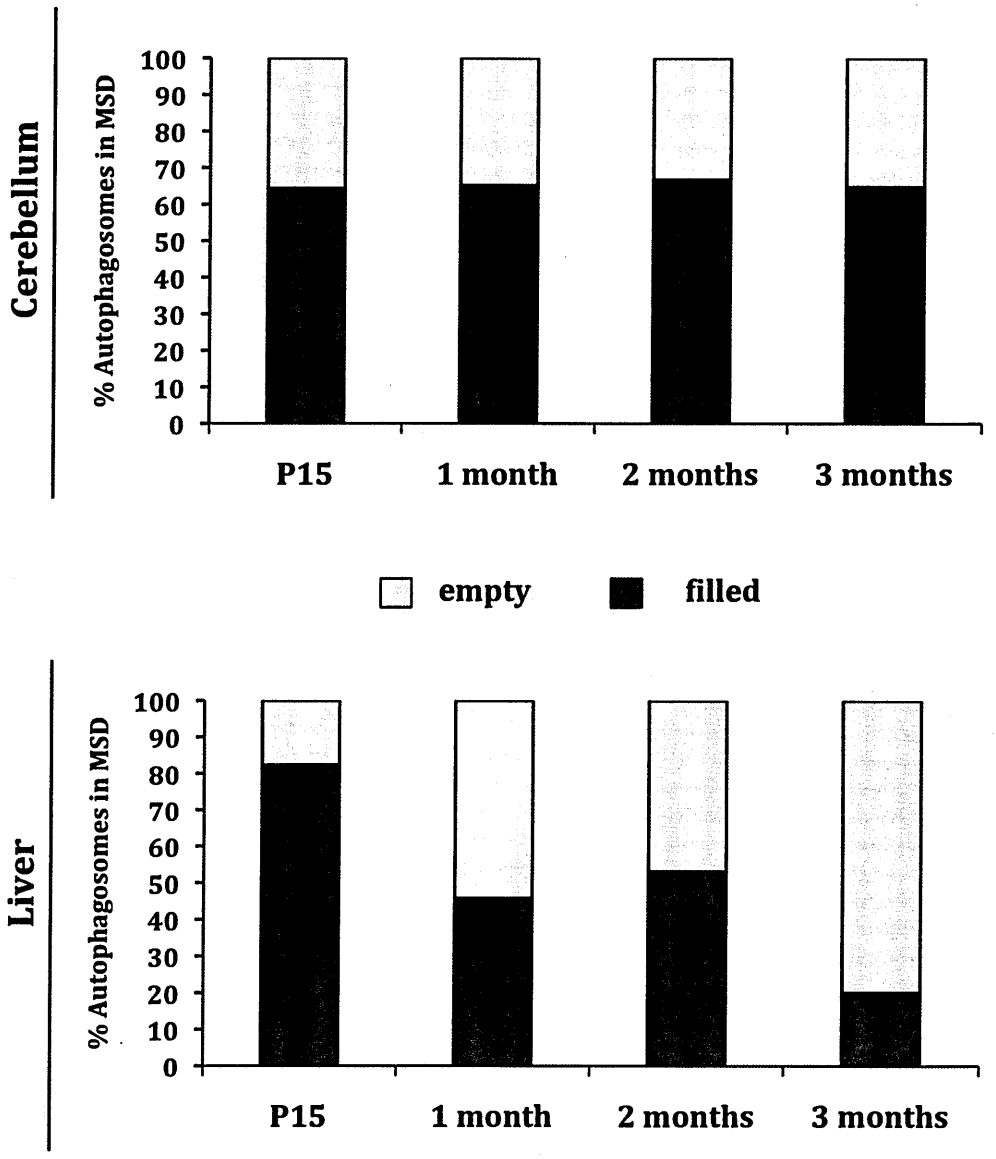

Figure 21. Analysis of autophagosomes content in MSD tissues. Electron microscopy analysis of autophagosomes of cerebellum and liver ultra-thin sections from MSD and control mice at 4 different time points (P15, 1-, 2-, and 3 months). Qualitatively, autophagosomes of MSD tissues have been classified into two categories: empty AVs (white arrows) and filled Avs (black arrows), based on the presence of clearly recognizable structures.

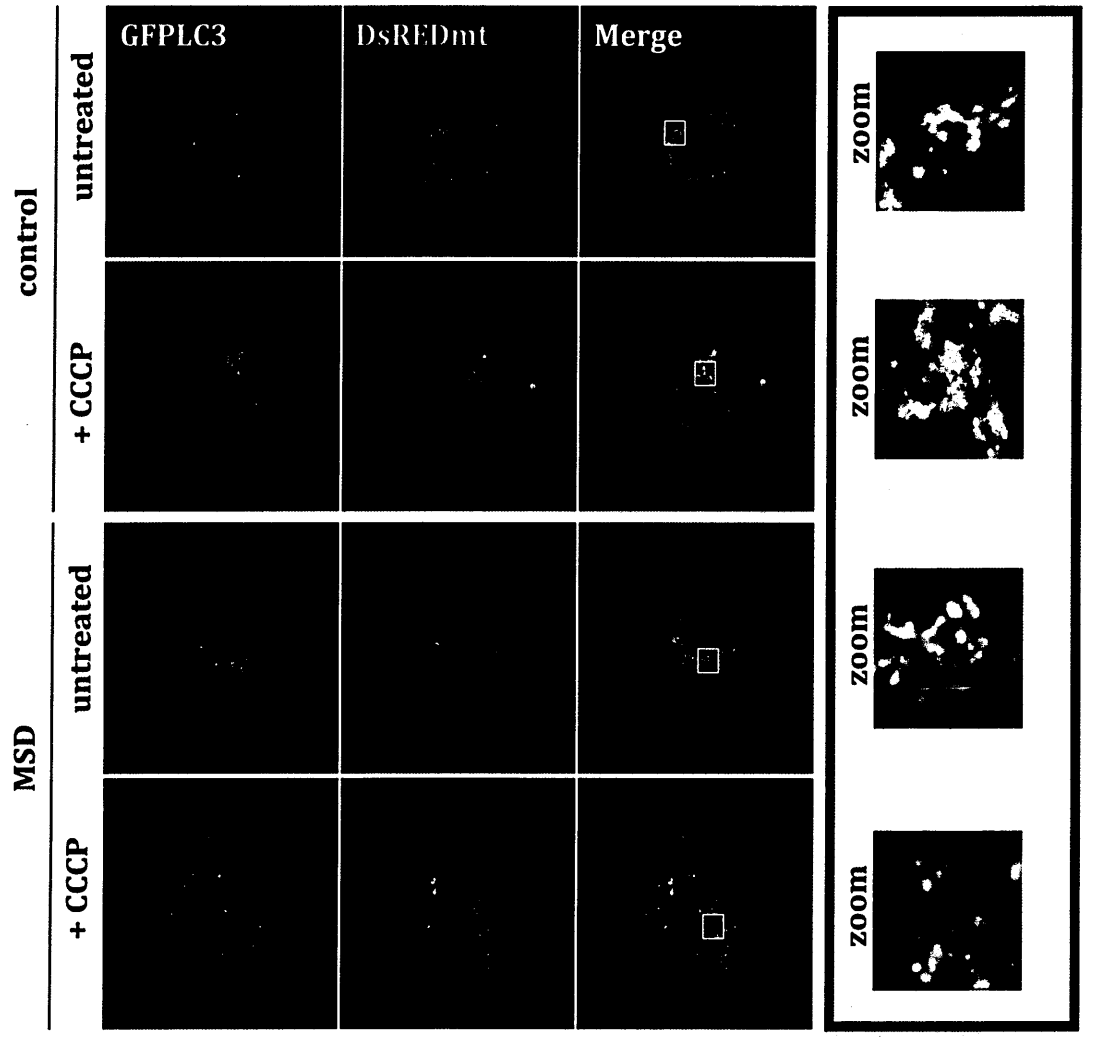

Figure 22. Depolarized mitochondria do not completely co-localize with the autophagic marker LC3 in MSD MEFs. Transient co-expression of GFP-LC3 (green) and DsREDmt (red) plasmids in MSD and control MEFs. 24-hours after transfection, cells were cultured in presence/absence of CCCP (20μM, 20h). Images were taken using a 63x/1.4 Oil DIC Plan Apo objective in a Zeiss LSM710 confocal microscope. Merge zoomed area is indicated with a white square.

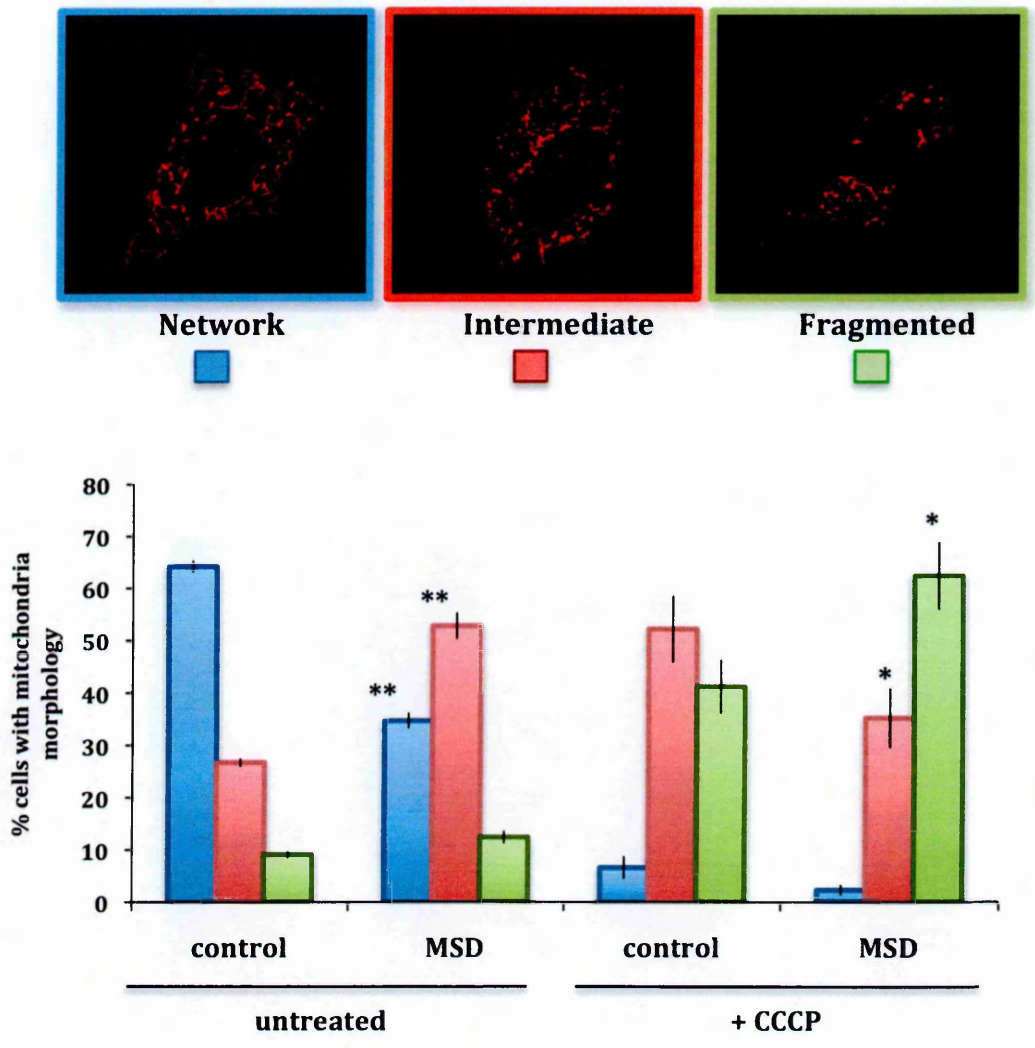

Figure 23. Mitochondrial morphology in MSD MEFs. Mitochondrial morphology has been classified following a pre-established criteria: "Network" for long interconnected mitochondria; "Fragmented" as for round-shaped mitochondria; and "Intermediate" for those cells with a half-and-a-half pattern. The graph represents the percentage of cells with a certain mitochondrial morphology in absence/presence of CCCP (20μM 6h). This value is an average value obtained from 4 independent experiments.

3. Impaired mitochondrial targeting is due to insufficient parkin-mediated mitochondrial ubiquitination

During mitochondrial priming, PINK1 recognizes depolarized mitochondria and recruits parkin to the OMM, where it exerts its E3 ubiquitin ligase activity. This step is crucial for proper mitochondrial recognition and degradation by autophagy. Therefore, we analyzed the efficiency of parkin-mediated ubiquitination in MSD tissues. To this end, we determined the total amount of ubiquitinated proteins in mitochondrial extracts obtained from both brain and liver of MSD and control mice (figure 24). . Analysis of the blots reveled equal amounts of ubiquitinated proteins in MSD brain mitochondrial fractions except for a slight increase at earl stages (1 month, 1.17 ± 0.015, p-value<0.05; 3 months, 0.97 ± 0.03). On the contrary, we observed lower levels of ubiquitinated proteins per mitochondrial number (ATPβase content) in MSD liver compared to control (1 month, 0.71 ± 0.04; 3 months, 0.70 ± 0.05, p-value> 0.05) thus suggesting an incomplete/partial ubiquitination of mitochondrial proteins that might probably result into inefficient cargo recognition.

Since OMM ubiquitination is carried out by parkin, we hypothesized that incomplete mitochondrial ubiquitination might be due to 1) inefficient translocation and/or 2) reduced levels of parkin. To address this issue, we evaluated the presence of parkin in tissue subcellular fractions obtained from both brain and liver of MSD and control mice.

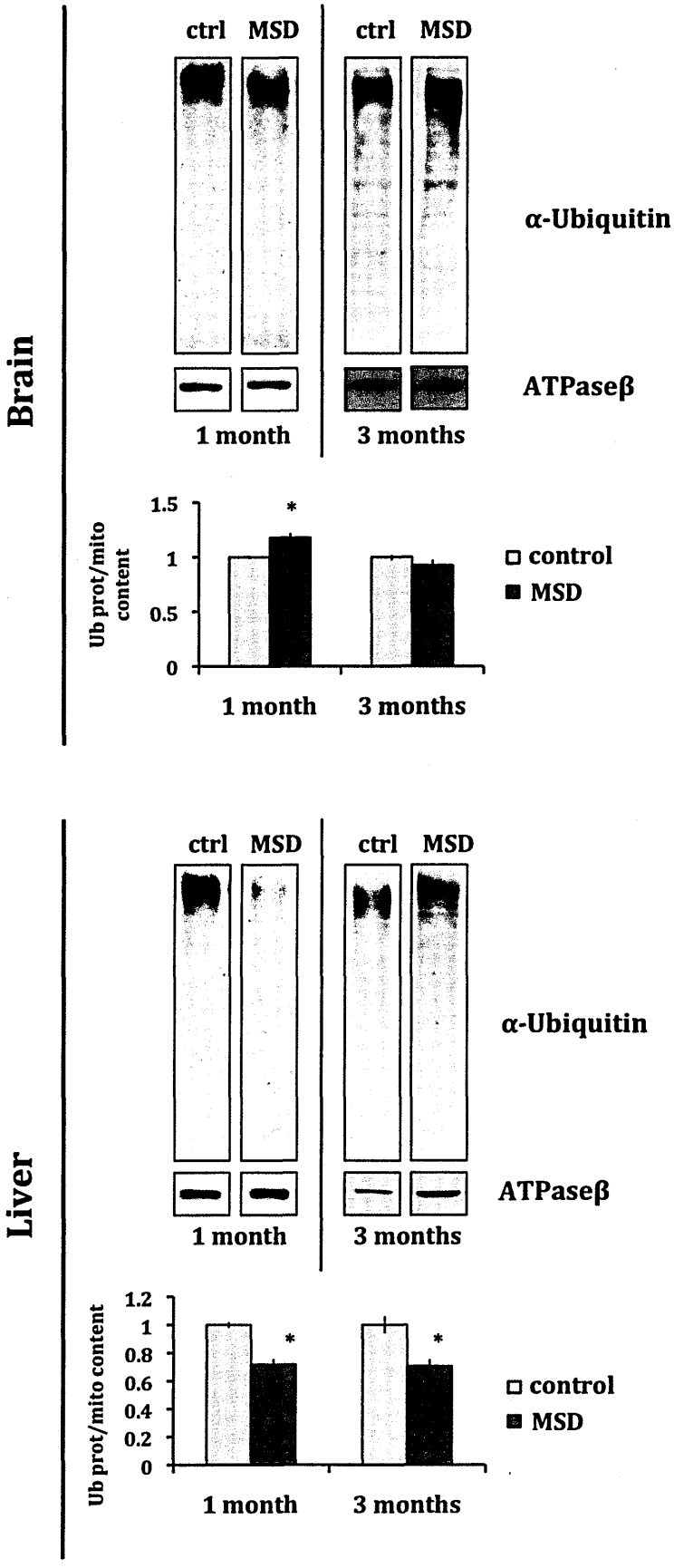
Brain
ctrl
MSD
ctrl
MSD
α-Ubiquitin
ATPaseβ
1 month
3 months
Ub prot/mito content
1.5
1
0.5
0
*
control
MSD
1 month
3 months
Liver
ctrl
MSD
ctrl
MSD
α-Ubiquitin
ATPaseβ
1 month
3 months
Ub prot/mito content
1.2
1
0.8
0.6
0.4
0.2
0
*
*
control
MSD
1 month
3 months

Figure 24. Ubiquitination of mitochondrial proteins in MSD tissues. Analysis of ubiquitinated proteins in mitochondrial fractions obtained from MSD (n=4) and control mice (n=4) at 1- and 3 months of age. Here we show the most representative blot as obtained after quantification with Image J software. Results have been expressed as the amount of ubiquitin respect to mitochondrial number. ** p-value< 0.01

As shown in figure 25, in MSD liver, parkin was predominantly localized in mitochondrial fractions when compared to control (1 month, cytosol control 42.2% MSD 13.99% p-value≤ 0.05, mitochondria control 57.7% MSD 86.1% p= 0.32; 3 months, cytosol control 39.1% MSD 17.6% p= 0.09, mitochondria control 60.8% MSD 82.4% p-value= 0.35) although total levels of the protein were significantly reduced (1 month, 0.48 ± 0.04; 3 months, 0.35 ± 0.03; p-value< 0.01) (figure 26). On the contrary, in MSD brain, parkin levels were comparable to those of control mice, being mostly localized in the cytosol (cytosol control 54.2% MSD 64.6% p-value= 0.14, mitochondria control 45.8% MSD 35.4% p-value= 0.06) (figure 25) and this was associated to unaltered amounts of parkin in total tissue homogenates (1 month, 1.26 ± 0.1; 3 months, 0.8 ± 0.11) (figure 26).

Proper parkin translocation was further confirmed in MSD MEFs. In this case, we transiently co-expressed GFP-parkin and DsREDmito plasmids in MSD and control cells, which were then incubated in absence/presence of the mitochondrial uncoupler CCCP (20μM, 20h). As shown in figure 27, parkin localization was entirely cytoplasmic in untreated cells. Upon CCCP treatment, massive depolarization of mitochondria induced the translocation of large amounts of parkin in both types of cell thus indicating that parkin is properly recruited to depolarized mitochondria in MSD cells.

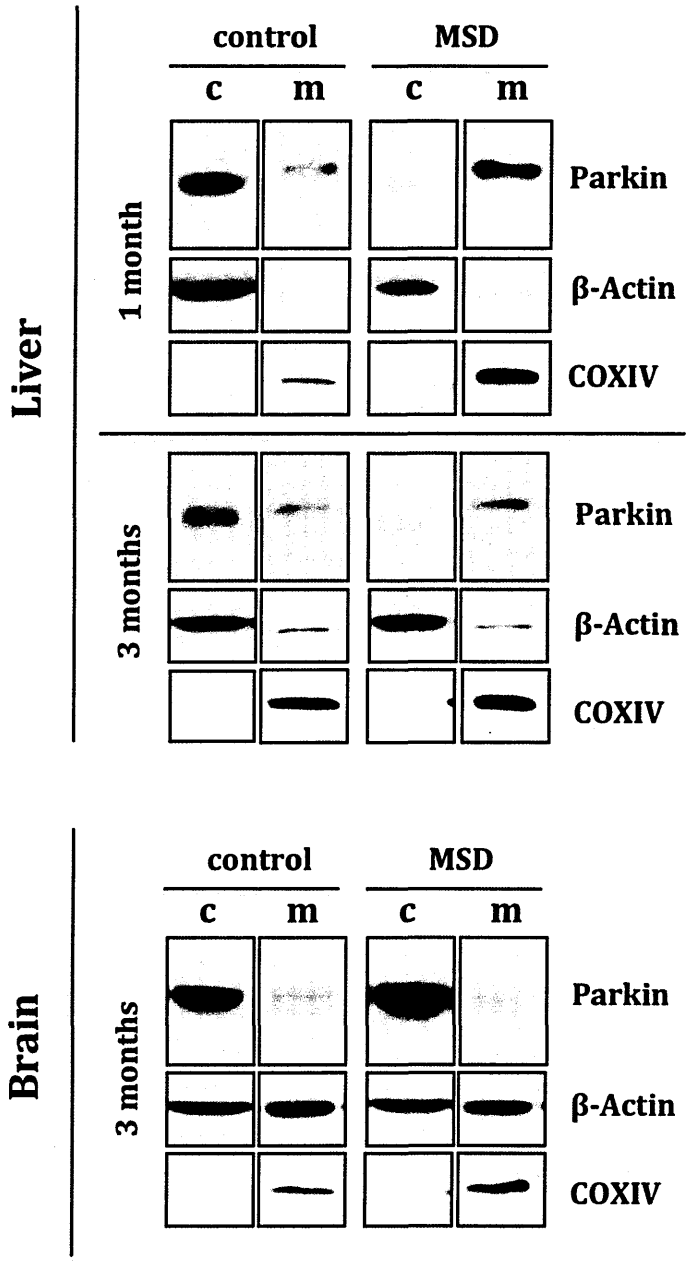

Figure 25. Parkin translocates to mitochondria in MSD tissues. Levels of parkin in cytosolic and mitochondrial fractions obtained from MSD (n=4) and control mice (n=4) at 1- and 3 months. Here we show the most representative blot as obtained after quantification with Image J software. COX IV has been used as loading control for mitochondrial fraction.

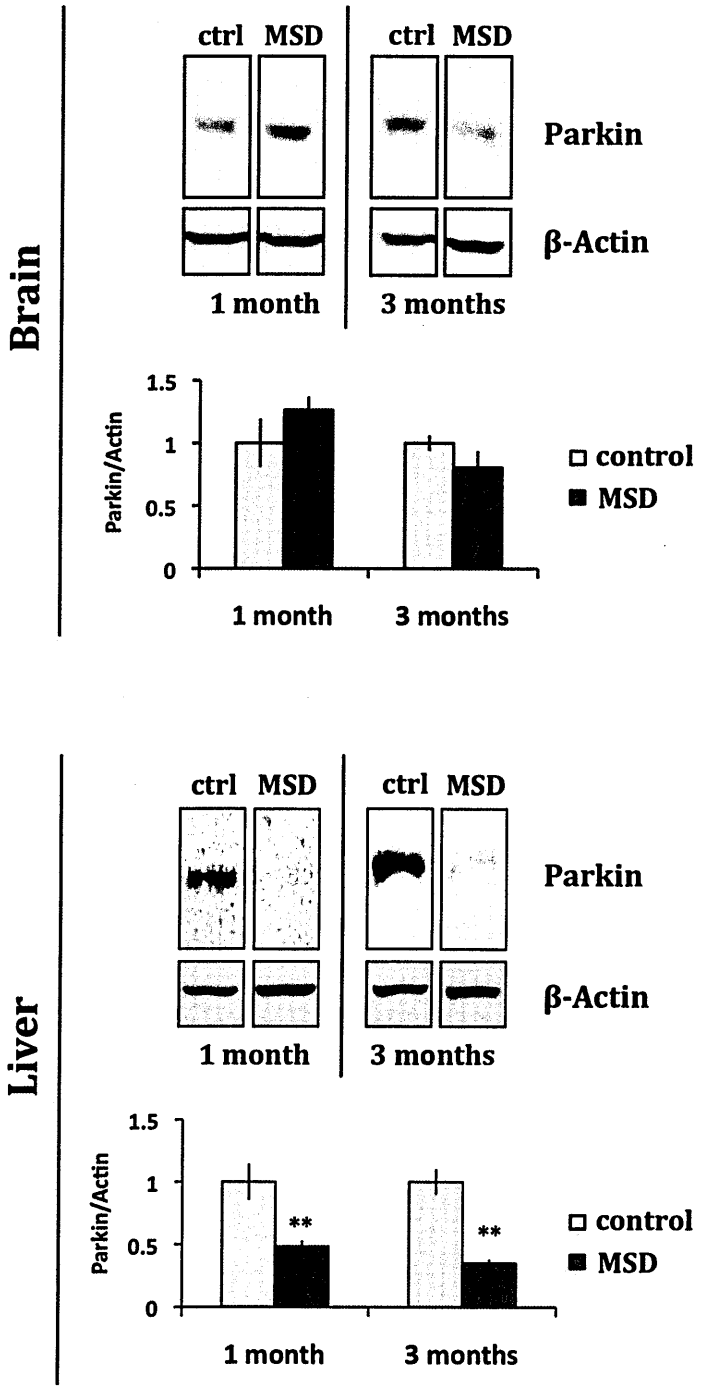

Figure 26. Parkin levels in MSD tissues. Western blot analysis of parkin in brain and liver total homogenates obtained from MSD (n=4) and control mice (n=4) at 1- and 3 months. Here we show the most representative blot as obtained after quantification with Image J software. The Parkin/Actin ratio has been expresses in terms of fold-change compared to control. ** p-value<0.01

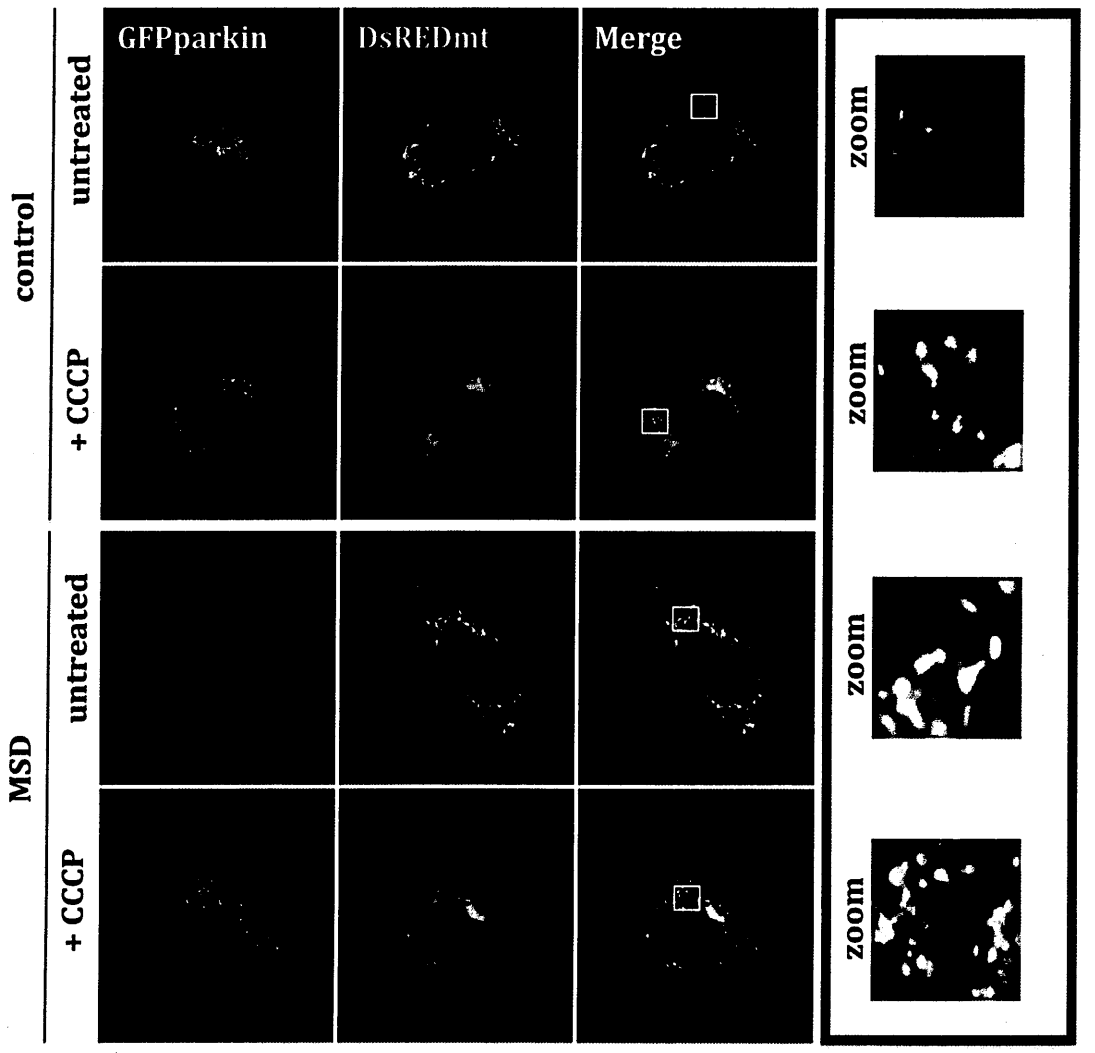

Figure 27. Parkin translocates to depolarized mitochondria in MSD MEFs. Transfection of GFP-parkin (green) and DsREDmt (red) constructs in MSD and control MEFs. 24-hours after transfection, cells were treated with 20μM CCCP for 20 hours. Images were taken with a 63x/1.4 Oil DIC Apo Plan lens in a Zeiss LSM710 confocal microscope. Merge zoomed area is indicated with a white square.

Our results indicate that despite parkin is able to efficiently translocate to mitochondria, levels of this protein are strongly reduced in MSD liver thus providing a suitable explanation for the incomplete mitochondrial ubiquitination observed in

this tissue. Moreover, we found that low parkin levels are likely due to enhanced posttranslational alterations since no significant differences were observed in *PARK2* relative expression (MSD brain, 1 month, 1.26 ± 0.08, p-value< 0.05; 3 months, 1.29 ± 0.18; MSD liver, 1 month, 0.51 ± 0.31; 3 months, 0.6 ± 0.28) (figure 28).

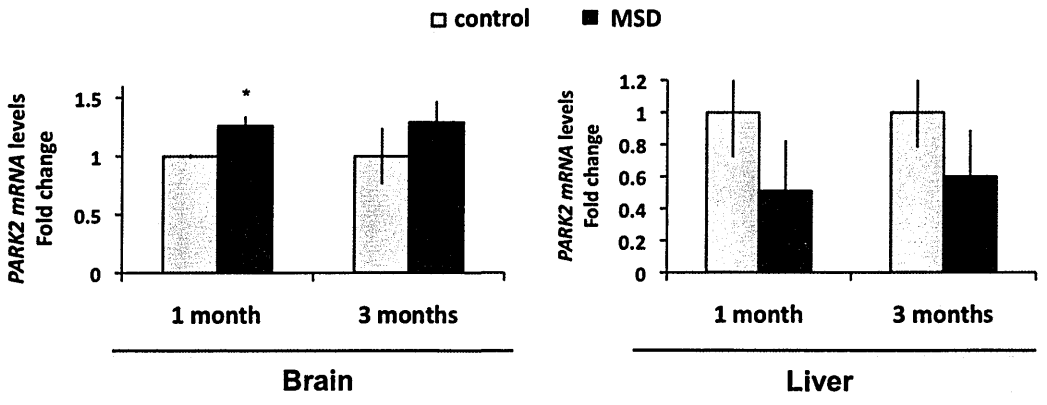

Figure 28. *PARK2* relative expression in MSD tissues. Analysis by qPCR of *PARK2* mRNA levels in brain and liver of MSD (n=3) and control mice (n=3) at 1- and 3 months. Results are represented in terms of fold-change compared to control. * p-value< 0.05

4. Inhibition of macroautophagy may contribute to defective mitochondrial removal

In a previous study, we described a defect in autophagosome maturation in LSDs (56, 64). We hypothesize that this autophagic distress may also affect the recycling of dysfunctional mitochondria thus exacerbating the mitochondrial phenotype already observed.

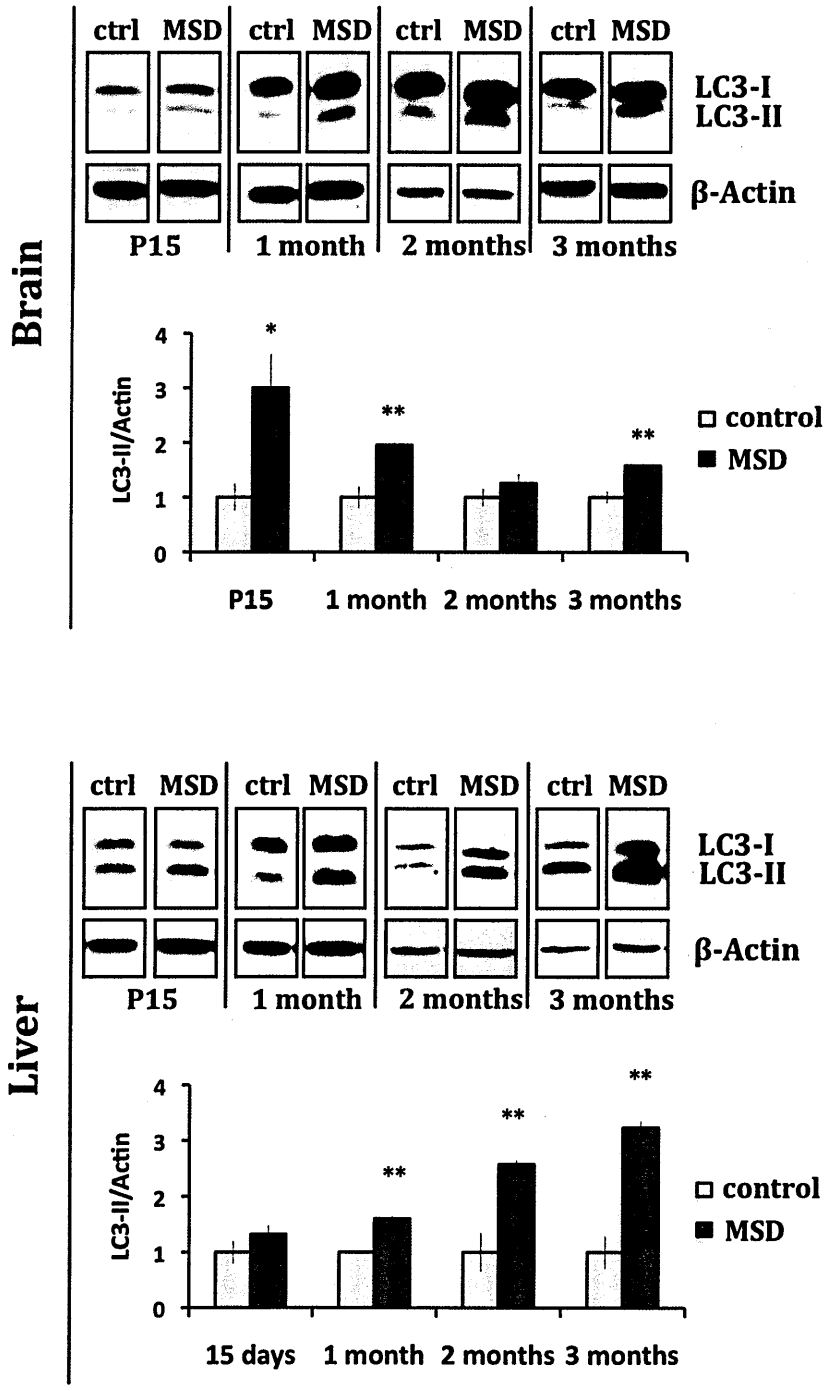

Figure 29. Autophagosome accumulation in MSD tissues. LC3 immunoblots on brain and liver total homogenates from MSD (n=4) and control mice (n=4) at P15, 1-, 2- and 3 months. Here we show the most representative blot as obtained after quantification with Image J software. Autophagosome accumulation has been expressed as the LC3-II/Actin ratio in terms of fold-change respect to control. * p-value< 0.05; ** p-value< 0.01

First, we monitored the accumulation of the autophagic marker LC3-II in MSD tissues (figure 29). LC3-II/Actin ratios in brain and liver total homogenates showed a significant accumulation of autophagosomes in MSD mice compared to control, both in brain (P15, 3 ± 0.625; 1 month, 1.95 ± 0.05; 2 months, 1.26 ± 0.17; 3 months, 1.58 ± 0.03) and liver (P15, 1.31 ± 0.15; 1 month, 1.6 ± 0.045; 2 months, 2.57 ± 0.075; 3 months, 3.2 ± 0.11). Nevertheless, the trend of accumulation differed between these two tissues. Indeed, whereas in MSD brain the LC3-II/Actin ratio remained constant over time (except for at P15), LC3-II levels gradually increased in liver. These results indicate a distinct autophagic dynamics between these tissues, which might be related to different metabolic requirements and/or stress conditions of each type of cell. This accumulation of LC3-II was in accordance with the block of autophagosome-lysosome fusion already reported (55, 63). However, we have never investigated whether this impairment in autophagosome maturation may somehow affect autophagy induction. The initial step of autophagosome formation depends in part on the phosphorylation-inactivation of the mTOR complex and/or levels of Beclin-1, which is part of the complex that mediates vesicle nucleation.

Therefore, we evaluated both the levels of Beclin-1 mRNA and protein in MSD (n=4) and control tissues (n=4) (figure 30). Immunoblots of MSD brain extracts showed a slight increase of protein levels only at 3 months (BECN1/Actin ratio at P15, 1 ± 0.03; 1 month, 0.98 ± 0.04; 2 months, 0.99 ± 0.01; 3 months, 1.12 ± 0.006), which matched with increased RNAm expression at the same time point (1.41 ± 0.11, p-value< 0.01).

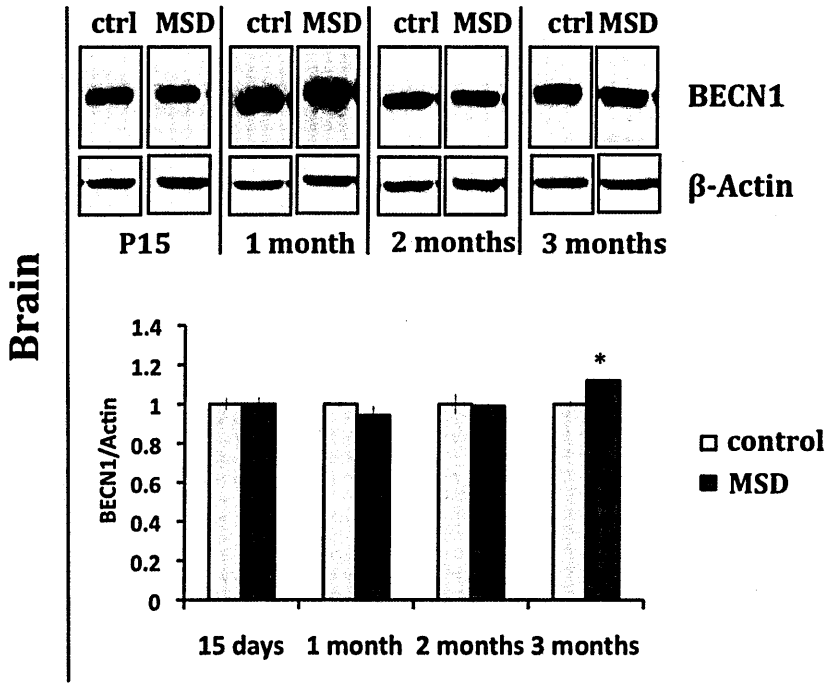
Brain
ctrl MSD ctrl MSD ctrl MSD ctrl MSD
BECN1
β-Actin
P15 1 month 2 months 3 months
BECN1/Actin
1.4
1.2
1
0.8
0.6
0.4
0.2
0
*
15 days 1 month 2 months 3 months
control
MSD

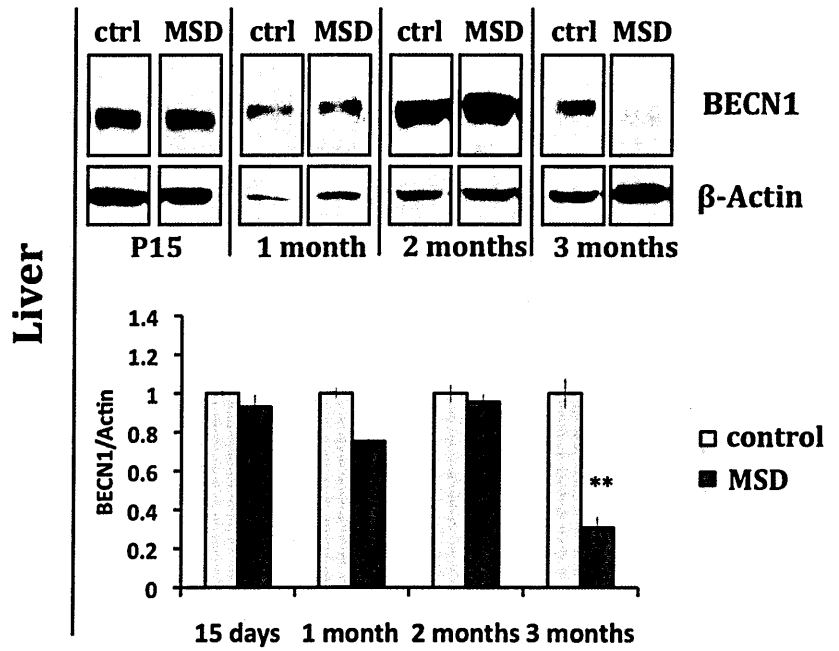
Liver
ctrl MSD ctrl MSD ctrl MSD ctrl MSD
BECN1
β-Actin
P15 1 month 2 months 3 months
BECN1/Actin
1.4
1.2
1
0.8
0.6
0.4
0.2
0
**
15 days 1 month 2 months 3 months
control
MSD

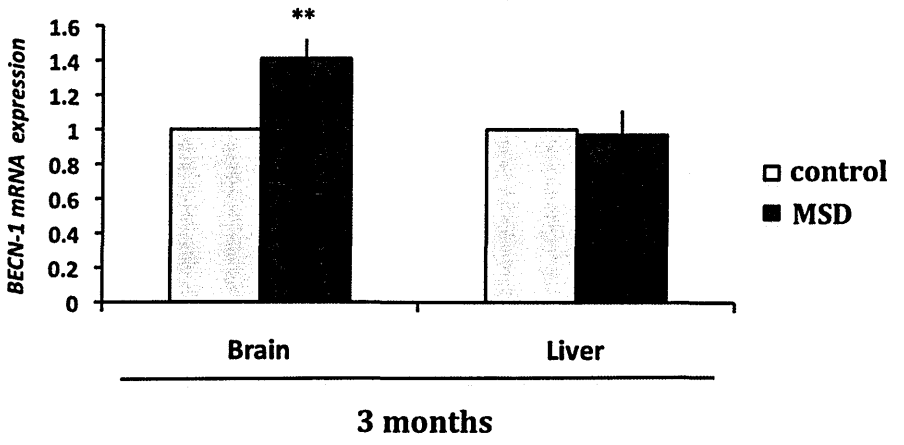

Figure 30. Autophagy is induced in MSD brain but not in liver. *previous page*, Beclin-1 protein levels in total lysates of brain and liver samples obtained from MSD (n=4) and control mice (n=4) at 4 different time points (P15, 1-, 2-, and 3 months). Here we show the most representative blot as obtained after quantification with Image J software. The BECN1/Actin is expressed in terms of fold-change compared to control. *this page*, *BECN-1* mRNA levels in brain and liver samples from MSD (n=4) and control mice (n=4) at 3 months. ** p-value< 0.01

Strikingly, Beclin-1 levels in liver were notably reduced at 3 months (BECN1/Actin ratio at P15, 0.93 ± 0.06; 1 month, 0.75 ± 0.01; 2 months, 0.95 ± 0.04; 3 months, 0.3 ± 0.05) although its RNAm expression was comparable to control (0.97 ± 0.14, p-value = 0.78). These results suggest that autophagy is differentially regulated in brain and liver of MSD mice: whereas in brain we observed a slight induction of autophagy at a late stage; in liver we detected reduced levels of Beclin-1, which may indicate a post-translational cleavage of Beclin-1 since mRNA levels appeared unaltered.

This inhibition of autophagy induction could further contribute to the impairment of mitochondrial removal observed in MSD liver.

5. Dysfunctional mitochondria release cytochrome *c* and trigger cell death in a tissue-specific fashion as a consequence of impaired mitophagy

Incomplete removal of mitochondria can have serious consequences for cell integrity. We have previously described a tissue-specific accumulation of morphologically altered mitochondria in our mouse model of lysosomal storage disorders.

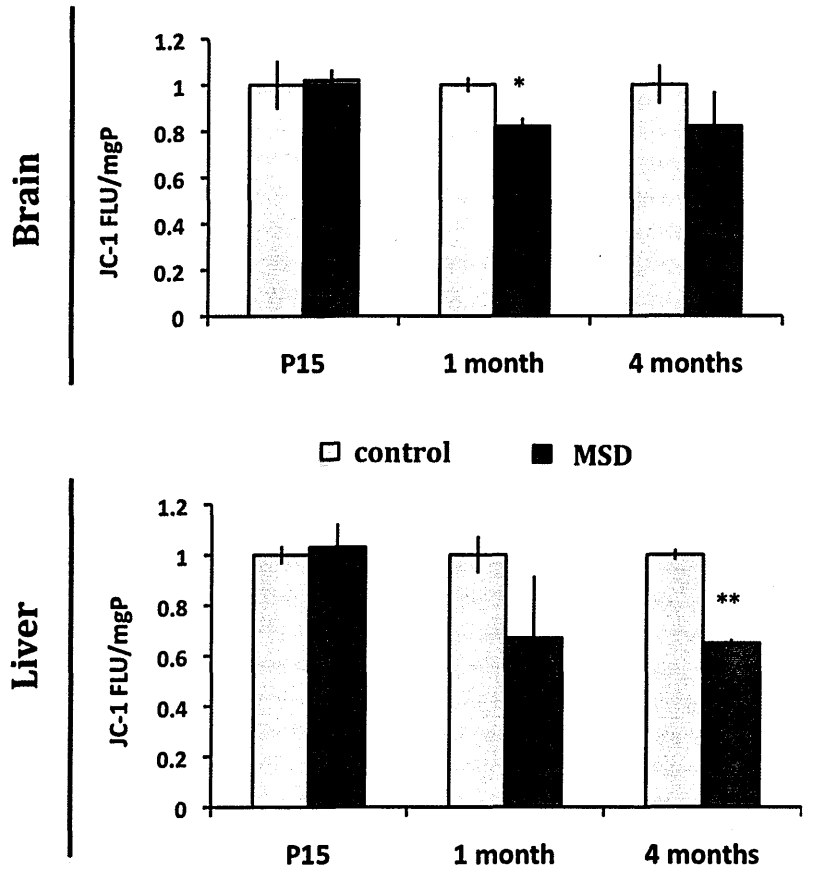

Figure 31. Loss of mitochondrial membrane integrity in MSD tissues. Measurement of JC-1 incorporation (JC-1 FLU/mg protein) in freshly isolated mitochondria obtained from brain and liver of MSD (n=3) and control mice (n=3) at three different stages (P15, 1- and 4 months). Values have been expressed in terms of fold-change respect to control. * p-value< 0.05; ** p-value< 0.01

In order to evaluate whether these mitochondria were potentially dangerous for cells, we performed a detailed analysis of mitochondrial functionality in MSD tissues. Initially, we evaluated the integrity of the mitochondrial membrane using JC-1, a fluorescent cationic dye that accumulates in mitochondria with intact electrochemical gradient. For this purpose we isolated mitochondria from both brain and liver of MSD (n=3) and control mice (n=3) and measured the incorporation of JC-1 (figure 31). Isolated mitochondria from MSD brain showed less retention of JC-1 at both 1 month (0.83 ± 0.03, p-value <0.05) and 4 months (0.83 ± 0.15) although the later result was not significant (p-value= 0.35). In liver, loss of membrane potential was evident at 1 month (0.67 ± 0.24, p-value= 0.27) and became significant at 4 months (0.65 ± 0.015, p-value< 0.01).

Since mitochondria are the main source of energy in cells, we used an ATP assay to further evaluate mitochondria functionality. For this analysis we used freshly isolated mitochondria from both brain and liver (n=3) and measured the relative amount of ATP in each mitochondrial fraction (figure 32). Although the results obtained in brain mitochondria were not significant (2 months, 0.61 ± 0.07, 4 months, 0.82 ± 0.06; p-value ≥ 0.05) they showed a slight decrease in ATP content in MSD compared to control mice samples. Instead, mitochondrial fractions from MSD

liver displayed a striking decrease in ATP levels at both time points (2 months, 0.19 ± 0.1; 4 months, 0.19 ± 0.04; p-value < 0.05).

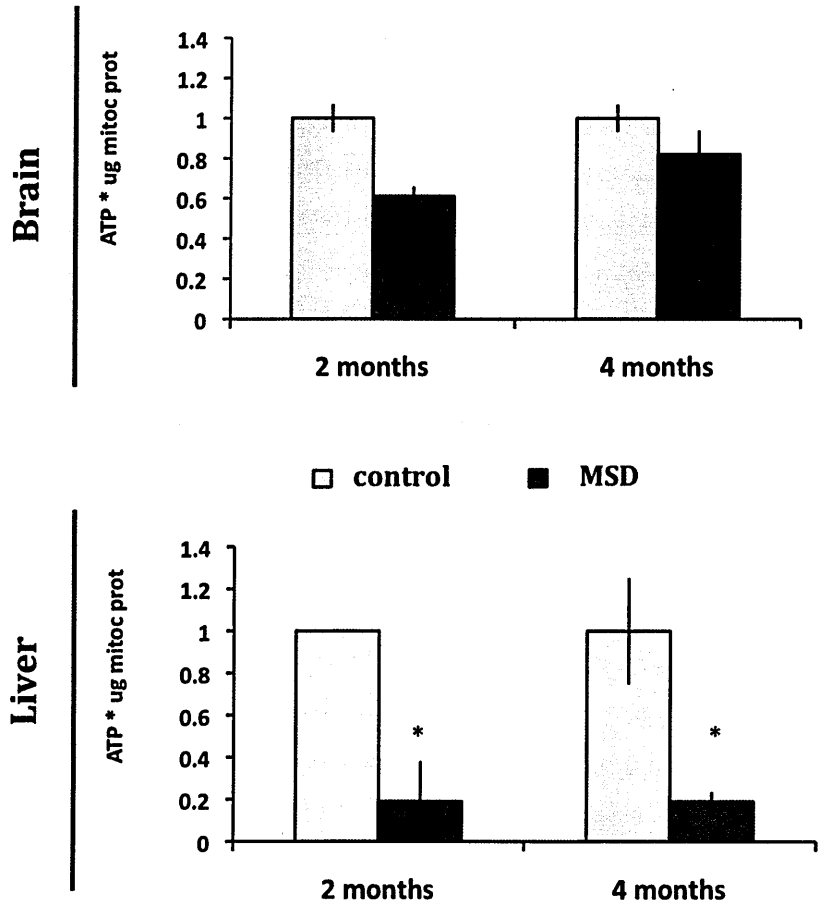

Figure 32. ATP content in mitochondria from MSD tissues. Measurement of ATP (ATP * µg mitochondrial protein^{-1}) in freshly isolated mitochondria from brain and liver of MSD (n=3) and control mice (n=3) at 2 different time points (2- and 4 months). Values have been expressed in terms of fold-change respect to control. * p-value< 0.01

Decreased ATP levels and increased permeabilization of the mitochondrial membrane can determine the fate of a cell. The opening of MPT pores can lead to mitochondrial swelling, OMM rupture and release of pro-apoptotic factors such as cytochrome *c* (41). We therefore evaluated whether mitochondria from brain and

liver of MSD mice were prone to release cytochrome *c* from the intermembrane space (IMS).

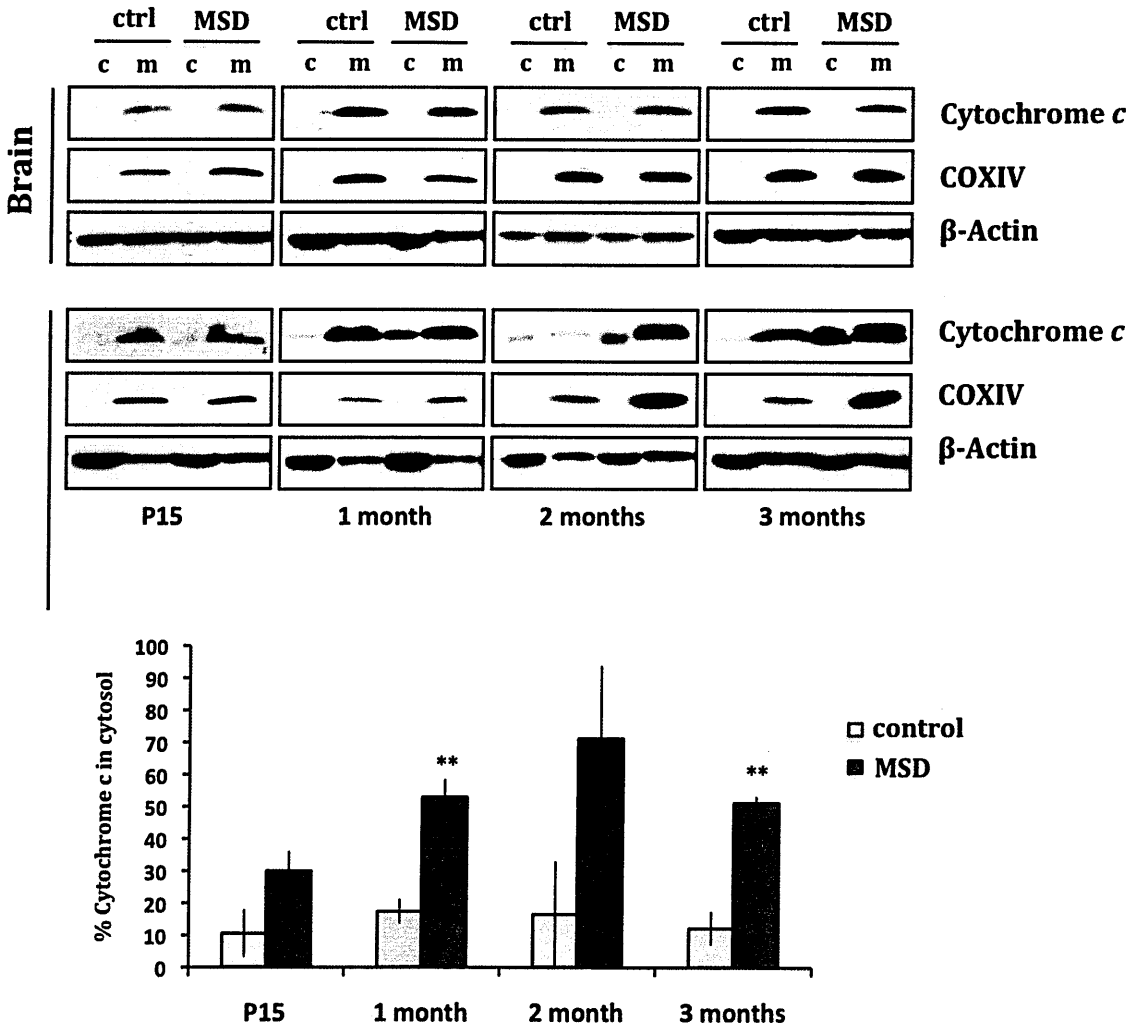

Figure 33. Analysis of cytochrome *c* release in MSD tissues. *top*, Western blot analysis of cytochrome *c* in subcellular fractions obtained from brain and liver samples of MSD (n=4) and control mice (n=4) at 4 different stages (P15, 1-, 2-, and 3 months). Here we show the most representative blot as obtained after quantification with Image J software. *bottom*, percentage of cytochrome *c* in cytosolic fractions from liver of MSD and control mice. ** p-value< 0.01

To this end, we isolated brain and liver samples from MSD (n=4) and control mice (n=4) at 4 different time points (P15, 1-, 2- and 3 months). Each sample was

processed separately and subcellular fractions were obtained by differential centrifugation. Equal amounts of both cytosolic and mitochondrial fractions were loaded into a SDS-PAGE followed by incubation with an antibody against cytochrome *c*. As shown in figure 33, no traces of cytochrome *c* were observed in cytosolic fractions of MSD brains at any of the stages analyzed. Nevertheless, we detected high levels of cytochrome *c* in cytosolic fractions of MSD liver as soon as 1 month of age (% Cyt c in cytosol at 1 month= 52.9 ± 5.6, 2 months= 71.1 ± 22.8 and 3 months= 51.1 ± 2.2). These data are consistent with the results shown in previous figures, that is, changes in mitochondrial morphology and membrane permeability precede the release of cytochrome *c* in liver but not in brain of MSD mice indicating that cell death is either mediated by different pathways or effectors in these organs.

To test whether the release of cytochrome *c* lead to cell death we performed an *in situ* apoptosis assay (TUNEL) on fixed- paraffin brain (cerebellum and cortex regions) and liver sections of MSD mice at an advanced stage of the disease (3 months) (figure 34). As expected, no TUNEL positive cells were detected on brain slices of MSD mice. This result correlates with the absence of cytochrome *c* in brain cytosolic fractions as shown by immunoblots. The absence of TUNEL positive cells suggests that commitment of cell death is mediated by a cytochrome *c*-independent mechanism in this tissue. Contrarily, MSD liver sections exhibited a massive presence of TUNEL positive cells per area analyzed.

Hence, we can conclude that mitochondria are the main effectors of cell death in MSD liver by releasing cytochrome *c* and subsequently activating downstream caspases.

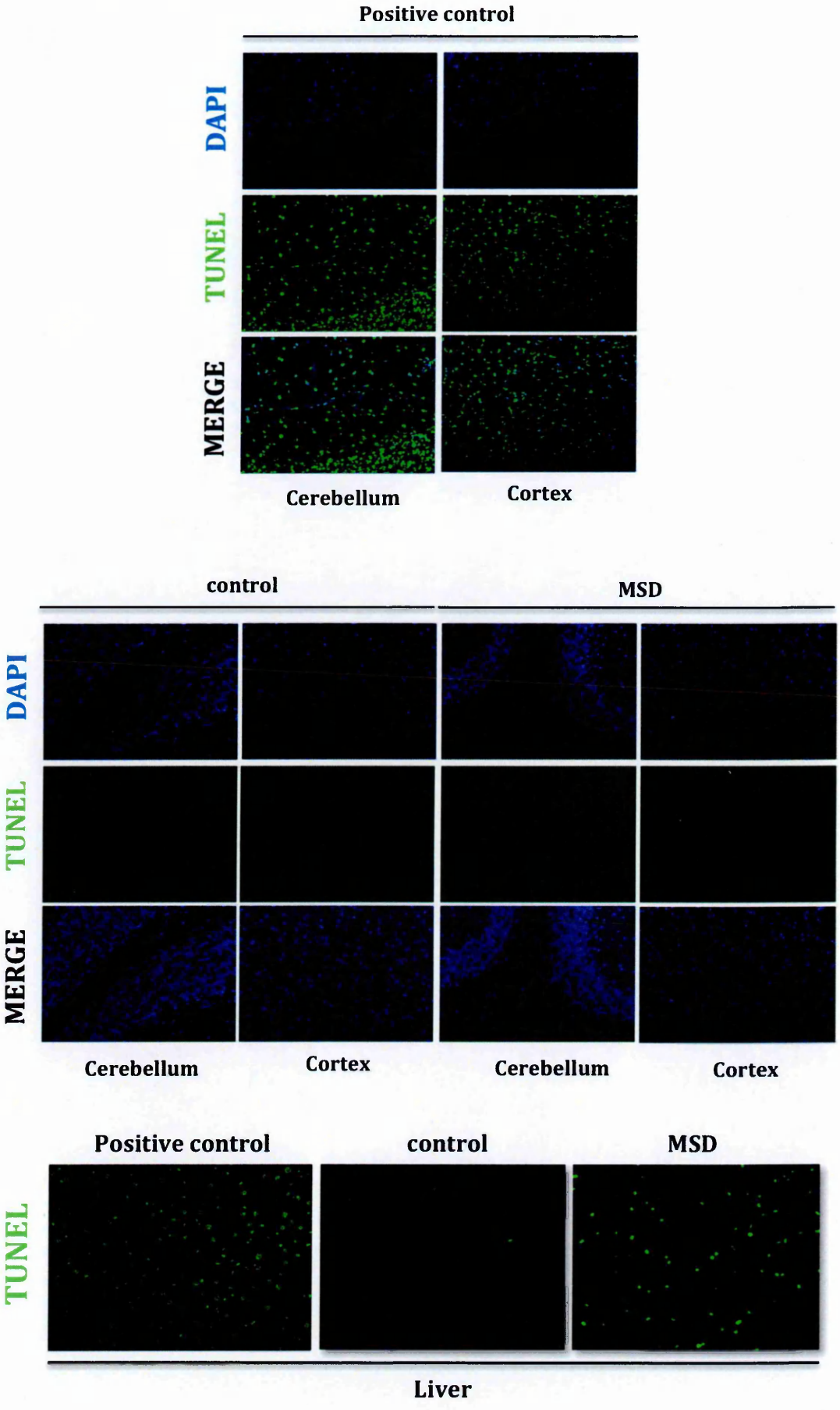
Positive control
DAPI
TUNEL
MERGE
Cerebellum
Cortex
control
MSD
DAPI
TUNEL
MERGE
Cerebellum
Cortex
Cerebellum
Cortex
Positive control
control
MSD
TUNEL
Liver

Figure 34. Release of cytochrome *c* triggers cell death in MSD liver. Detection of apoptotic nuclei (green) on brain (cerebellun and cortex regions) and liver paraffin sections (7μM) of MSD and control mice at 3 months by TUNEL assay. Images were taken in a Zeiss Axioimager A.1 fluorescence microscope (20x objective).

CONCLUSIONS

Mitochondrial aberrations are a hallmark of many neurodegenerative disorders. In Alzheimer's disease (AD), beta-amyloid (Aβ) fragments have been described to directly interact with mitochondria thus resulting in mitochondrial dysfunction (66). Over-expression of wild-type APP in both M17 and primary hippocampal neurons induced a severe mitochondrial fragmentation concomitantly with a reduction in the number of mitochondria (67). However, evidence showing mitophagy in AD is scarce and controversial: whilst Moreira and collaborators (68) showed increased mitochondrial sequestration in autophagosomes, a previous study had demonstrated cytosolic accumulation of mitochondria as a result of inefficient autophagic-lysosomal degradation (69). Similar to AD, mutant huntingtin (htt) has been described to localize to the mitochondrial outer membrane (OMM) in Huntington disease (HD) (70). The association of mutant htt with mitochondria is responsible for structural changes, decreased mitochondrial trafficking and impairment of mitochondrial dynamics (71). Recently, a study carried out by Martinez-Cuervo and collaborators (53) have revealed the existence of cargo recognition defects that result in the accumulation of dysfunctional mitochondria in HD cells.

Mitochondrial dysfunction has also been involved in the pathogenesis of lysosomal storage disorders. Recently, Sano and collaborators (72) reported that the accumulation of GM1 at the mitochondria-associated ER membranes leads to calcium-dependent mitochondrial apoptosis. Changes in mitochondrial morphology

and function have been described in a list of different LSDs (see *Chapter 4* - 4.3). However, while in AD and HD mutant proteins directly have been shown to interact with mitochondria, the origin of organelle dysfunction in LSDs may be associated to different mechanisms indirectly correlated with the storage.

As previously demonstrated by our group, the accumulation of effete mitochondria was initially related to an impairment of autophagosome maturation (56, 64). Nevertheless, the results obtained in the present study demonstrate that mitochondria accumulation is not a mere consequence of defective autophagosome-lysosome fusion but may involve a more specific mechanism that mediates mitochondrial priming and targeting to autophagosomes. Furthermore, our findings highlight the tissue-specificity of this phenomenon, which appeared to be compromised in liver but not in brain of MSD mice.

In brains of MSD mice, we have reported the up-regulation of *PARK2* expression and the increase in parkin levels. We believe that this higher transcriptional activation may more efficiently control the elimination of potentially dangerous mitochondria. In fact, as consequence of higher parkin activity indicated by the increased levels of ubiquitination of mitochondrial fractions, we do not observe any differences in mitochondrial content. Moreover, the characterization of isolated mitochondria from MSD brain did not reveal significant changes in either mitochondrial integrity (JC-1 assay and cytochrome *c* release) or functionality (ATP production). Only at an advanced stage of the disease, presumably as a consequence of accumulated metabolic stress, mitochondria from cortical neurons appeared fragmented. Mitochondrial fission has been demonstrated to trigger autophagy (73). In fact, simultaneously to morphological changes, we observed an

increase of beclin-1 levels. The induction of autophagy may reflect the urgent necessity to eliminate fragmented mitochondria that might compromise tissue homeostasis. In a previous study, loss of Purkinje cells has been described in MSD mice as soon as 2 months (28). However, no TUNEL-positive cells have been detected at any of the stages analyzed. We therefore speculate that, under the third month of age, neurodegeneration may not be directly correlated with mitochondria dysfunction but might result as a consequence of both direct accumulation of undegraded material inside lysosomes and the formation of toxic aggregates due to impaired autophagosome maturation (56).

Contrarily to what observed in brain of MSD mice, the analysis of liver samples showed a time-related accumulation of mitochondria as indicated by COX IV levels. Morphological analysis revealed an increase in mitochondrial size, a characteristic that was detected as soon as 15 days after birth. Mitochondrial enlargement can be a consequence of 1) defective fission, 2) a high rate of fusion and 3) impaired mitophagy. We have reported a reduction in DLP-1 levels, which may in part account for the accumulation of enlarged mitochondria. However, in the majority of cases, the presence of giant mitochondria is a result of defective mitochondrial turnover (74). Actually, the qualitative analysis of autophagosome content revealed the presence of a high percentage of vesicles without any recognizable structure inside. Notably, this percentage increased over time concomitantly with the accumulation of mitochondria. From a detailed analysis of key steps of mitophagy emerged that, despite proper translocation, reduced levels of parkin resulted in inefficient ubiquitination of mitochondrial proteins in MSD liver. We hypothesize that this incomplete ubiquitination might in turn derive in an

inadequate cargo recognition by the adaptor protein p62/SQSTM1. However, further analysis need to be performed in order to check whether p62/SQSTM1 is able to recognize ubiquitinated mitochondria in MSD. On the other hand, the non-induction of autophagy, represented by unaltered levels of beclin-1, together with a defect in autophagosome maturation may contribute to the phenotype observed by limiting the availability of new autophagic vesicles. Moreover, at an advanced stage of the pathology, beclin-1 levels appear surprisingly reduced. It has been reported that the mitochondrial proteins Bcl-2 and Bcl-XL negatively regulate autophagy by binding beclin-1, which is then cleaved by caspases (75). These data indicate that apoptosis and autophagic cell death cannot co-exist in the same cell. In line with this, our data demonstrate that the impaired removal and subsequent accumulation of mitochondria may trigger apoptosis thus leading to autophagy inhibition. In fact, detailed analysis of mitochondrial functionality showed the collapse of mitochondrial membrane potential (Ψ_m). Many mitochondrial reactions such as ATP generation, ROS production and Ca^{+2} uptake depend on mitochondrial Ψ_m. Therefore, loss of membrane integrity results in a strong decrease in ATP content and in the opening of the MTP pore, leading to the release of pro-apoptotic proteins. In MSD liver, cytochrome *c* has been detected in cytosolic fractions as soon as 1 month of age. Once released, cytochrome *c* contributes to the formation of the apoptosome, which in turns recruits caspases and triggers a cascade of events leading to cell death. Actually, TUNEL analysis on liver sections have confirmed the presence of many apoptotic nuclei in MSD sections thus indicating that in this tissue, mitochondrial dysfunction is directly linked to cell death by the release of pro-apoptotic factors

We believe that the differences observed in our study might be associated to tissue energetic requirements. Mitochondria are the main power- house of cells since the major production of energy (ATP) occurs through oxidative phosphorilation. The brain contains a mixture of both post-mitotic (neurons) and mitotic (astrocytes and microglia) cell types. Neurons contain a high number of mitochondria, approximately 10,000 mitochondria per cell, which play an important role in synaptic maintenance through their ability to buffer Ca^{+2}. For this reason, post-mitotic cells are expected to be particularly vulnerable to changes in mitochondrial activity. It is then not surprising that mitochondrial turnover would be a very tightly controlled event in neurons since oxidative damage is considered one of the principal mediators for the progressive decline in cellular function. Actually, it is believed that neuronal populations subjected to higher levels of stress have higher levels of autophagy that allows the proper removal of ROS-producing mitochondria. In fact, not all neurons show the same level of susceptibility to impaired autophagy thus supporting the existence of different compensatory mechanisms. In fact, in a recent study, Van Laar and collaborators (76) have hypothesized the existence of a parkin-independent mechanism of mitochondrial turnover that would depend on cellular ATP levels. However, further analysis must be performed to corroborate this theory.

We have proposed a new working model (figure 35): in non-pathological conditions, parkin molecules are able to recognize depolarized mitochondria and promote their elimination by autophagy. In MSD, reduced levels of parkin impair the degradation of mitochondria thus leading to the accumulation of

morphologically and functional- altered mitochondria. At the same time, the block of autophagosome and lysosome fusion may in turn contribute to the phenotype observed by inhibiting the formation of new autophagic vesicles.

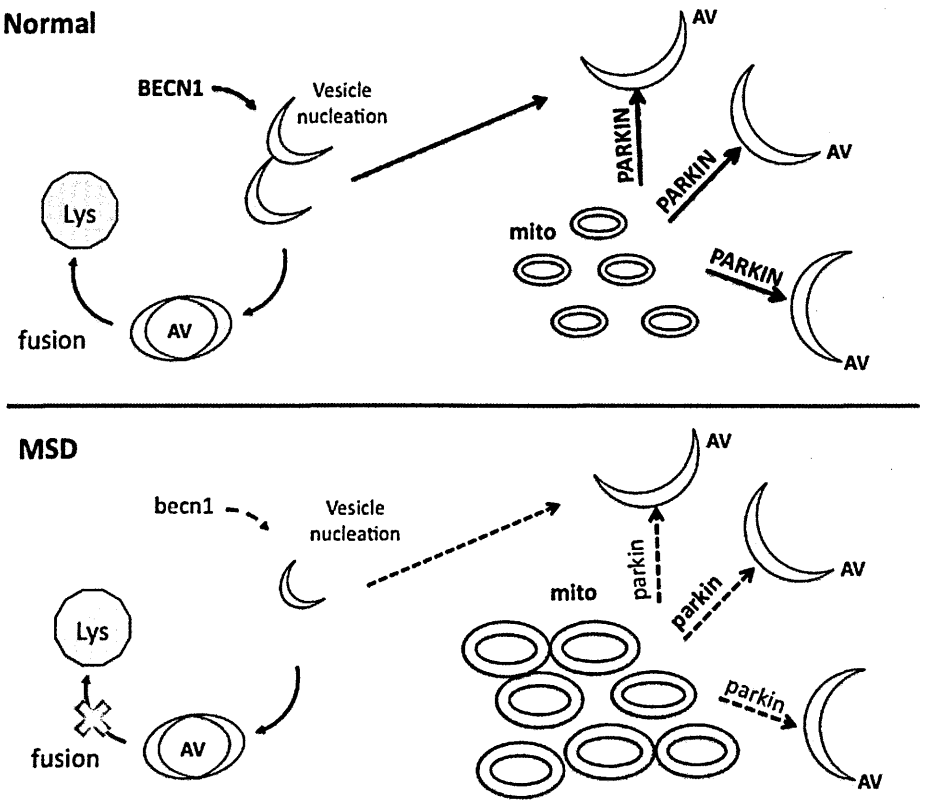

Figure 35. Proposed working model.

It is not clear whether the reduced levels of parkin are a consequence of impaired autophagy or it is an independent cause non-related to defects in autophagy. Parkin degradation is controlled by another E3 ubiquitin ligase called Nrdp1. The over-expression of Nrdp1 has been described to reduce the half-life of parkin from 5 to 2.5 hours (77). However, further studies must be performed in order to understand the real causes of parkin reduction and whether it can be directly correlated to SUMF1 deficiency.

In addition, it would be interesting to transduce MSD liver with a vector expressing *PARK2* and analyze whether the introduction of exogenous parkin is able to rescue the phenotype observed in this tissue. Actually, the analysis of parkin translocation in MEFs (GFP-Parkin/DsREDmito) was performed upon parkin over-expression conditions. It is possible then that what we observed in cells was a result of parkin over-expression, which might in turn mask the real phenotype.

Recent publications have described a parkin-dependent proteasomal degradation of OMM proteins, which seems to be a critical step for mitophagy (78-80). Moreover, other studies showed that p62/SQSTM1- null cells have no defects in parkin-mediated mitophagy thus suggesting that this cargo adaptor merely participates in mitochondrial aggregation around the perinuclear region (81,82). These new observations rise up the necessity to further analyze this selective process to better understand its real function.

Differently to other prototypical neurodegenerative disorders such as AD and HD, MSD is characterized not only by progressive neurodegeneration but has a prominent involvement of many systemic organs. In fact, from the analysis of different tissues at the same age has raise up the existence of different degrees of phenotype severity. In this study, many of the markers analyzed have been monitored over time thus making possible to correlate some events with the progression of the pathology. Establishing the onset of a specific molecular event may be of great importance in order to develop new therapeutic strategies. Moreover, since neurodegeneration has a slower progression, the generation of a

SUMF1 conditional mouse strain in brain would be useful to elucidate the contribution of mitochondria to the neurodegenerative process.

1 De Duve, C., Passau, L. and Maisin, J. (1955) Acid phosphatase and beta-glucuronidase activities in the livers from rats fed 4-dimethylaminoazobenzene. *Acta Unio Int Contra Cancrum*, 11, 638-639.

2 Saftig, P. (2005) *Lysosomes*. Landes Bioscience.

3 Barranger, J.A. and Cabrera-Salzar, M.A. (2007) *Lysosomal Storage Disorders*. Springer Science.

4 Neufeld, E.F. (1991) Lysosomal storage diseases. *Annu Rev Biochem*, 60, 257-280.

5 Vellodi, A. (2005) Lysosomal storage disorders. *Br J Haematol*, 128, 413-431.

6 Sardiello, M., Palmieri, M., di Ronza, A., Medina, D.L., Valenza, M., Gennarino, V.A., Di Malta, C., Donaudy, F., Embrione, V., Polishchuk, R.S. *et al.* (2009) A gene network regulating lysosomal biogenesis and function. *Science*, 325, 473-477.

7 Futerman, A.H. and van Meer, G. (2004) The cell biology of lysosomal storage disorders. *Nat Rev Mol Cell Biol*, **5**, 554-56

8 Wenger, D.A., Coppola, S. and Liu, S.L. (2003) Insights into the diagnosis and treatment of lysosomal storage diseases. *Arch Neurol*, 60, 322-328.

9 Beck, M. (2010) Therapy for lysosomal storage disorders. *IUBMB Life*, **62**, 33-40.

10 Platt, F.M., Neises, G.R., Dwek, R.A. and Butters, T.D. (1994) N-butyldeoxynojirimycin is a novel inhibitor of glycolipid biosynthesis. *J Biol Chem*, 269, 8362-8365.

11 Patterson, M.C., Vecchio, D., Prady, H., Abel, L. and Wraith, J.E. (2007) Miglustat for treatment of Niemann-Pick C disease: a randomised controlled study. *Lancet Neurol*, 6, 765-772.

12 Yam, G.H., Bosshard N., Zuber C., Steinman B. and Roth J. (2006) Pharmacological chaperone corrects lysosomal stoarge in Fabry disease caused by trafficking-incompetent variants. *Am J Physiol Cell Physiol*, 290, C1076 –C1082.

13 Sands M.S. and Davidson B.L. (2006) Gene therapy for Lysosomal Storage Disorders. *Molecular Therapy*, 13, 839-849.

14 Hopwood JJ, Ballabio A (1997). in The Metabolic and Molecular Basis of the Inherited Disease (McGraw–Hill, New York), pp 3725–3732.

15 Hanson, S.R., Best, M.D. and Wong, C.H. (2004) Sulfatases: structure, mechanism, biological activity, inhibition, and synthetic utility. *Angew Chem Int Ed Engl*, **43**, 5736-5763.

16 Sardiello, M., Annunziata, I., Roma, G. and Ballabio, A. (2005) Sulfatases and sulfatase modifying factors: an exclusive and promiscuous relationship. *Hum Mol Genet*, **14**, 3203-3217.

17 Diez-Roux, G. and Ballabio, A. (2005) Sulfatases and human disease. *Annu Rev Genomics Hum Genet*, **6**, 355-379.

18 See the website: http://us.expasy.org/cgi-bin/prosite (PDOC00117).

19 Dierks, T., Lecca, M.R., Schlotterhose, P., Schmidt, B. and von Figura, K. (1999) Sequence determinants directing conversion of cysteine to formylglycine in eukaryotic sulfatases. *EMBO J*, **18**, 2084-2091.

20 Knaust, A., Schmidt, B., Dierks, T., von Bulow, R. and von Figura, K. (1998) Residues critical for formylglycine formation and/or catalytic activity of arylsulfatase A. *Biochemistry*, **37**, 13941-13946.

21 Dierks, T., Schmidt, B., Borissenko, L.V., Peng, J., Preusser, A., Mariappan, M. and von Figura, K. (2003) Multiple sulfatase deficiency is caused by mutations in the gene encoding the human C(alpha)-formylglycine generating enzyme. *Cell*, **113**, 435-444.

22 Cosma, M.P., Pepe, S., Annunziata, I., Newbold, R.F., Grompe, M., Parenti, G. and Ballabio, A. (2003) The multiple sulfatase deficiency gene encodes an essential and limiting factor for the activity of sulfatases. *Cell*, **113**, 445-456.

23 Annunziata, I., Bouche, V., Lombardi, A., Settembre, C. and Ballabio, A. (2007) Multiple sulfatase deficiency is due to hypomorphic mutations of the SUMF1 gene. *Hum Mutat*, **28**, 928.

24 Dierks, T., Schlotawa, L., Frese, M.A., Radhakrishnan, K., von Figura, K. and Schmidt, B. (2009) Molecular basis of multiple sulfatase deficiency, mucolipidosis II/III and Niemann-Pick C1 disease - Lysosomal storage disorders caused by defects of non-lysosomal proteins. *Biochim Biophys Acta*, **1793**, 710-725.

25 Schlotawa, L., Steinfeld, R., von Figura, K., Dierks, T. and Gartner, J. (2008) Molecular analysis of SUMF1 mutations: stability and residual activity of mutant formylglycine-generating enzyme determine disease severity in multiple sulfatase deficiency. *Hum Mutat*, **29**, 205.

26 Artigalas, O.A., da Silva, L.R., Burin, M., Pastores, G.M., Zeng, B., Macedo, N. and Schwartz, I.V. (2009) Multiple sulfatase deficiency: clinical report and

description of two novel mutations in a Brazilian patient. *Metab Brain Dis*, **24**, 493-500.

27 Spampanato,C., De Leonibus, E., Dama, P., Gargiulo, A., Fraldi, A., Sorrentino, N.C., Russo, F., Nusco, E., Auricchio, A., Surace, E.M. and Ballabio, A. (2010). Efficacy of a combined intracerebral and systemic gene delivery approach for the treatment of a severe lysosomal storage disorder. *Mol Ther*.

28 Settembre, C., Annunziata, I., Spampanato, C., Zarcone, D., Cobellis, G., Nusco, E., Zito, E., Tacchetti, C., Cosma, M.P. and Ballabio, A. (2007) Systemic inflammation and neurodegeneration in a mouse model of multiple sulfatase deficiency. *Proc Natl Acad Sci U S A*, **104**, 4506-4511.

29 Settembre, C., Arteaga-Solis, E., McKee, M.D., de Pablo, R., Al Awqati, Q., Ballabio, A. and Karsenty, G. (2008) Proteoglycan desulfation determines the efficiency of chondrocyte autophagy and the extent of FGF signaling during endochondral ossification. *Genes Dev*, **22**, 2645-2650.

30 Klionsky, D.J. and Emr, S.D. (2000) Autophagy as a regulated pathway of cellular degradation. *Science*, **290**, 1717-1721.

31 Martinez-Vicente, M. and Cuervo, A.M. (2007) Autophagy and neurodegeneration: when the cleaning crew goes on strike. *Lancet Neurol*, **6**, 352-361.

32 Eskelinen, E.L. and Saftig, P. (2009) Autophagy: a lysosomal degradation pathway with a central role in health and disease. *Biochim Biophys Acta*, **1793**, 664-673.

33 Dunn, W.A., Jr. (1990) Studies on the mechanisms of autophagy: formation of the autophagic vacuole. *J Cell Biol*, **110**, 1923-1933.

34 Hailey, D.W., Rambold, A.S., Satpute-Krishnan, P., Mitra, K., Sougrat, R., Kim, P.K. and Lippincott-Schwartz, J. (2010) Mitochondria supply membranes for autophagosome biogenesis during starvation. *Cell*, **141**, 656-667.

35 Ravikumar, B., Moreau, K., Jahreiss, L., Puri, C. and Rubinsztein D.C. (2010) Plasma mebrane contributes to the formation of pre-autophagosomal structures. *Nat Cell Biol*, **12**, 747-757

36 Kabeya, Y., Mizushima, N., Ueno, T., Yamamoto, A., Kirisako, T., Noda, T., Kominami, E., Ohsumi, Y. and Yoshimori, T. (2000) LC3, a mammalian homologue of yeast Apg8p, is localized in autophagosome membranes after processing. *Embo J*, **19**, 5720-5728.

37 Hales, K.G. and Fuller, M.T. (1997) Developmentally regulated mitochondrial fusion mediated by a conserved, novel, predicted GTPase. *Cell*, 90, 121-129.

38 Koshiba, T., Detmer, S.A., Kaiser, J.T., Chen, H., McCaffery, J.M. and Chan, D.C. (2004) Structural basis of mitochondrial tethering by mitofusin complexes. *Science*, 305, 858-862.

39 Cipolat, S., Martins de Brito, O., Dal Zilio, B. and Scorrano, L. (2004) OPA1 requires mitofusin 1 to promote mitochondrial fusion. *Proc Natl Acad Sci U S A*, 101, 15927-15932.

40 Lee, Y.J., Jeong, S.Y., Karbowski, M., Smith, C.L. and Youle, R.J. (2004) Roles of the mammalian mitochondrial fission and fusion mediators Fis1, Drp1, and Opa1 in apoptosis. *Mol Biol Cell*, 15, 5001-5011.

41 Karbowski, M. and Youle, R.J. (2003) Dynamics of mitochondrial morphology in healthy cells and during apoptosis. *Cell Death Differ*, 10, 870-880.

42 Twig, G., Elorza, A., Molina, A.J., Mohamed, H., Wikstrom, J.D., Walzer, G., Stiles, L., Haigh, S.E., Katz, S., Las, G. *et al.* (2008) Fission and selective fusion govern mitochondrial segregation and elimination by autophagy. *Embo J*, 27, 433-446.

43 Kissova, I., Deffieu, M., Manon, S. and Camougrand, N. (2004) Uth1p is involved in the autophagic degradation of mitochondria. *J Biol Chem*, 279, 39068-39074.

44 Okamoto, K., Kondo-Okamoto, N. and Ohsumi, Y. (2009) Mitochondria-anchored receptor Atg32 mediates degradation of mitochondria via selective autophagy. *Dev Cell*, 17, 87-97.

45 Matsuda, N., Sato, S., Shiba, K., Okatsu, K., Saisho, K., Gautier, C.A., Sou, Y.S., Saiki, S., Kawajiri, S., Sato, F. *et al.* (2010) PINK1 stabilized by mitochondrial depolarization recruits Parkin to damaged mitochondria and activates latent Parkin for mitophagy. *J Cell Biol*, 189, 211-221.

46 Narendra, D.P., Jin, S.M., Tanaka, A., Suen, D.F., Gautier, C.A., Shen, J., Cookson, M.R. and Youle, R.J. (2010) PINK1 is selectively stabilized on impaired mitochondria to activate Parkin. *PLoS Biol*, 8, e1000298.

47 Vives-Bauza, C., Zhou, C., Huang, Y., Cui, M., de Vries, R.L., Kim, J., May, J., Tocilescu, M.A., Liu, W., Ko, H.S. *et al.* (2010) PINK1-dependent recruitment of Parkin to mitochondria in mitophagy. *Proc Natl Acad Sci U S A*, 107, 378-383.

48 Geisler, S., Holmstrom, K.M., Skujat, D., Fiesel, F.C., Rothfuss, O.C., Kahle, P.J. and Springer, W. (2010) PINK1/Parkin-mediated mitophagy is dependent on VDAC1 and p62/SQSTM1. *Nat Cell Biol*, 12, 119-131.

49 Ziviani, E., Tao, R.N. and Whitworth A.J. (2010) *Drosophila* parkin requires PINK1 for mitochondrial translocation and ubiquitinates mitofusin. *Proc Natl Acad Sci U S A*, 107, 5018-5023

50 Clark, I.E., Dodson, M.W., Jiang, C., Cao, J.H., Huh, J.R., Seol, J.H., Yoo, S.J., Hay, B.A., and Guo M. (2006) Drosophila pink1 is required for mitochondrial function and interacts genetically with parkin. *Nature*, 441, 1162-1166.

51 Tanaka, A. (2010) Parkin-mediated selective mitochondrial autophagy, mitophagy: Parkin purges damaged organelles from the vital mitochondrial network. *FEBS Lett*, 584, 1386-1392.

52 Van Laar, V.S. and Berman, S.B. (2009) Mitochondrial dynamics in Parkinson's disease. *Exp Neurol*, 218, 247-256.

53 Martinez-Vicente, M., Talloczy, Z., Wong, E., Tang, G., Koga, H., Kaushik, S., de Vries, R., Arias, E., Harris, S., Sulzer, D. *et al.* (2010) Cargo recognition failure is responsible for inefficient autophagy in Huntington's disease. *Nat Neurosci*, 13, 567-576

54 Levine, B. and Kroemer, G. (2008) Autophagy in the pathogenesis of disease. *Cell*, **132**, 27-42.

55 Wong, E. and Cuervo, A.M. (2010) Autophagy gone awry in neurodegenerative diseases. *Nat Neurosci*, **13**, 805-811.

56 Settembre, C., Fraldi, A., Jahreiss, L., Spampanato, C., Venturi, C., Medina, D., de Pablo, R., Tacchetti, C., Rubinsztein, D.C. and Ballabio, A. (2008) A block of autophagy in lysosomal storage disorders. *Hum Mol Genet*, **17**, 119-129.

57 Takamura, A., Higaki, K., Kajimaki, K., Otsuka, S., Ninomiya, H., Matsuda, J., Ohno, K., Suzuki, Y. and Nanba, E. (2008) Enhanced autophagy and mitochondrial aberrations in murine G(M1)-gangliosidosis. *Biochem Biophys Res Commun*, 367, 616-622.

58 Bi, X. and Liao, G. (2007) Autophagic-lysosomal dysfunction and neurodegeneration in Niemann-Pick Type C mice: lipid starvation or indigestion? *Autophagy*, **3**, 646-648.

59 Cao, Y., Espinola, J.A., Fossale, E., Massey, A.C., Cuervo, A.M., MacDonald, M.E. and Cotman, S.L. (2006) Autophagy is disrupted in a knock-in mouse model of juvenile neuronal ceroid lipofuscinosis. *J Biol Chem*, **281**, 20483-20493.

60 Jennings, J.J., Jr., Zhu, J.H., Rbaibi, Y., Luo, X., Chu, C.T. and Kiselyov, K. (2006) Mitochondrial aberrations in mucolipidosis Type IV. *J Biol Chem*, 281, 39041-39050.

61 Tanaka, Y., Guhde, G., Suter, A., Eskelinen, E.L., Hartmann, D., Lullmann-Rauch, R., Janssen, P.M., Blanz, J., von Figura, K. and Saftig, P. (2000) Accumulation of autophagic vacuoles and cardiomyopathy in LAMP-2-deficient mice. *Nature*, **406**, 902-906.

62 Raben, N., Shea, L., Hill, V. and Plotz, P. (2009) Monitoring autophagy in lysosomal storage disorders. *Methods Enzymol*, **453**, 417-449.

63 Rubinsztein, D.C., Cuervo, A.M., Ravikumar, B., Sarkar, S., Korolchuk, V., Kaushik, S. and Klionsky, D.J. (2009) In search of an "autophagomometer". *Autophagy*, **5**, 585-589.

64 Fraldi, A., Annunziata, F., Lombardi, A., Kaiser, H.J., Medina, D.L., Spampanato, C., Fedele, A.O., Polishchuk, R., Sorrentino, N.C., Simons, K. *et al.* (2010) Lysosomal fusion and SNARE function are impaired by cholesterol accumulation in lysosomal storage disorders. *EMBO J.*

65 Otomo, T., Higaki, K., Nanba, E., Ozono, K. and Sakai, N. (2009) Inhibition of autophagosome formation restores mitochondrial function in mucolipidosis II and III skin fibroblasts. *Mol Genet Metab*, 98, 393-399.

66 Santos, R.X., Correia, S.C., Wang, X., Perry, G., Smith, M.A., Moreira, P.I. and Zhu, X. (2010) A synergistic dysfunction of mitochondrial fission/fusion dynamics and mitophagy in Alzheimer's disease. *J Alzheimers Dis*, 20 (Suppl 2): S401-S412.

67 Wang, X., Su, B., Siedlak, S.L., Moreira, P.I., Fujioka, H., Wang, Y., Casadesus, G. and Zhu, X. (2008) Amyloid-beta overproduction causes abnormal mitochondrial dynamics via differential modulation of mitochondrial fission/fusion proteins. *Proc Natl Acad Sci U S A*, 105, 318-323.

68 Moreira, P.I., Siedlak, S.L., Wang, X., Santos, M.S., Oliveira, C.R., Tabaton, M., Nunomura, A., Szweda, L.I., Aliev, G., Smith, M.A., Zhu, X. and Perry, G. (2007) Increased autophagic degradation of mitochondria in Alzheimer disease. *Autophagy*, 3, 614-615.

69 Hirai, K., Aliev, G., Nunomura, A., Fujioka, H., Russell, R.L., Atwood, C.S., Johnson, A.B., Kress, Y., Vinters, H.V., Tabaton, M., Shimohama, S., Cash, A.D., Siedlak, S.L., Harris, P.L., Jones, P.K., Petersen, R.B., Perry, G. and Smith, M.A. (2001) Mitochondrial abnormalities in Alzheimer's disease. *J Neurosci*, 21, 017-023

70 Panov, A.V., Gutekunst, C.A., Leavitt, B.R., Hayden, M.R., Burke, J.R., Strittmatter, W.J. and Greenamyre, J.T. (2002) Early mitochondrial calcium defects in Huntington's disease are a direct effect of polyglutamines. *Nat Neurosci*, 5, 731-736.

71 Damiano, M., Galvan, L., Dégion, N. and Brouillet, E. (2010) Mitochondria in Huntington's disease. *Biochim Biophys Acta*, 1802, 52-61

72 Sano, R., Annunziata, I., Patterson, A., Moshiach, S., Gomero, E., Opferman, I., Forte, M. and d'Azzo, A. (2009) GM1-ganglioside accumulation at the mitochondria-associated ER membranes links ER stress to Ca (2+)-dependent mitochondrial apoptosis. *Mol Cell,* 36, 500-511.

73 Gomes, L.C. and Scorrano, L. (2008) High levels of Fis1, a pro-fission mitochondrial protein, trigger autophagy. *Biochim Biophys Acta*, 1777, 860-866.

74 Navratil, M., Terman, A. and Arriaga, E.A. (2007) Giant mitochondria do not fuse and exchange their contents with normal mitochondria. *Exp Cell Research*, 314, 164-172

75 Luo, S. and Rubinsztein, D.C. (2010) Apoptosis blocks Beclin 1-dependent autophagosome synthesis – an effect rescued by Bcl-xL. *Cell Death Differ*, 17, 268-277.

76 Van Laar, V.S., Arnold, B., Cassady, S.J., Chu, C.T., Burton, E.A. and Berman, S.B. Bioenergetics of neurons inhibit the translocation response of parkin following rapid mitochondrial depolarization. *Hum Mol Genet*, 2010 Dec 7.

77 Zhong, L., Tan, Y., Zhou, A., Yu, Q. and Zhou J. (2005). RING finger ubiquitin-protein isopeptide ligase Nrdp1/FLRF regulates parkin stability and activity. *J Biol Chem*, 280, 9425-9430.

78 Yoshii, S.R., Kishi, C., Ishihara, N. and Mizushima, N. Parkin mediates proteasome-dependent protein degradation and rupture of the outer mitochondrial membrane. *J Biol Chem*, 2011 Mar 18.

79 Chan, N.C., Salazar, A.M., Pham, A.H., Sweredoski, M.J., Kolawa, N.J., Graham, R.L., Hess, S. and Chan, D.C. (2011) Broad activation of the ubiquitin-proteasome system by Parkin is critical for mitophagy. *Hum Mol Genet*, **20**, 1726-1737

80 Tanaka, A., Cleland, M.M., Xu, S., Narendra, D.P., Suen, D.F., Karbowski, M. and Youle, R.J. (2010) Proteasome and p97 mediate mitophagy and degradation of mitofusins induced by Parkin. *J Cell Biol,* **191,** 1367-80.

81 Okatsu, K., Saisho, K., Shimanuki, M., Nakada, K., Shitara, H., Sou, Y.S., Kimura, M., Sato, S., Hattori, N., Komatsu, M. *et al.* (2010) p62/SQSTM1 cooperates with Parkin for perinuclear clustering of depolarized mitochondria. *Genes Cells,* **15,** 887-900.

82 Narendra, D., Kane, L.A., Hauser, D.N., Fearnley, I.M. and Youle, R.J. (2010) p62/SQSTM1 is required for Parkin-induced mitochondrial clustering but not mitophagy; VDAC1 is dispensable for both. *Autophagy,* **6,** 1090-106.

Human Molecular Genetics, 2007, Vol. 16, No. ? *1–11*
doi:10.1093/hmg/ddm289
Advance Access published on xxx

A block of autophagy in lysosomal storage disorders

Carmine Settembre[1,†], Alessandro Fraldi[1,†], Luca Jahreiss[2], Carmine Spampanato[1], Consuelo Venturi[3,4], Diego Medina[1], Raquel de Pablo[1], Carlo Tacchetti[3,4], David C. Rubinsztein[2,‡] and Andrea Ballabio[1,*]

[1]Telethon Institute of Genetics and Medicine (TIGEM), Naples, Italy [2]Department of Medical Genetics, Cambridge Institute for Medical Research, Cambridge, UK [3]Department of Experimental Medicine and [4]MicroSCoBiO Research Center and IFOM Center of Cell Oncology and Ultrastructure, University of Genoa, Genoa, Italy and [5]Medical Genetics, Department of Pediatrics, Federico II University, Naples, Italy

Received August 5, 2007; Revised and Accepted September 30, 2007

Most lysosomal storage disorders (LSDs) are caused by deficiencies of lysosomal hydrolases. While LSDs were among the first inherited diseases for which the underlying biochemical defects were identified, the mechanisms from enzyme deficiency to cell death are poorly understood. Here we show that lysosomal storage impairs autophagic delivery of bulk cytosolic contents to lysosomes. By studying the mouse models of two LSDs associated with severe neurodegeneration, multiple sulfatase deficiency (MSD) and mucopolysaccharidosis type IIIA (MPSIIIA), we observed an accumulation of autophagosomes resulting from defective autophagosome-lysosome fusion. An impairment of the autophagic pathway was demonstrated by the inefficient degradation of exogenous aggregate-prone proteins (i.e. expanded huntingtin and mutated alpha-synuclein) in cells from LSD mice. This impairment resulted in massive accumulation of polyubiquitinated proteins and of dysfunctional mitochondria which are the putative mediators of cell death. These data identify LSDs as 'autophagy disorders' and suggest the presence of common mechanisms in the pathogenesis of these and other neurodegenerative diseases.

INTRODUCTION

Deficiencies of specific lysosomal hydrolases in lysosomal storage disorders (LSDs) cause accumulation of their undegraded target substrates. However, it is not clear if these substrates themselves are the primary mediators of toxicity. Indeed, the biological pathways from lysosomal enzyme deficiency to cellular dysfunction are still largely unknown (1,2). Interestingly, despite the great structural diversity of the accumulating substrates in the different LSDs, these disorders share many phenotypic similarities, suggesting the presence of common pathogenetic mechanisms. Many LSDs are associated with progressive and severe neurodegeneration which represents the most difficult challenge for their therapy (2). In previous studies, we detected severe neurodegeneration in murine models of mucopolysaccharidoses type II and IIIA (MPSII and MPSIIIA, respectively) and of multiple sulfatase deficiency (MSD) (3–6).

The degradation of intracellular proteins is performed by two major mechanisms: the ubiquitin-proteasome system (UPS) and macroautophagy (hereafter referred to as autophagy). The latter is a lysosomal-dependent catabolic pathway through which long-lived cytosolic proteins and organelles, such as mitochondria, are sequestered by double membrane vesicles (autophagosomes) and ultimately degraded after autophagosome-lysosome fusion (7). Many of the aggregate-prone proteins causing late-onset neurodegenerative conditions, such as Huntington's and familial forms of Parkinson's

*To whom correspondence should be addressed at: Telethon Institute of Genetics and Medicine (TIGEM), Via P. Castellino 111, 80131 Napoli, Italy. Tel: +39 0816132207; Fax: +39 0815790919; Email: ballabio@tigem.it
†The authors wish it to be known that, in their opinion, the first two authors should be regarded as joint First Authors.
‡Both D.C.R. and A.B. should be regarded as senior authors.

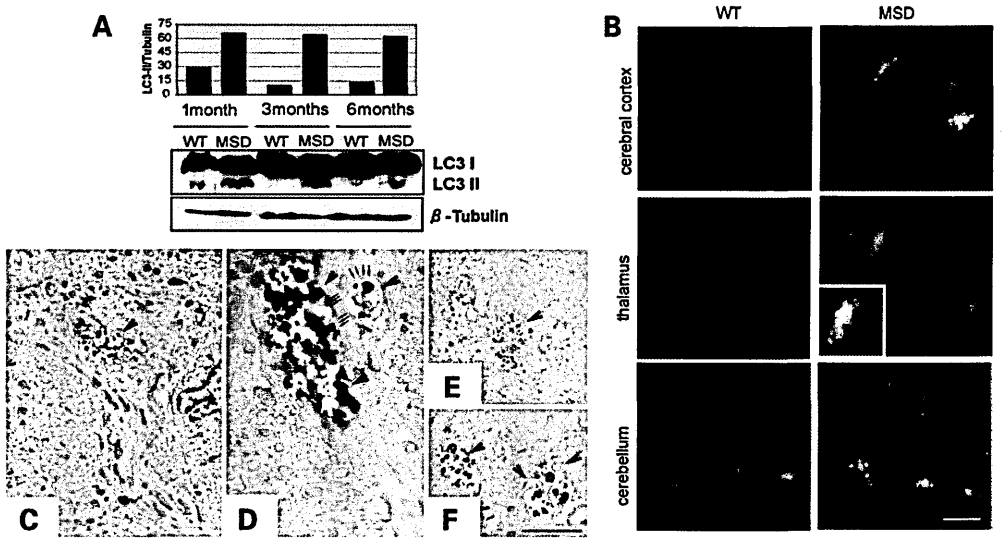

Figure 1. Accumulation of autophagosomes in MSD brain. (**A**) Anti-LC3 western blot of total brain homogenates prepared from 1, 3 and 6-month-old MSD and wild-type mice. (**B**) Immuno-fluorescence staining of LC3 in different brain regions of MSD mice and wild-type littermates. Bar = 15 μm. (**C–F**) Electron micrographs of both cerebellum (C and D) and cerebral cortex (E and F) from an MSD mouse. A neural process from a Purkinje cell, containing a large autophagosome (black arrowhead) and an enlargement of a portion of a neural process from a Purkinje cell are shown in (C). (D) Three autophagosomes (black arrowheads) in Purkinje cells surrounded by a double membrane (arrows) and containing remnants of cellular organelles. Membrane cisterns pile up in stacks (white arrowheads) by the autophagosomes. (E and F) Electron micrographs of autophagosomes (black arrowheads) in cerebral cortex. Bar: $d = 3.0$ μm; $e = 1.6$ μm; $f = 9.3$ μm; $g = 5.6$ μm.

diseases, are autophagy substrates (8). In addition, knock-out of autophagy genes causes abnormal protein accumulation in ubiquitinated inclusions and neurodegeneration in mice (9,10).

We hypothesized that LSDs are associated with a lysosomal dysfunction that impairs the autophagic pathway ultimately leading to cell death. To test this hypothesis, we studied the mouse models of two LSDs: MSD, which is caused by the deficiency of the sulfatase modifying factor 1 (*SUMF1*) gene involved in the post-translational modification of sulfatases (6,11,12), and MPS-IIIA, caused by sulfamidase deficiency (13). Our results revealed a block of autophagic pathway occurs as a consequence of decreased ability of lysosomes to fuse with autophagosomes. This results in the cellular accumulation of toxic substrates which are the putative mediators of cell death.

RESULTS

Increased autophagosome number in MSD

We assessed autophagosome number in brain sections from MSD mice by using an antibody detecting the autophagosome marker LC3 (14). During autophagosome formation, the LC3-I isoform is converted into LC3-II, whose amount (compared to actin or tubulin) correlates with the number of autophagosomes (14). LC3-II is the only known protein that specifically associates with autophagosomes and not with other vesicular structures. LC3-II levels were clearly raised in whole brain homogenates from MSD mice, compared to wild-type littermates at 1, 3 and 6 months of age (Fig. 1A). Furthermore, immuno-fluorescence analysis revealed increased numbers of LC3-positive vesicles in the cerebral cortex, cerebellum and thalamus of MSD mice, compared to corresponding brain regions of wild-type mice (Fig. 1B). Electron microscopy evaluation of cerebellum (Fig. 1C and D) and cerebral cortex (Fig. 1E and F) sections from MSD mice showed abnormally abundant autophagosomes. Interestingly, the morphology of autophagic vacuoles accumulating in MSD mice resembled that of early immature autophagosomes (15,16) (Fig. 1C–F), suggesting the presence of a defective maturation.

A similar increase in LC3-II levels was observed in mouse embryonic fibroblasts (MEFs) and embryonic liver macrophages (ELMs) (Fig. 2A)—macrophages were previously identified as the primary site of lysosomal storage in MSD mice (6). The increase in both number and size of autophagosomes was confirmed in MEFs by quantitative analysis (Fig. 2B and C).

Autophagosome-lysosome fusion is impaired in MSD

Clearance of autophagosomes occurs via fusion with lysosomes. We postulated that accumulation of autophagosomes

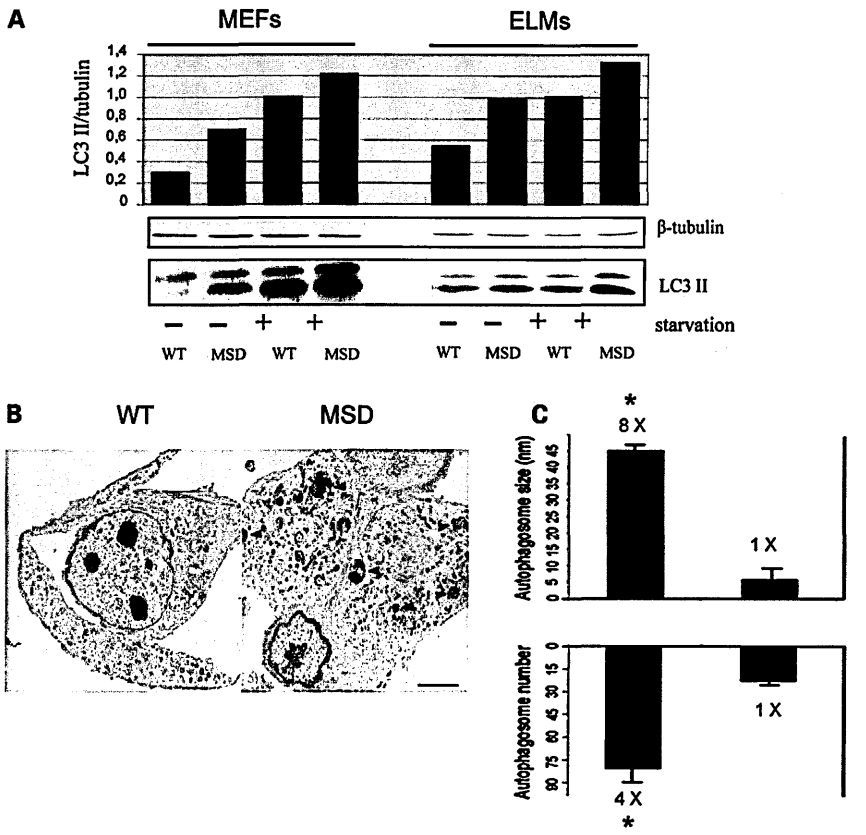

Figure 2. Accumulation of autophagosomes in MSD cultured cells. **(A)** Anti-LC3 western blot of protein extracts prepared from MEFs and ELMs derived from MSD and wild-type mice in both normal and starved conditions. **(B)** MSD MEFs display several autophagosomes (arrowheads), compared to wild-type. Bar = 9.3 μm. **(C)** Morphometric evaluation revealed that autophasomes were more numerous and larger in MSD MEFs compared to those observed in wild-type MEFs. $^{*}P < 0.05$.

in MSD is due to defective clearance caused by impaired autophagosome-lysosome fusion. To test this hypothesis, we analyzed the subcellular localization of the lysosomal marker lgp120 (LAMP1) and the autophagosomal marker LC3 by confocal microscopy. These experiments demonstrated that the extent of lgp120/LC3 co-localization was significantly reduced (ranging from 40 to 50%) in MSD compared to wild-type MEFs, thus indicating impaired autophagosome-lysosome fusion (Fig. 3A and B). This was observed both in normal medium (basal autophagy) (Fig. 3A) and in starved cells (induced autophagy) (Fig. 3B).

To characterize this impairment, we used drugs which either induce or inhibit autophagy. Autophagy stimulation with rapamycin increased LC3-II levels in both MSD and wild-type MEFs (Fig. 4). Moreover, LC3-II levels in MSD MEFs were further increased with bafilomycin A1, an inhibitor autophagosome-lysosome fusion (17), alone or in combination with rapamycin, suggesting that the block of autophagy is not complete (Fig. 4).

Decreased ability of MSD cells to degrade exogenous aggregate-prone proteins

Defective autophagosome-lysosome fusion may lead to an impairment of autophagy. We investigated the ability of MSD cells to degrade aggregate-prone proteins which are autophagy substrates (18). These include the mutant huntingtin and A53T α-synuclein which are involved in Huntington and familial Parkinson diseases, respectively. Mutant huntingtin exon 1 constructs aggregate readily in tissue culture and form inclusions readily visible by light microscopy. The proportion of cells with such inclusion is linearly related to the expression levels of the construct (19). The A53T α-synuclein construct does not form overt inclusions in the cell lines we

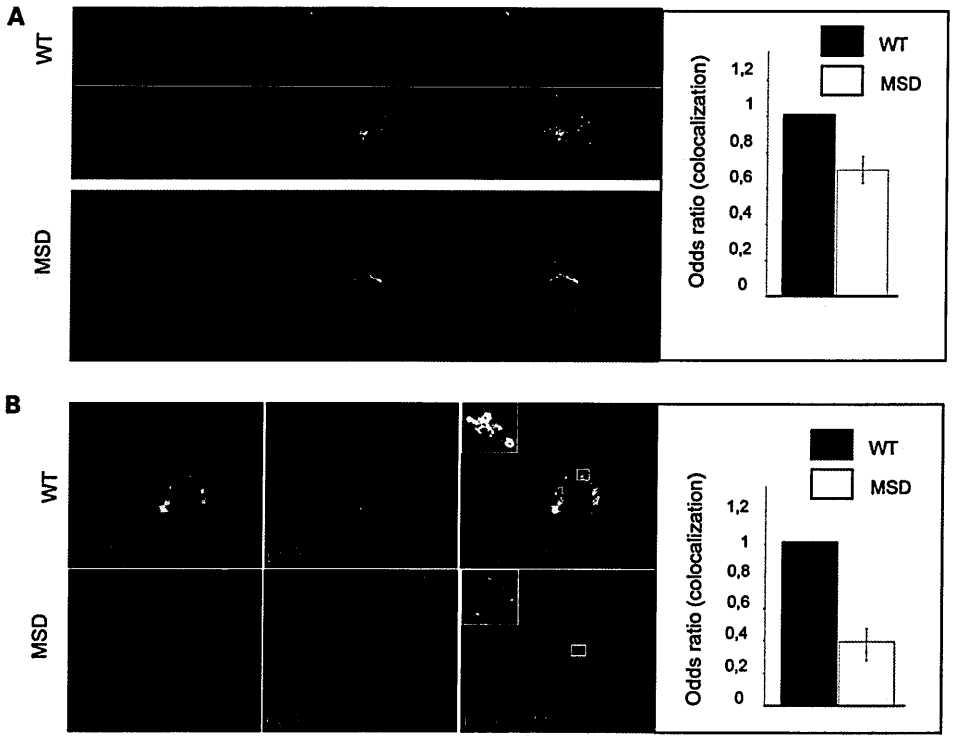

Figure 3. Defective autophagosome-lysosome fusion in MSD MEFs. (**A** and **B**) Co-localization of LAMP1 and LC3 in wild-type and MSD MEFs stained for LAMP1 (red) and LC3 (green). Confocal microscopy shows a reduction in the extent of co-localization of LAMP1 and LC3 proteins. The figure was selected to illustrate the basis for the assays we have quantified. The number of autophagosome-lysosome fusion events in MSD MEFs was quantified both in normal (A) and starved (B) serum conditions, as described in the Methods section.

have studied (20). We expressed these mutant proteins in MSD cells to test the functionality of the autophagic pathway. The Gln_{74};Q74 huntingtin, which encodes the first exon of huntingtin with 74 glutamine repeats, and the A53T α-synuclein were fused to green fluorescent protein (GFP) and transiently expressed in both MEFs and ELMs derived from MSD mice. Forty-eight hours after transfection, cells were collected and GFP-fused proteins were detected by western blot. Figure 5A shows an increased accumulation of both types of mutant proteins in MSD compared to wild-type cells. In addition, immuno-fluorescence analysis revealed that the number of GFP-Q74 aggregates was also significantly higher in MSD MEFs and ELMs compared to wild-type cells (Fig. 5B and C). Notably, when cells were analyzed at earlier time points, no significant differences in the accumulation of GFP-Q74 were observed between wild-type and MSD cells (Supplementary Material), this indicating that only at later time points accumulation of overexpressed proteins occurs. Moreover, GFP alone did not accumulate in MSD cells (Supplementary Material) demonstrating that increased levels of GFP-Q74 and GFP-A53T are due to autophagic defective degradation and not to difference in transfection efficiency.

Taken together, these data indicate a dysfunction of autophagy with consequent decreased ability of MSD cells to degrade aggregate-prone proteins.

Polyubiquitinated proteins progressively accumulate in MSD neurons

Autophagy is responsible for constitutive protein turnover (8). This function appears to be particularly important in neuronal cells and is relevant to neurodegenerative diseases (21,22). Knockout of autophagy genes results in suppression of autophagy and accumulation of inclusion bodies, which contain polyubiquitinated proteins, in neurons (9,10). We detected a massive and progressive accumulation of ubiquitin-positive inclusions in the cerebral cortex as well as in other brain regions of MSD mice by both anti Ub immuno-histochemical and immuno-fluorescence analyses (Fig. 6A and B and data not shown). Co-localization of Ubiquitin with NeuN neuronal marker indicates that

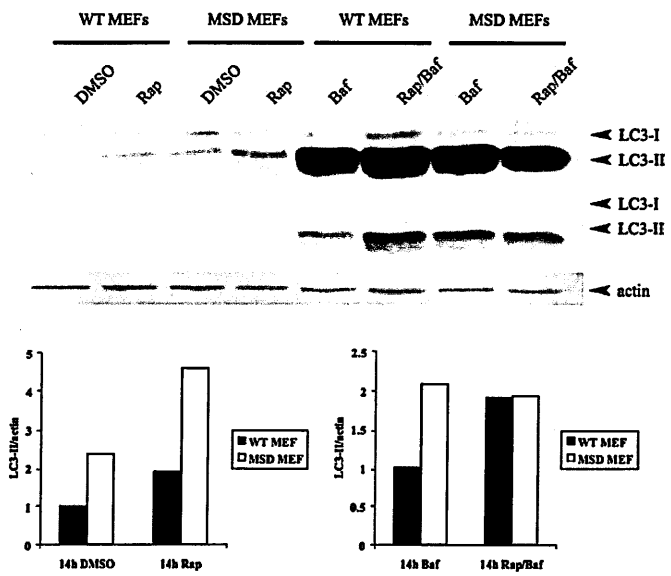

Figure 4. Evaluation of LC3 levels in MSD and wild-type MEFs after induction and/or inhibition of autophagy. Both wild-type and MSD MEFs were treated with indicated drugs. Western-blot analysis (top) was performed using anti-LC3 antibodies. Quantitation (bottom) was performed by normalizing with actin levels. The middle lane in the western blot is a lower exposure of the upper lane.

ubiquitin inclusions are located in neurons (Fig. 6B). Progressive accumulation of polyubiquitinated proteins was also detected by western blotting of brain homogenates (Fig. 6C). Importantly, analysis of chymotrypsin-like proteasome activity in MSD brain at several ages revealed that proteasome function is not affected in MSD mice (data not shown), indicating that the accumulation of ubiquitinated proteins is due to defective autophagy rather than to UPS impairment.

In addition, we found that P62/SQSTM1 significantly accumulates (Fig. 6D), and co-localizes with ubiquitin-positive inclusions (Fig. 6E) in brain from MSD mice. The p62/SQSTM1 protein is known to be a common component of ubiquitin-positive protein aggregates in neurodegenerative diseases (23), being involved in the targeting of polyubiquitinated proteins to the autophagosomes and selectively degraded via the autophagic pathway (24).

Accumulation of dysfunctional mitochondria in MSD mice

Autophagy also plays a crucial role in the degradation and turnover of cellular organelles like mitochondria. Indeed, it has been suggested that autophagy selectively degrades dysfunctional mitochondria (25). Fragmented and dysfunctional mitochondria have been reported to accumulate in patients with mucolipidosis types II, III and IV and in patients with neuronal ceroid lipofuscinosis 2 (NCL2), suggesting that lysosomal storage in these diseases impairs autophagy-mediated mitochondrial turnover (26,27). Electron microscopy analysis revealed an increased number of mitochondria in MSD brain sections and MEFs (Fig. 7A and B). Consistently, an increase of Cox4 (a mitochondrial marker) levels was detected by western blotting in MSD brain samples (Fig. 7C). To examine the function of accumulating mitochondria, we measured the mitochondrial membrane potential ($\Delta\Psi m$) in WT and MSD MEFs by using a mitochondria-specific voltage dependent dye ($DiOC_6$). As shown in Fig. 7D, MSD MEFs show a significant reduction in the $\Delta\Psi m$ compared to wild-type cells in both normal and starved conditions, thus indicating that mitochondria accumulating in MSD are dysfunctional.

Impairment of autophagy in MPSIIIA

Overall, our data identify an impairment of autophagy in MSD, leading to the accumulation of polyubiquitinated proteins and of dysfunctional mitochondria. To investigate whether this applies to other LSDs caused by defective hydrolases, we analyzed the autophagic pathway in the murine model of MPSIIIA, which is also associated with severe neurodegeneration (4,5). The results obtained in MPSIIIA mice were similar to those of MSD mice. We detected increased LC3II levels in MPSIIIA MEFs (Fig. 8A) as well as accumulation of autophagosomes in brain samples (Fig. 8B). Consequently, accumulation of ubiquitin-positive inclusions (Fig. 8C) and P62/SQSTM1 (Fig. 8D) were observed in the brain of MPSIIIA mice. In addition, electron microscopy analysis revealed an increased number of mitochondria in

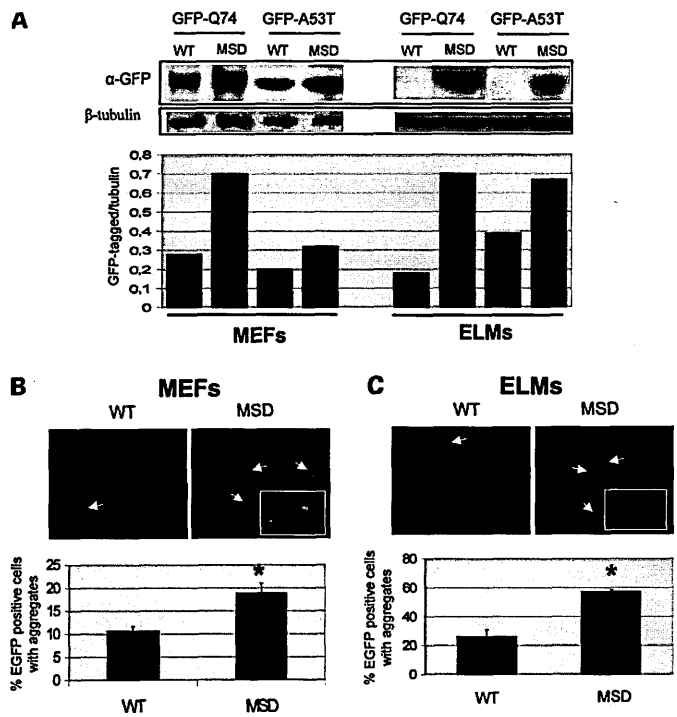

Figure 5. Decreased ability of MSD cells to degrade exogenous aggregate-prone proteins. (A) Gln_{74}:Q74 huntingtin (encoding the first exon of expanded huntingtin containing 74 glutamine repeats) or A53T α-synuclein were transiently expressed (48 h) as GFP-tagged proteins along with GFP (GFP proteins:GFP 1,5:1 ratio) in both MEFs and ELMs derived from MSD and wild-type mice. The amount of GFP-Q74 and GFP-A53T proteins was then assessed by anti-GFP western blot. (**B** and **C**) Fluorescence microscopy evaluation of GFP-aggregates in MEFs (B) and ELMs (C) expressing GFP-Q74 huntingtin. Transfected MSD MEFs and ELMs displayed a significant increase in percentage of GFP-positive cell containing aggregates compared to transfected wild-type cells. Cell counts were performed on three independent experiments and 50 cells were analyzed in each experiment. $^*P < 0.05$.

MPSIIIA brain (data not shown). Similarly to MSD, accumulation of toxic substrates was observed in the absence of any detectable impairment of proteasome function (data not shown).

DISCUSSION

Mucopolysaccharidoses represent a substantial proportion (~25%) of all LSDs (28). Our results in MSD and MPSIIIA indicate that lysosomal storage in these diseases causes cellular dysfunction by blocking autophagic protein clearance. We provide evidence for this block at both structural (i.e. defective autophagosome-lysosome fusion) and functional levels (i.e. impaired ability of cells to degrade exogenous aggregate-prone proteins, and accumulation of endogenous substrates, such as ubiquitinated proteins, P62 and mitochondria).

Accumulation of ubiquitinated proteins was also observed in mice with autophagy gene knockouts and likely results from increased ubiquitination of substrates by virtue of their longer half-lives. These mice show severe neurodegeneration, suggesting that neurons, compared to other cell types, are more susceptible to a block of autophagy. This may be because non-mitotic cells cannot dilute accumulating cytosolic contents by cell division. This may also explain the prevalence of a neurological phenotype in LSDs.

Furthermore, our data provide an explanation for previous reports of autophagosome accumulation in other types of LSDs, namely Danon disease (15), NCL2 (26,29), Glycogenosis type II (Pompe disease) (30) and Mucolipidosis IV (27). Note that these previous studies did not resolve the crucial issue if the autophagosome accumulation was due to increased formation of autophagosomes (which would lead to increased degradation of autophagic substrates), or decreased autophagosome-lysosome fusion (which results in decreased degradation of such substrates). Clearly, these different scenarios result in vastly different pathological consequences. An induction, rather than a block, of autophagy was observed in NPC types 1 and 2, associated with increased levels of beclin-1 expression (31,32). However, NPC represents the 'atypical' type of LSD as it is caused by mutations in cholesterol transporters, thus suggesting a direct role of lipid

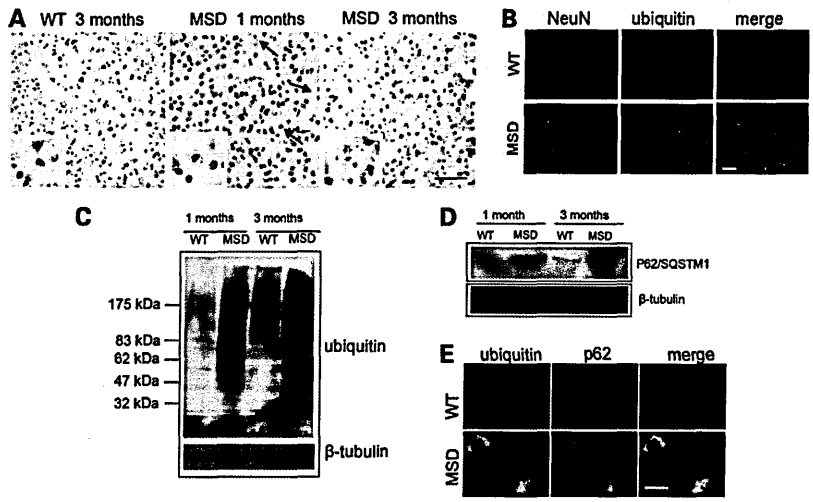

Figure 6. Accumulation of ubiquitin-positive inclusions and of P62 in MSD brain. **(A)** Immuno-histochemical staining of ubiquitinated proteins in the cerebral cortex of a 1-month-old wild-type mouse and of 1 and 3 month-old MSD mice. Bar = 30 μm. **(B)** Anti-Ub (green) and anti-NeuN (red) immuno-fluorecence of cerebral cortex sections derived from MSD and wild-type mice showing the presence of ubiquitin-positive inclusions in MSD neurons. Bar = 20 μm. **(C)** Anti-Ub western blot from total brain homogenates derived from 1 and 3 month-old MSD mice and wild-type littermates. **(D)** Western blot analysis of total brain homogenates showing progressive accumulation of P62 in MSD. **(E)** Immuno-fluorescence with anti-P62 (red) and anti-Ub (green) showed significant co-localization of P62 with polyubiquitinated proteins in the brain of MSD mice. Bar = 12 μm.

trafficking in the regulation of autophagy (32). Accordingly, we found no differences in beclin-1 expression between tissues from MSD mice and wild-type littermates (data not shown).

We propose a model which identifies a block of autophagy as a crucial component in the pathogenesis of LSDs (Fig. 9). According to this model, lysosomal accumulation of undegraded substrates results in defective fusion between autophagosomes and lysosomes and causes a block of the autophagic pathway. As a consequence of this block, toxic proteins and dysfuctional mitochondria accumulate, ultimately leading to apoptosis, either directly or through the induction of chronic inflammation and cytokine release (6). Indeed, cells with impaired autophagy have an increased susceptibility to mitochondria-mediated apoptosis (33,34). It is interesting to note that bafilomycin A1, a proton-pump inhibitor which attenuates lysosomal acidification, results in similar blocks in autophagosome-lysosome fusion as LSDs, suggesting that there may be ways that defective lysosomal function feed back to inhibit autophagosome-lysosome fusion.

Importantly, we found that the ubiquitin-proteasome degradation is not impaired in our LSD mouse models. Proteasome dysfunction may lead to the accumulation of ubiquitinated inclusions (35) and has been associated to neurodegenerative diseases (36–38). The finding that UPS is functional in our LSD models allows us to conclude that the block of autophagy pathway is the only mechanism accounting for the accumulation of ubiquitinated proteins which are the putative mediators of cell death in LSDs. Interestingly, a recent work from Pandey *et al.* (39) showed that autophagy and proteasome are compensatory interacting systems, and pointed to the role of autophagy in rescuing protein degradation deficiency due to the proteasome impairment. This finding raises the possibility to exploit new therapeutic approaches for LSDs based on pharmacological induction of proteasome function in order to compensate for autophagy deficiency.

Our model defines LSDs as 'autophagy disorders', resembling more common neurodegenerative diseases such as Alzheimer (AD), Parkinson (PD) and Huntington (HD) diseases. While there are major differences in the initial steps involved in all these diseases (i.e. impaired degradation of polyubiquitinated proteins in LSDs versus expression of aggregate-prone proteins in AD, PD and HD), our data suggest that they may share common mechanisms suggesting the possibility of overlapping therapeutic strategies.

METHODS

Generation of MEFs and ELMs

MEFs were isolated by trypsinization of littermate embryos isolated at E14 and grown in DMEM supplemented with 20% FBS and penicillin/streptomycin. Fetal liver cells were isolated from E14.5 embryos by mechanical homogenization and filtering through a 40 μm cell-strained. The cells were resuspended in DMEM plus 10% fetal bovine serum and allowed to attach to plastic. Adherent macrophages (obtained by washing wells in DMEM to remove non-adherent cells) were cultured in macrophage medium (PAA) and repurified by immune-separation using CD11b-coating magnetic beads

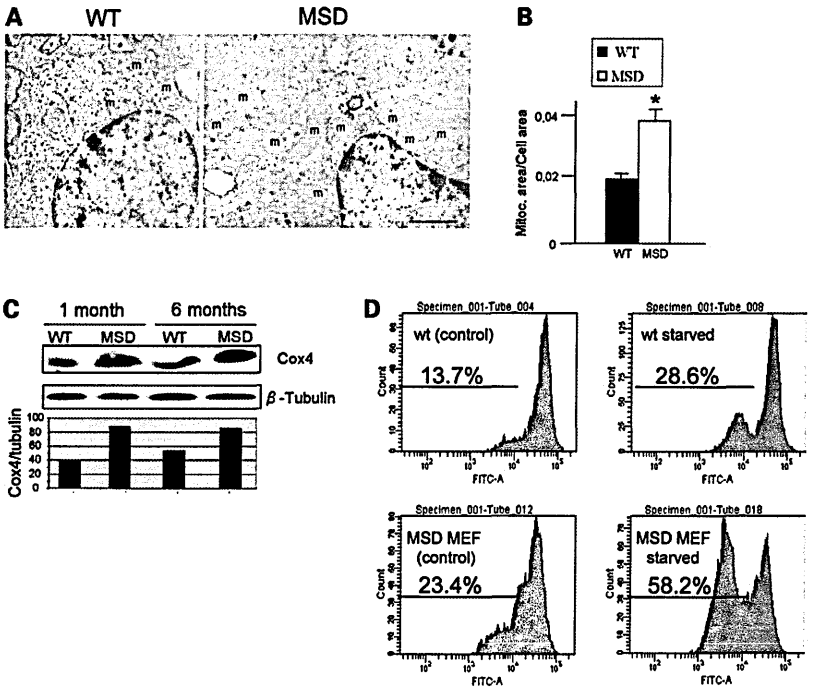

Figure 7. Accumulation of dysfunctional mitochondria in MEFs and brain of MSD mice. (**A** and **B**) Electron microscopy analysis of the brain cortex neurons from MSD mice and wild-type littermates (bar: wild-type = 2.1 μm; MSD = 1.8 μm). MSD neurons contain a significantly higher number of mitochondria (m) compared to wild type neurons as also evident from quantitative analysis (B) (*$P < 0.05$). (**C**) Western blot analysis using antibodies recognizing Cox4, a mitochondrial marker, shows increased levels of Cox4 in MSD compared to wild-type MEFs. (**D**) Wild-type and MSD MEFs were grown in either normal serum or starved conditions (4 h). Cells were then stained with 40 nM DiOC6 and 1 μg/ml propidium iodine. ΔΥm was measured by flow cytometry. Propidium iodine was used as counterstain. All experiments were performed in triplicate and analyzed using Stat-View software and ANOVA test. Results were considered significant if $P < 0.05$.

(MACs technology, Miltenyi Biotec). Macrophages were characterized by the expression of MOMA-2, and F4/80 antigens by immuno-fluorescence.

Transfections and drug treatments

Sub-confluent cells (MEFs or ELMs) were transfected using lipofectamine™ 2000 (Invitrogen) according manufacturer's protocols. For co-localization experiments in normal serum conditions, sub-confluent MEFs were co-transfected with 0.5 μg lgp120-GFP and 1 μg mCherry-LC3mCherry-LC3 and cultured in full medium for 24 h. For drug treatments, cells were treated for 14 h with 0.2 mg/ml rapamycin (Sigma), 200 nM bafilomycin A1 (Upstate).

Cloning of mCherry-hLC3B construct

Human LC3B was subcloned from pGEX-6P-1 into pcDNA3 (Invitrogen) using BamHI and EcoRI (both NEB). mCherry pRSET-B was amplified by PCR with the following primers: 5'-TA CCG AGC TCG GTA CCC GCC ACC AT-3' and 3'-G CTG TAC AAG CAA GGA TCC TGC-5'. The resulting fragments were purified, digested with KpnI and EcoRI (both NEB) and sub-cloned in frame into the 5' end of hLC3B pcDNA3.

Antibodies

Primary antibodies were: rabbit polyclonal anti-LC3 (Novus Biological), rat monoclonal anti-mouse LAMP1 (Developmental Studies Hybridoma Bank, Iowa), rabbit polyclonal anti-ubiquitin (DakoCytomation), mouse monoclonal anti-NeuN (Chemicon), mouse monoclonal P62/SQSTM1 (BD), rabbit polyclonal anti-tubulin (Cell signaling), rabbit polyclonal anti-actin (Sigma) and mouse monoclonal anti-COX4 (Clontech). Secondary antibodies were: goat anti-rabbit or anti-rat conjugated to Alexa Fluor 488 or 594 (Molecular Probes, Eugene, OR, USA). HRP-conjugated anti-mouse or anti-rabbit IgG (Amersham); biotinylated donkey anti-rabbit (Jackson ImmunoReasearch).

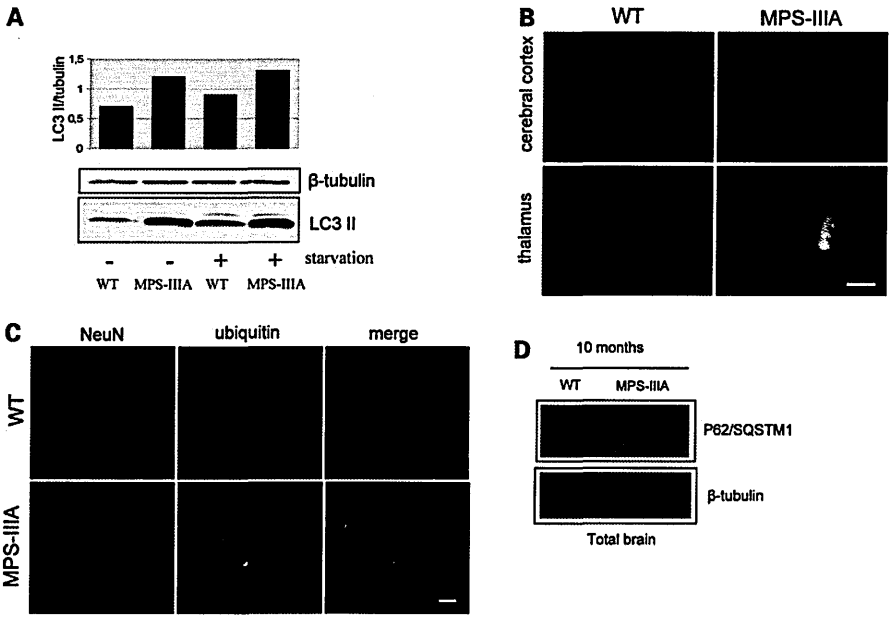

Figure 8. Autophagy impairment in MPSIIIA mice. (**A**) Anti-LC3 western blot of MPSIIIA and wild-type MEFs in either normal or starved serum conditions. Quantification of LC3 protein levels shows an increase of the LC3-II isoform in MPSIIIA MEFs in either normal or starved serum conditions. (**B**) Immunofluorescence staining of LC3 in the thalamus and cerebral cortex of MPSIIIA and wild-type mice. Bar = 7 μm. (**C**) Anti-Ub immuno-fluorescence analysis of MPSIIIA mouse brain showing accumulation of ubiquitinated proteins (green) in neurons (NeuN marker:red). Bar = 20 μm. (**D**) Anti-P62 western blot of total brain homogenates from MPSIIIA and wild-type mice. The levels of P62 protein are significantly higher in MPSIIIA mouse brain.

Western blot

Cells were lysed in cold lysis buffer (20 mM Tris–HCl, pH 7.4,150 mM NaCl, 1% TritonX-100) in the presence of protease inhibitors (Roche Diagnostics) for 30 min on ice. Brain tissue samples were homogenized in sucrose buffer, centrifuged and resulting supernatants lysed in TritonX-100. Proteins were transferred onto nitrocellulose membrane (Amersham Pharmacia Biotech). Primary and (HRP)-conjugated antibodies were diluted in 5% milk. Bands were visualized using the ECL detection reagent (Pierce). Proteins were quantified by the Bradford method.

GFP analysis and immuno-staining

Cells were grown on coverslips and fixed in PBS pH 7.4 4% paraformaldehyde (GFP analysis) for 20 min. Tissues were fixed overnight in PBS pH 7.4 4% paraformaldehyde and were embedded in optimal cutting temperature compound (Tissue Tek). Cryostat sections were cut at 10 mM. For immunofluorescence analysis, cells/tissues were permeabilized and incubated with appropriate primary and secondary antibodies (diluted in PBS+1% FBS). Immuno-histochemistry was performed using Vectastain ABC kit (Vector Laboratories, Burlingame, CA, USA) according to standard protocols. Cells/tissue slides were mounted and cover-slipped in glycerol/DAPI and viewed on an epi-fluorescent microscope or counterstained with hematoxylin and viewed on a light microscope (immuno-histochemical analysis).

Confocal microscopy

For co-localization analysis in normal serum conditions, cover slips were blinded and 20 cells per cell line per experiment were imaged on a Zeiss Axiovert 200 M microscope with a LSM 510 confocal attachment using a ×63 1.4 NA Plan Apochromat oil-immersion lens. Laser lines at 488 nm (lgp120-GFP) and 543 nm (mCherry-LC3) were used. The detector pinholes were set to give a 0.9 μm optical slice. Acquisition was performed using Zeiss LSM 510 software. These cells were then analysed in *Zeiss LSM Image Browser 3.5* as follows: first, only mCherry-LC3+ vesicles were counted and marked, by switching off the GFP-channel. Then, the GFP-channel was switched back on and the number of co-localized vesicles was counted. From these two values, the fraction of co-localized vesicles was then determined. The number of autophagosome-lysosome fusion events in starved MSD and wild-type MEFs were determined by the analysis of confocal images [obtained by a Leica TCS SP2 AOBS confocal microscope with a ×63 Neofluor Pan-Apo 1.3 nm oil objective with laser lines at 488 nm (LC3) and 594 nm (LAMP1)] utilizing Volocity 3.7.0 software

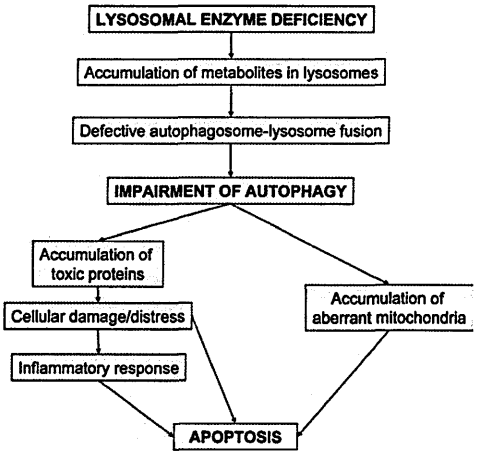

Figure 9. A proposed model for the pathogenesis of LSDs. A defect in lysosomal degradation results in the accumulation of substrates in the lysosomes. Lysosomal storage leads to a reduced ability of lysosomes to fuse with autophagosomes with a consequent block of autophagy. Polyubiquitinated protein aggregates and dysfunctional mitochondria accumulate and promote apoptosis-mediated cell death. The inflammatory response to cell damage further contributes to cell death.

(Improvision). Pearson's correlation was used as a value of co-localization between autophagosomes and lysosomes.

Mitochondrial membrane potential measurements

PBS-washed 1×10^6 cells were incubated in 40 nM $DiOC_6$ (Sigma-Aldrich) and 1 μg/ml PI (Sigma-Aldrich) for 15 min at 37°C. After washing, cells were suspended in 1 ml PBS (pH 7.4) and were subsequently analyzed using flow cytometry. For the $DiOC_6$-stained samples, PI-negative cells were excluded of the analysis. Normal and starved MSD and wild-type MEFs were analyzed at the same passage and treated in the same way. At least 10 000 cells were analyzed for each sample. The experiments were performed at least in triplicate, and all statistical analyses were performed using Stat-View 5.0 (Statsoft, USA).

Electron microscopy analysis

MEFs were fixed at room temperature, in 2.5% glutaraldehyde (Polysciences, Inc., Warrington, PA, USA), 0.1 M sodium cacodylate–HCl buffer, pH 7.3, for 10 min, scraped off the dish, pelletted by centrifugation and postfixed in 1% OsO4 (Polyscience) in the same buffer, for 20 min. After en bloc staining with 1% uranyl acetate for 1 h and ethanol dehydration, cells were embedded in LX112 (Polyscience). Tissue preparations were performed as previously described (26). Grey-silver sections were visualized using FEICM10 and Tecnai12G2 microscopes. Morphometry assessment of both number and size of the autophagosomes in MSD and wild-type MEFs was performed by the point intersection method.

Assay of proteasome activity

Chymotrypsin-like activity of 20S proteasomes was measured on brain homogenates using Suc-LLVY-AMC as substrate (20S proteasome activity assay kit; Chemicon).

Data analysis

Data were analyzed by one-way ANOVA (analysis of variance). A P-value <0.05 was considered to be statistically significant. Odds ratios for co-localization LAMP1-LC3 were determined by unconditional logistical regression analysis, using the general log-linear analysis option of *SPSS* 9 software (SPSS, Chicago).

SUPPLEMENTARY MATERIAL

Supplementary Material is available at HMG Online.

ACKNOWLEDGEMENTS

We are grateful to G. Andria, P. Ducy, G. Karsenty and R. Sitia for critical reading of the manuscript, to M. Mizuguchi for human LC3B, to P.Luzio for GFP-lgp120, and to R. Tsien for mCherry. C. Settembre is the recipient of a pre-doctoral fellowship of the European School of Molecular Medicine (SEMM).

Conflict of Interest statement. The authors declare that they have no competing financial interests.

FUNDING

Financial support from the Italian Telethon Foundation is gratefully acknowledged. We are also grateful to MRC (Grant to D.C.R. and studentship for L.J.), Wellcome Trust (Senior Fellowship in Clinical Science to D.C.R.), MIPAF (grant to A.B.), FIRB and MIUR (grants to C.T.) for funding. Electron microscopy has been performed at the Telethon facility for EM (grant GTF03001 to C.T.).

REFERENCES

1. Futerman, A.H. and van Meer, G. (2004) The cell biology of lysosomal storage disorders. *Nat. Rev. Mol. Cell. Biol.*, **5**, 554–565.
2. Jeyakumar, M., Dwek, R.A., Butters, T.D. and Platt, F.M. (2005) Storage solutions: treating lysosomal disorders of the brain. *Nat. Rev. Neurosci.*, **6**, 713–725.
3. Cardone, M., Polito, V.A., Pepe, S., Mann, L., D'Azzo, A., Auricchio, A., Ballabio, A. and Cosma, M.P. (2006) Correction of Hunter syndrome in the MPSII mouse model by AAV2/8-mediated gene delivery. *Hum. Mol. Genet.*, **15**, 1225–1236.
4. Hemsley, K.M. and Hopwood, J.J. (2005) Development of motor deficits in a murine model of mucopolysaccharidosis type IIIA (MPS-IIIA). *Behav. Brain Res.*, **158**, 191–199.
5. Fraldi, A., Hemsley, K., Crawley, A., Lombardi, A., Lau, A., Sutherland, L., Auricchio, A., Ballabio, A. and Hopwood, J. (2007) Functional correction of CNS lesions in a MPS-IIIA mouse model by intracerebral

RESEARCH COMMUNICATION

Proteoglycan desulfation determines the efficiency of chondrocyte autophagy and the extent of FGF signaling during endochondral ossification

Carmine Settembre,[1,2] Emilio Arteaga-Solis,[1] Marc D. McKee,[3] Raquel de Pablo,[2] Qais Al Awqati,[1] Andrea Ballabio,[2,4] and Gerard Karsenty[1,5]

Department of Genetics and Development, College of Physicians and Surgeons, Columbia University, New York, New York 10032, USA; Telethon Institute of Genetic and Medicine (TIGEM), Naples 80131, Italy; Faculty of Dentistry, and Department of Anatomy and Cell Biology, McGill University, Montreal, Quebec H3A 2B2, Canada; Medical Genetics, Department of Pediatrics, Federico II University, Naples 80131, Italy

Cartilage extracellular matrix (ECM) contains large amounts of proteoglycans made of a protein core decorated by highly sulfated sugar chains, the glycosaminoglycans (GAGs). GAGs desulfation, a necessary step for their degradation, is exerted by sulfatases that are activated by another enzyme, Sulfatase-Modifying Factor 1 (SUMF1), whose inactivation in humans leads to severe skeletal abnormalities. We show here that despite being expressed in both osteoblasts and chondrocytes *Sumf1* does not affect osteoblast differentiation. Conversely, in chondrocytes it favors ECM production and autophagy and promotes proliferation and differentiation by limiting FGF signaling. Thus, proteoglycan desulfation is a critical regulator of chondrogenesis.

Supplemental material is available at http://www.genesdev.org.

Received June 28, 2008; revised version accepted August 11, 2008.

Endochondral ossification, a multistep process responsible for embryonic bone formation and postnatal longitudinal bone growth (Kronenberg 2003), begins once mesenchymal cells condense, forming the blueprint of the future skeleton. Then, these mesenchymal cells differentiate into resting and proliferating chondrocytes that express *Aggrecan* and α *(II) Collagen* while cells at the periphery express α *(I) Collagen* and form the perichondrium. Subsequently, chondrocytes in the center of this structure further differentiate into hypertrophic chondrocytes expressing α *(X) Collagen* but not *Aggrecan* and α *(II) Collagen*. The extracellular matrix (ECM) secreted by hypertrophic chondrocytes allows vascular invasion, degradation of the calcified ECM, and initiation of osteogenesis. Thus, the ECM plays important functions during skeletal development (Olsen et al. 2000).

Alongside collagen fibrils the cartilagineous ECM contains large amounts of proteoglycans that protect these fibrils and provide resistance against compression. Proteoglycans are composed of a protein core to which one or more highly sulfated polysaccharide chains (glycosaminoglycan [GAG]) bind. The GAGs moiety of proteoglycans can regulate the distribution and binding ability of several signaling molecules, thereby influencing developmental processes. GAGs fulfill these functions according to their degree of sulfation (Esko and Selleck 2002; Perrimon and Hacker 2004) a process determined by two classes of intracellular enzymes: the sulfotransferases, that catalyze incorporation of sulfated groups into a nascent molecule, and the sulfatases, that remove them (Diez-Roux and Ballabio 2005; Bulow and Hobert 2006).

There are at least 17 different sulfatases in vertebrates, whose function is determined by their subcellular localization in the lysosomes, cell surface, or ER/Golgi, and by substrates specificity (Diez-Roux and Ballabio 2005). In addition, sulfatase becomes active following a post-translational formylglycination catalyzed by the enzyme Sulfatase-Modifying Factor 1 (Sumf1) (Cosma et al. 2003). To date, no other substrates besides the sulfatases have been identified for Sumf1 (Diez-Roux and Ballabio 2005); hence, it can be viewed as the master regulator of proteoglycan desulfation. Further underscoring the biological importance of Sumf1 and of proteoglycan desulfation a broad spectrum of diseases, most of them including skeletal abnormalities, results from loss of function mutations in various sulfatases or in Sumf1 itself (Diez-Roux and Ballabio 2005). In most of these diseases, called mucopolysaccharidoses, the lack of lysosomal sulfatases causes a block in GAG degradation and an intralysosomal GAG accumulation (Neufeld and Muenzer 2001).

In order to define the importance of proteoglycan desulfation during skeletogenesis we studied mice lacking *Sumf1* (Settembre et al. 2007). We show here that although *Sumf1* is expressed in osteoblasts during skeletogenesis, it has no overt function in osteoblasts. In contrast, *Sumf1* and, as a result, proteoglycan desulfation, favors ECM production, chondrocyte autophagy, and promotes chondrocyte proliferation and differentiation. Genetic and biochemical evidence show that *Sumf1* regulation of chondrocyte proliferation and differentiation occurs by inhibiting FGF signaling.

Results and Discussion

Sumf1 expression during skeletogenesis

To determine whether *Sumf1* is an appropriate tool to study the role(s) of proteoglycan desulfation during skeletogenesis we examined its pattern of expression using a *LacZ* gene inserted in the *Sumf1* locus (Settembre et al. 2007). β-Galactosidase staining of whole embryos showed that *Sumf1* starts to be expressed in skeletal elements as early as embryonic day 14.5 (E14.5) (Fig. 1A–C). Histological analysis revealed that this staining was

Keywords: Proteoglycan; desulfation; FGF; chondrocytes]
Corresponding author.
E-MAIL gk2172@columbia.edu; FAX (212) 923-2090.
Article is online at http://www.genesdev.org/cgi/doi/10.1101/gad.1711308.

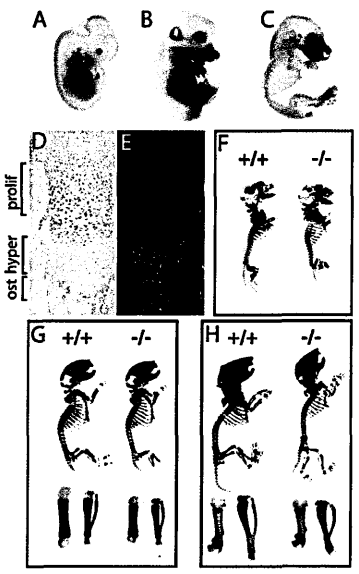

Figure 1. Skeletal development in *Sumf1*$^{-/-}$ embryos and mice. (*A–C*) X-gal-stained *Sumf1*$^{+/-}$ E12.5, E14.5, and E16.5 embryos. *LacZ* was expressed in all cartilagineous elements starting at E14.5. (*D*) Femoral growth plate section showing *LacZ* staining in proliferating chondrocytes and osteoblasts. (*E*) In situ hybridization of *Sumf1* in E16.5 growth plate. (*F–H*) Alcian blue/alizarin red staining of E16.5 (*F*), newborn (*G*), and P4 (*H*) wild-type and *Sumf1*$^{-/-}$ embryos and mice. (*G,H*) Femur and tibia magnification of newborn and P4 *Sumf1*$^{-/-}$ and wild-type mice.

equally strong in proliferating chondrocytes of the growth plate and in osteoblasts of the developing bones, while staining in hypertrophic chondrocytes was weak (Fig. 1D); in situ hybridization analysis of *Sumf1* expression while confirming that *Sumf1* was expressed in proliferating chondrocytes and osteoblasts also revealed a strong expression in hypertrophic chondrocytes (Fig. 1E). Thus, *Sumf1* is a molecular marker of all cell types in the developing skeleton.

Proteoglycan desulfation affects endochondral ossification

As a first approach to study the importance of proteoglycan desulfation during skeletogenesis we analyzed skeletal preparations of *Sumf1*$^{-/-}$ embryos and mice stained with alcian blue for unmineralized cartilagineous ECMs and alizarin red for mineralized cartilagineous and bony ECMs. E14.5 *Sumf1*$^{-/-}$ embryos were indistinguishable from wild-type littermates (data not shown), an observation consistent with the fact that *Sumf1* is not express in the developing skeleton before this stage. In contrast, examination of E16.5 embryos revealed that femurs were significantly shorter in *Sumf1*$^{-/-}$ than in wild-type embryos (3.0 mm wild type vs. 2.8 mm *Sumf1*$^{-/-}$; $n = 3$, $P < 0.05$). This dwarfism, that worsened in newborn *Sumf1*$^{-/-}$ mice (4.2 mm wild type vs. 3.8 mm *Sumf1*$^{-/-}$; $n = 5$, $P < 0.01$) was generalized, as every bone analyzed (femurs, vertebrae, mandibles, components of the skull) were shorter in *Sumf1*$^{-/-}$ than in wild-type littermates (Fig. 1F,G; data not shown). These morphological abnormalities that were not caused by a decrease in insulin growth factor 1 production (Supplemental Fig. 1A), illustrate that the extent of proteoglycan desulfation is an important determinant of the growth of most skeletal elements during embryonic development.

Proteoglycan desulfation affects growth plate cellularity

Next, we performed histological and gene expression analyses. Consistent with the absence of morphological defects in E14.5 *Sumf1*$^{-/-}$ embryos there was no difference in the morphology of the various populations of chondrocytes between *Sumf1*$^{-/-}$ and wild-type embryos at that stage and expression of α_1*(II) Collagen*, a marker of proliferating chondrocytes, and of α_1*(X) Collagen*, a marker of hypertrophic chondrocytes, was similar in *Sumf1*$^{-/-}$ and wild-type embryos at E14.5 (Fig. 2A). At E16.5 the zone of proliferating chondrocytes, determined by cell morphology and the extent of α_1*(II) Collagen* expression, was significantly shorter in *Sumf1*$^{-/-}$ than in wild-type embryos (Fig. 2B). The intensity of α_1*(X) Collagen* expression was also weaker in E16.5 *Sumf1*$^{-/-}$ than in wild-type embryos (Fig. 2B). At birth, the classical columnar organization of the proliferating chondrocytes was lost in the *Sumf1*$^{-/-}$ growth plate and expression of α_1*(II) Collagen* and of α_1*(X) Collagen* was again noticeably weaker in mutant than in wild-type growth plate (Fig. 2C). Remarkably, despite the high level of *Sumf1* expression in osteoblasts, bone formation defined by the presence of bone trabeculae and expression of α_1*(I) Collagen* was not affected by *Sumf1* inactivation (Fig. 2B,C,D). Taken together, these results suggest that inactivation of *Sumf1*—i.e., inhibition of proteoglycan desulfation—affects more severely chondrogenesis than osteogenesis during development.

We next investigated whether the weaker expression of α_1*(II)* and α_1*(X) Collagen* in the *Sumf1*$^{-/-}$ growth plate was reflecting a decrease in chondrocyte number. We observed that there was a significant decrease in chondrocyte number in *Sumf1*$^{-/-}$ growth plates at E16.5 and at postnatal day 0 (P0) (Fig. 3A), indicating that the extent of proteoglycan desulfation regulates, in ways studied below, chondrocyte survival and/or proliferation during endochondral ossification.

Proteoglycan desulfation influences ECM production and turnover

Since abnormalities in proteoglycan desulfation result in lysosomal defects in several tissues in vertebrates (Neufeld and Muenzer 2001), we asked if lysosomal function was affected in *Sumf1*$^{-/-}$ chondrocytes and/or osteoblasts.

Electron microscopic (EM) analysis of wild-type and mutant growth plates did not reveal any morphological difference between *Sumf1*$^{-/-}$ and wild-type chondrocytes at E14.5 (Fig. 3C), while in E16.5 *Sumf1*$^{-/-}$ embryos and newborn mice the cytoplasm of chondrocytes was filled with vacuolar structures that had characteristic appearance of lysosomes filled with GAGs as seen in cells from patients affected by mucopolysaccharidoses (Neufeld and Muenzer 2001) (Fig. 3D,E, inset; Supplemental Fig.

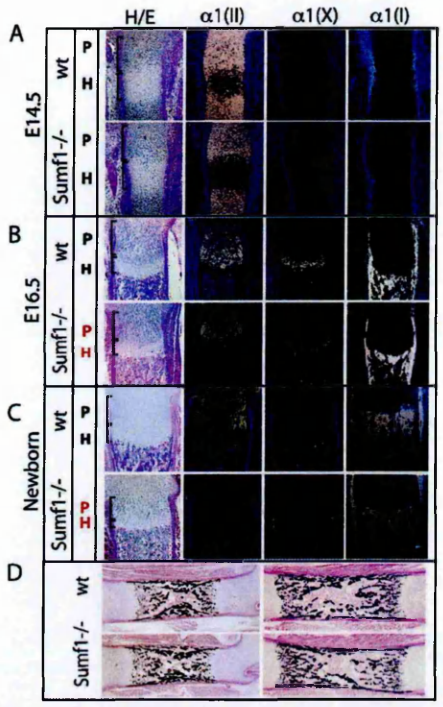

Figure 2. *Sumf1*$^{-/-}$ deficiency affects chondrogenesis but not osteogenesis. (*A*) Hematoxylin/eosin (H/E) staining and in situ hybridization analysis of femoral sections. No differences between *Sumf1*$^{-/-}$ and wild-type growth plates are observed in E14.5 embryos, while in E16.5 (*B*) and newborn (*C*) there is a progressive shortening of both proliferative and hypertrophic area in mutant mice. Expression of *α1(II)* and *α1(X) Collagen* was decreased in newborn *Sumf1*$^{-/-}$ compared with wild-type mice. *α1(I) Collagen* expression was similar in wild-type and *Sumf1*$^{-/-}$ samples at all stages analyzed. (*D*) Von Kossa-Van Gieson staining of femoral sections showed normal mineralization (black staining) in E16.5 and newborn *Sumf1*$^{-/-}$ mice. Magnification: *A–C*, 100×, *D*, 50×.

1B). Lysosomal vacuolization in osteoblasts was not nearly as dramatic, further suggesting that proteoglycan desulfation is a more important process during chondrogenesis than osteogenesis (Fig. 3F).

This impaired lysosomal degradation of GAGs in chondrocytes led us to ask whether the amount of GAGs present in the ECM was affected by the absence of *Sumf1* in chondrocytes by measuring the amount of GAGs in wild-type and in *Sumf1*$^{-/-}$ chondrocytes. As hypothesized, mutant chondrocytes produced 30% fewer membrane-bound GAGs than wild-type chondrocytes; GAG secretion in the medium was also reduced by 50% (Fig. 3G). This explained why staining with alcian blue, a dye marking proteoglycans, was significantly weaker in *Sumf1*$^{-/-}$ than in wild-type growth plates (Fig. 3H). EM analysis of ER and Golgi did not shown any morphological differences between wild-type and *Sumf1*$^{-/-}$ chondrocytes at E16.5 or P0, indicating that the reduced amount of ECM is not caused by a block in the GAGs biosynthetic pathway (Supplemental Fig. 1C).

Chondrocyte autophagy is hampered in the absence of proteoglycan desulfation

We next asked what were the mechanisms leading the decrease in chondrocyte number in *Sumf1*$^{-/-}$ growth plate. There was no overt increase in chondrocyte apoptosis in *Sumf1*$^{-/-}$ mice before or after birth (data not shown). BrdU incorporation did not reveal any significant difference in chondrocyte proliferation between *Sumf1*$^{-/-}$ and wild-type embryos at E14.5 and E16.5 either, although chondrocyte proliferation was significantly decreased after birth in *Sumf1*$^{-/-}$ mice (Fig. 4A). Thus, at least two mechanisms explain the paucity of chondrocytes in the *Sumf1*$^{-/-}$ growth plate: a decrease in chondrocyte proliferation beyond birth, and another one, yet to be determined, during embryonic development.

Macroautophagy (hereafter referred as autophagy) is a lysosomal process of cellular self-digestion required for turnover of cytoplasmic structure and for producing energy in conditions of cellular starvation (Mizushima 2007). Since chondrocytes reside in a hypoxic and avascular environment (Schipani et al. 2001) we hypothesized that autophagy may be a physiological means al-

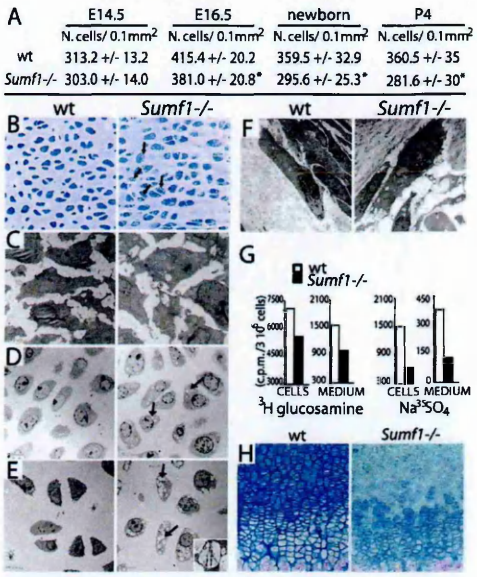

Figure 3. Defective ECM in *Sumf1*$^{-/-}$ growth plate. (*A*) Chondrocyte number in the growth plate proliferative zone. Values are the mean ± SD. Student's test (*) $P < 0.05$. (*B*) Toluidin blue staining of chondrocostal cartilage of newborn *Sumf1*$^{-/-}$ and wild-type littermates. Note the presence of cytoplasmatic vacuolization in *Sumf1*$^{-/-}$ chondrocytes. (*C*) EM analysis of E14.5 *Sumf1*$^{-/-}$ and wild-type chondrocytes showing no evidence of lysosomal vacuolization in *Sumf1*$^{-/-}$ embryos. (*D,E*) Cytoplasmatic vacuoles in E16.5 (*D*) and newborn (*E*) *Sumf1*$^{-/-}$ chondrocytes filled with amorphous material (GAGs) and partially degraded collagen fiber (*E, inset*). (*F*) *Sumf1*$^{-/-}$ osteoblasts are less affected than chondrocytes by lysosomal vacuolization. (*G*) ECM proteoglycan produced by *Sumf1*$^{-/-}$ and wild-type primary chondrocytes labeled with ^{3}H-glucosamine and $Na^{35}SO_4$. ECM amount was estimated by ^{3}H and ^{35}S incorporation and normalized for cells number. (*H*) Decreased alcian blue staining in P7 *Sumf1*$^{-/-}$ compared with wild-type growth plate.

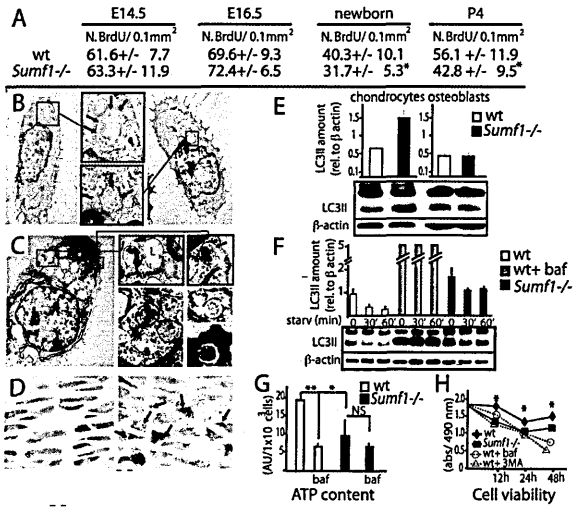

Figure 4. Abnormal autophagy in *Sumf1* ′ chondrocytes. (*A*) Number of BrdU positive cells present in the proliferative zone of the growth plate. Values are the mean ± SD. Student's test (*) $P < 0.05$. (*B*) EM analysis of newborn chondrochostal cartilage revealed the presence of autophagosomes in wild-type chondrocytes. (Boxed *inset*) Note the double membrane vesicles surrounding a portion of cytoplasm (arrows). (*C*) Chondrocyte from newborn *Sumf1* ′ showing more autophagosomes (AV) surrounded by enlarged lysosomes (L). (*D*) Confocal microscopy analysis of *Sumf1* ′ ;GFP-LC3 and wt;GFP-LC3 growth plate. In GFP-LC3 chondrocytes (*left*) the GFP fluorescence was more diffused throughout the cytoplasm while in *Sumf1* ′ ;GFP-LC3 it was aggregated in cytoplasmatic dots (*right*). (*E*) Western blot analysis showing a 2.5-fold increase in LC3II level in newborn *Sumf1* ′ chondrocytes. No difference was observed in osteoblasts. Values shown are means of triplicate experiments. (*F*) Abnormal autophagy in *Sumf1* ′ chondrocytes during serum and nutrient starvation. Wild-type and *Sumf1* ′ chondrocytes were starved for the indicated period of time, harvested, and subjected to LC3 immunoblotting. *Sumf1* ′ chondrocytes and wild type stimulated with Baf presented an increased amount of LC3II compared with wild-type chondrocytes at all time points analyzed. (*G*) ATP amount is decreased in wild-type chondrocytes when autophagy is inhibited with Baf. *Sumf1* ′ chondrocytes displayed a lower level of ATP compared with wild-type and Baf treatment did not affected significantly ATP concentration. (*H*) Wild-type and *Sumf1* ′ chondrocytes were cultured in serum and glucose-free medium for 2 d. Wild-type chondrocytes were also treated with baf and 3-methyladenine, another inhibitor of autophagy. Cell viability was monitored after 12 h, 24 h, and 48 h. Error bars represent SEM. Student's test (*) $P < 0.05$; (**) $P < 0.01$.

lowing them to survive, and that impairment in this process could cause chondrocyte death in *Sumf1* ′ embryos. Indeed, EM analysis of E16.5 embryos and newborn wild-type mice identified vacuoles containing a portion of cytoplasm and degraded organelles, a feature characteristic of autophagy (Mizushima 2007) (Fig. 4B, arrows). Remarkably, the number of autophagosome vacuoles (autophagosomes) was greatly increased in mutant chondrocytes (Fig. 4C).

To establish rigorously that the number of autophagosomes was increased in *Sumf1* ′ chondrocytes we used in vivo and biochemical approaches. First, we generated *Sumf1* ′ mice harboring in all cells a transgene expressing a GFP-tagged LC3 protein (Mizushima et al. 2004). During autophagy the free cytoplasmatic LC3I isoform of the LC3 protein is converted into LC3II, a specific marker of autophagosomes (Kabeya et al. 2000). Consistent with an increase in the number of autophagosomes GFP immunoreactivity was noticeably stronger in *Sumf1* ′ ;*GFP-LC3* than in *GFP-LC3* chondrocytes (Supplemental Fig. 1D). Moreover, while the GFP fluorescence was distributed throughout the cytoplasm in wild-type chondrocytes, it was clustered in autophagosomes in *Sumf1* ′ ;*GFP-LC3* chondrocytes (Fig. 4D, arrows). Western blot quantification of LC3II proteins showed also a 2.5-fold increase in *Sumf1* ′ compared with wild-type growth plates (Fig. 4E). This was not observed in *Sumf1* ′ osteoblasts (Fig. 4E), further illustrating that these cells are not overtly influenced by the absence of *Sumf1*.

Since GAGs accumulation can inhibit lysosomal function (Li et al. 2004), we tested whether this increase in the number of autophagosomes in *Sumf1*$^{-/-}$ chondrocytes was reflecting a failure of lysosome to digest autophagosomes by treating wild-type and *Sumf1* ′ chondrocytes with bafilomycin (Baf), an inhibitor of the autophagosome–lysosome fusion (Yamamoto et al. 1998), a necessary step during autophagy (Mizushima 2007). Baf treatment of wild-type chondrocytes triggered an increase in autophagosome accumulation as measured by LC3-II level and a significant decrease of energy (ATP) production (Fig. 4F,G). In contrast, in *Sumf1* ′ chondrocyte the level of LC3II was higher than in wild-type chondrocytes, and Baf did not decrease energy production significantly (Fig. 4F,G). These results support the notion that autophagy is impaired in *Sumf1* ′ chondrocytes. To determine if this impairment of autophagy could lead to chondrocyte death, wild-type and mutant chondrocytes were cultured in glucose-free and serum-free medium, a condition in which autophagy is required for energy production and cell survival (Lum et al. 2005). LC3-II immunoreactivity decreased rapidly upon nutrient starvation, suggesting that autophagosomes were efficiently digested by lysosomes in wild-type but not in *Sumf1* ′ chondrocytes (Fig. 4F). Moreover, when measured with colorimetric assay, cell viability was decreased in *Sumf1* ′ chondrocytes compared with wild-type cells (Fig. 4H).

In summary, in vivo and cell-based assays establish that autophagy is used by wild-type chondrocytes to produce energy and suggest that disruption of intralysosomal GAG digestion impairs autophagy in *Sumf1* ′ chondrocytes. This impairment in turn leads to cell death.

Proteoglycan desulfation regulates chondrocyte proliferation and differentiation

To explain the decrease in chondrocyte proliferation noted in *Sumf1* ′ mice we asked whether *Sumf1* expression modulates growth factor signaling. We first looked at Indian Hedgehog (Ihh), since its signaling is influenced in vivo by GAGs (Koziel et al. 2004), but failed to detect any difference in the level of expression of *Ihh* or of its receptor *Patched* (*Ptch*) between *Sumf1* ′ and wild-type chondrocytes at E16.5, P0, or P4 (Supplemental Fig. 2; data not shown). These observations indicate that *Sumf1* deletion does not affect overtly *Ihh* signaling during endochondral ossification.

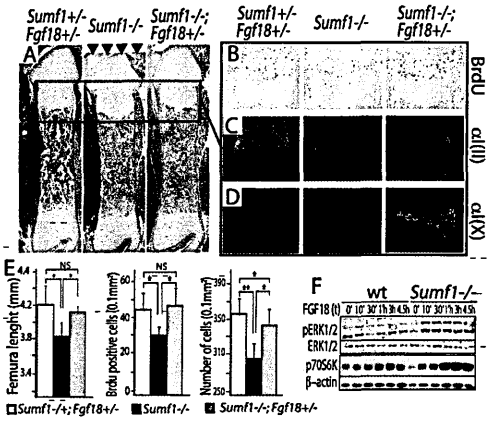

Figure 5. *Sumf1* regulates FGF18 activity during endochondral ossification. (*A*) H/E staining of femurs showing shortening of *Sumf1* $^{-/-}$ bone length (arrowheads) and its rescue in *Sumf1* $^{-/-}$;*fgf18*$^{+/}$ mice. Brdu staining (*B*) and in situ expression of α1(II) *Collagen* (*C*) and α1(*X*) *Collagen* (*D*) in wild-type (*left*), *Sumf1* $^{-/-}$ (*middle*), and *Sumf1* $^{-/-}$;*fgf18*$^{+/}$ mice. (*E*) Quantification of femoral length, BrdU index, and cell number in newborn wild-type, *Sumf1* $^{-/-}$, and *Sumf1* $^{-/-}$;*fgf18*$^{+/}$ mice. At least three mice were analyzed per each genotype. Error bars represent SEM. Student's test (*) $P < 0.05$; (**) $P < 0.01$. (*F*) Primary chondrocytes from wild-type and *Sumf1* $^{-/-}$ mice treated with Fgf18 (20 ng/mL) for the indicated period of time. Note the more sustained phosophorylation of ERK and 70S6k in *Sumf1* $^{-/-}$ than in wild-type chondrocytes following Fgf18 treatment.

The defect in chondrocyte proliferation and differentiation noticed in *Sumf1* $^{-/-}$ mice was reminiscent of what is observed in mice harboring an increase in FGF signaling (Ornitz and Marie 2002). To determine if FGF signaling was increased we generated *Sumf1* $^{-/-}$ mice lacking one copy of *Fgf18*, a known regulator of chondrocyte proliferation (Liu et al. 2002). Several lines of evidence indicate that proteoglycan desulfation indeed regulates, directly or indirectly, FGF signaling.

First, skeletal preparation showed that removing one allele of *Fgf18* rescued *Sumf1* $^{-/-}$ mice short stature at P0 as determined by femur length (Fig. 5A [arrowhead], quantification in E). Second, chondrocyte proliferation measured by BrdU incorporation, which was reduced by 20% in the P0 *Sumf1* $^{-/-}$, was indistinguishable from wild-type in *Sumf1* $^{-/-}$;*Fgf18*$^{+/}$ P0 mice (Fig. 5B, quantification in E). As a result, the zone of hypertrophic chondrocytes was larger, and there was a significant increase of growth plate cellularity in *Sumf1* $^{-/-}$;*Fgf18*$^{+/}$ compared with *Sumf1* $^{-/-}$ mice (Fig. 5E). Third α_1*(II) Collagen* and α_1*(X) Collagen* expression was restored almost to its normal intensity in *Sumf1* $^{-/-}$;*Fgf18*$^{+/}$ newborn mice (Fig. 5C,D). Together, these data support the notion that the absence of *Sumf1* results in an increase in FGF signaling, explaining the decrease in chondrocyte proliferation observed in *Sumf1* $^{-/-}$ mice. Of note, removing one Fgf18 allele did not normalize the chondrocyte number (Fig. 5E), indicating that the abnormal autophagy seen in the Sumf1 $^{-/-}$ embryos is not secondary to the increase in FGF signaling.

To identify the cause(s) of this increased FGF signaling in *Sumf1* $^{-/-}$ chondrocytes we first compared *Fgf18* expression in *Sumf1* $^{-/-}$ and wild-type newborn mice but failed to detect any significant difference (Supplemental Fig. 3), thus ruling out that *Sumf1* is not a regulator of *Fgf18* expression. It has been proposed that proteoglycans, through their degree of sulfation, modulate the affinity of FGFs for their cognate receptors (Bishop et al. 2007). To determine if this was the case in *Sumf1* $^{-/-}$ mice we stimulated wild-type and *Sumf1* $^{-/-}$ primary chondrocytes with FGF18 and measured activation of FGF signaling. Both the ERK kinase and the ribosomal protein S6, which are involved in FGF signaling (Murakami et al. 2004), were more phosphorylated in *Sumf1* $^{-/-}$ than in wild-type chondrocytes (Fig. 5F). These results support the hypothesis that *Sumf1*, and more generally proteoglycan desulfation, influence FGF signaling in chondrocytes during skeletal development.

Sulfatases catalyze desulfation of the GAGs moiety of proteoglycans in the intracellular and extracellular space. These enzymes are substrates of *Sumf1* whose only known function is to activate sulfatases. By studying endochondral ossification in *Sumf1* $^{-/-}$ mice we show that proteoglycan desulfation regulates several aspects of chondrocyte biology. Indeed, the block in proteoglycan desulfation caused by *Sumf1* $^{-/-}$ deletion severely decreases chondrocytes viability by hampering their capacity to generate enough energy through autophagy to survive in their avascular environment. Our data suggest that this defect in autophagy is caused, in part, by the engulfment of lysosomes by undigested GAGs that leads to an impairment of the autophagosome–lysosome fusion (Settembre et al. 2008).

Growth plate cartilage is a hypoxic structure in which the transcription factor *Hif1α* is required for chondrocytes survival. The fact that hypoxia stimulate autophagy (Mizushima 2007) suggests that autophagy could be one pathway through which *Hif1α* allows chondrocytes to survive. Moreover, chondrocytes starvation does not increase the autophagosome number as commonly observed in other cellular lines, suggesting that in this cell type autophagy is a constitutive rather than an adaptive pathway.

Our study also shows that proteoglycan desulfation is a negative regulator of *Fgf18* signaling during endochondral ossification. This may be a direct consequence of the level of desulfation of certain proteoglycans such as heparan sulphate proteoglycan (HSPG) rather than a secondary effect of the engulfment of lysosomes with GAGs. Our results are in agreement with the notion that, in cell culture, ECM proteoglycans, and particularly HSPG bind members of FGF family (Bishop et al. 2007). It is likely that the two main sulfatases involved in this regulatory pathways are *Sulf1* and *Sulf2*, which are strongly expressed in chondrocytes and whose substrate is HSPG (Lum et al. 2007). Together, our data show that proteoglycan desulfation eventually affects several aspects of chondrocyte biology during skeletal development not only by determining lysosomal function but also by modulating growth factor signaling.

Materials and methods

Animals

Sumf1 $^{-/-}$, *Fgf18* $^{-/-}$, and *GFP-LC3* transgenic mice were described previously (Liu et al. 2002; Mizushima et al. 2004; Settembre et al. 2007). Genotyping was performed by genomic PCR.

Skeletal preparation
Skeletons were fixed in 100% ethanol overnight and stained with alcian blue and alizarin red according to standard protocols. At least three mice of each genotype were analyzed per stage.

LacZ staining and BrdU labeling
Embryos were fixed in 1% paraformaldehyde, 0.2% glutalaldehyde, and stained overnight with X-Gal (Roche). Specimens were embedded in paraffin, sectioned at 6 µm, and counterstained with eosin (Sigma). Embryos were labeled with BrdU by injecting pregnant females with 500 µL of 10 mM BrdU 1 h before harvest. BrdU incorporation was detected using a Zymed BrdU staining kit (Invitrogen). Three to five embryos/mice were analyzed for each genotype and age group. Statistical significance was assessed by the Student's test. ([*] $P < 0.05$; [**] $P < 0.01$).

Light and electron microscopy
Tibia were fixed in a 4% paraformaldehyde/1% glutaraldehyde fixative solution (pH 7.4), in 0.1 M sodium cacodylate buffer, dehydrated in ethanol, and embedded in plastic resin. Ultrathin sections (80 nm) were examined with a transmission electron microscope operated at 80 kV.

Cell cultures, Western blot analyses, and in situ hybridization
See the Supplemental Material.

Isolation of radiolabeled GAGs
Primary chondrocytes were cultured in presence of 10 µCi/mL $Na^{35}SO_4$ (25–40 Ci/mg) and 20 µCi/mL D-[6-^{3}H]glucosamine (40 Ci/mmol) for 3 d in sulfate and glucose-free medium. GAG extraction, purification, and analysis were performed as described previously (Bame and Esko 1989).

Acknowledgments

We are indebted to Drs. D.M. Ornitz and N. Mizushima for providing Fgf18-deficient mice and GFP-LC3 transgenic mice. C.S thanks M.P. Cosma, P. Ducy, A. Fraldi, and G. Parenti for their critical reading of the manuscript. C.S is the recipient of a predoctoral fellowship of the European School of Molecular Medicine (SEMM). This work was supported by grants from the NIH to G.K.

References

Bame, K.J. and Esko, J.D. 1989. Undersulfated heparan sulfate in a Chinese hamster ovary cell mutant defective in heparan sulfate N-sulfotransferase. *J. Biol. Chem.* **264:** 8059–8065.

Bishop, J.R., Schuksz, M., and Esko, J.D. 2007. Heparan sulphate proteoglycans fine-tune mammalian physiology. *Nature* **446:** 1030–1037.

Bulow, H.E. and Hobert, O. 2006. The molecular diversity of glycosaminoglycans shapes animal development. *Annu. Rev. Cell Dev. Biol.* **22:** 375–407.

Cosma, M.P., Pepe, S., Annunziata, I., Newbold, R.F., Grompe, M., Parenti, G., and Ballabio, A. 2003. The multiple sulfatase deficiency gene encodes an essential and limiting factor for the activity of sulfatases. *Cell* **113:** 445–456.

Diez-Roux, G. and Ballabio, A. 2005. Sulfatases and human disease. *Annu. Rev. Genomics Hum. Genet.* **6:** 355–379.

Esko, J.D. and Selleck, S.B. 2002. Order out of chaos: Assembly of ligand binding sites in heparan sulfate. *Annu. Rev. Biochem.* **71:** 435–471.

Kabeya, Y., Mizushima, N., Ueno, T., Yamamoto, A., Kirisako, T., Noda, T., Kominami, E., Ohsumi, Y., and Yoshimori, T. 2000. LC3, a mammalian homologue of yeast Apg8p, is localized in autophagosome membranes after processing. *EMBO J.* **19:** 5720–5728.

Koziel, L., Kunath, M., Kelly, O.G., and Vortkamp, A. 2004. Ext1-dependent heparan sulfate regulates the range of Ihh signaling during endochondral ossification. *Dev. Cell* **6:** 801–813.

Kronenberg, H.M. 2003. Developmental regulation of the growth plate. *Nature* **423:** 332–336.

Li, Z., Yasuda, Y., Li, W., Bogyo, M., Katz, N., Gordon, R.E., Fields, G.B., and Bromme, D. 2004. Regulation of collagenase activities of human cathepsins by glycosaminoglycans. *J. Biol. Chem.* **279:** 5470–5479.

Liu, Z., Xu, J., Colvin, J.S., and Ornitz, D.M. 2002. Coordination of chondrogenesis and osteogenesis by fibroblast growth factor 18. *Genes & Dev.* **16:** 859–869.

Lum, J.J., Bauer, D.E., Kong, M., Harris, M.H., Li, C., Lindsten, T., and Thompson, C.B. 2005. Growth factor regulation of autophagy and cell survival in the absence of apoptosis. *Cell* **120:** 237–248.

Lum, D.H., Tan, J., Rosen, S.D., and Werb, Z. 2007. Gene trap disruption of the mouse heparan sulfate 6-O-endosulfatase gene, Sulf2. *Mol. Cell. Biol.* **27:** 678–688.

Mizushima, N. 2007. Autophagy: Process and function. *Genes & Dev.* **21:** 2861–2873.

Mizushima, N., Yamamoto, A., Matsui, M., Yoshimori, T., and Ohsumi, Y. 2004. In vivo analysis of autophagy in response to nutrient starvation using transgenic mice expressing a fluorescent autophagosome marker. *Mol. Biol. Cell* **15:** 1101–1111.

Murakami, S., Balmes, G., McKinney, S., Zhang, Z., Givol, D., and de Crombrugghe, B. 2004. Constitutive activation of MEK1 in chondrocytes causes Stat1-independent achondroplasia-like dwarfism and rescues the Fgfr3-deficient mouse phenotype. *Genes & Dev.* **18:** 290–305.

Neufeld, E. and Muenzer, J. 2001. *The metabolic and molecular bases of inherited disease.* McGraw-Hill, New York.

Olsen, B.J., Reginato, A.M., and Wang, W. 2000. Bone development. *Annu. Rev. Cell Dev. Biol.* **16:** 191–220.

Ornitz, D.M. and Marie, P.J. 2002. FGF signaling pathways in endochondral and intramembranous bone development and human genetic disease. *Genes & Dev.* **16:** 1446–1465.

Perrimon, N. and Hacker, U. 2004. Wingless, hedgehog and heparan sulfate proteoglycans. *Development* **131:** 2509–2511.

Schipani, E., Ryan, H.E., Didrickson, S., Kobayashi, T., Knight, M., and Johnson, R.S. 2001. Hypoxia in cartilage: HIF-1α is essential for chondrocyte growth arrest and survival. *Genes & Dev.* **15:** 2865–2876.

Settembre, C., Annunziata, I., Spampanato, C., Zarcone, D., Cobellis, G., Nusco, E., Zito, E., Tacchetti, C., Cosma, M.P., and Ballabio, A. 2007. Systemic inflammation and neurodegeneration in a mouse model of multiple sulfatase deficiency. *Proc. Natl. Acad. Sci.* **104:** 4506–4511.

Settembre, C., Fraldi, A., Jahreiss, L., Spampanato, C., Venturi, C., Medina, D., de Pablo, R., Tacchetti, C., Rubinsztein, D.C., and Ballabio, A. 2008. A block of autophagy in lysosomal storage disorders. *Hum. Mol. Genet.* **17:** 119–129.

Yamamoto, A., Tagawa, Y., Yoshimori, T., Moriyama, Y., Masaki, R., and Tashiro, Y. 1998. Bafilomycin A1 prevents maturation of autophagic vacuoles by inhibiting fusion between autophagosomes and lysosomes in rat hepatoma cell line, H-4-II-E cells. *Cell Struct. Funct.* **23:** 33–42.

Legatoria - Tipografia - RICCO - Via Mezzocannone, 105 Napoli
Tel./Fax 081.551.66.55 - e-mail: tipografiaricco@libero.it
Premiata con Medaglia d'oro "Premio Minerva 1988"